Chairman: Prof. Dr. Jan Colpaert

Promoter: Prof. Dr. Wouter Maes

Copromoters: Prof. Dr. Dirk Vanderzande

                             Dr. Laurence Lutsen

Members of the Jury: Prof. Dr. Tanja Junkers, UHasselt

                             Prof. Dr. Seth Marder,
Georgia Institute of Technology

                             Prof. Dr. Michael M. Singleton,
Université Catholique de Louvain

                             Prof. Dr. ir. Guy Van Assche,
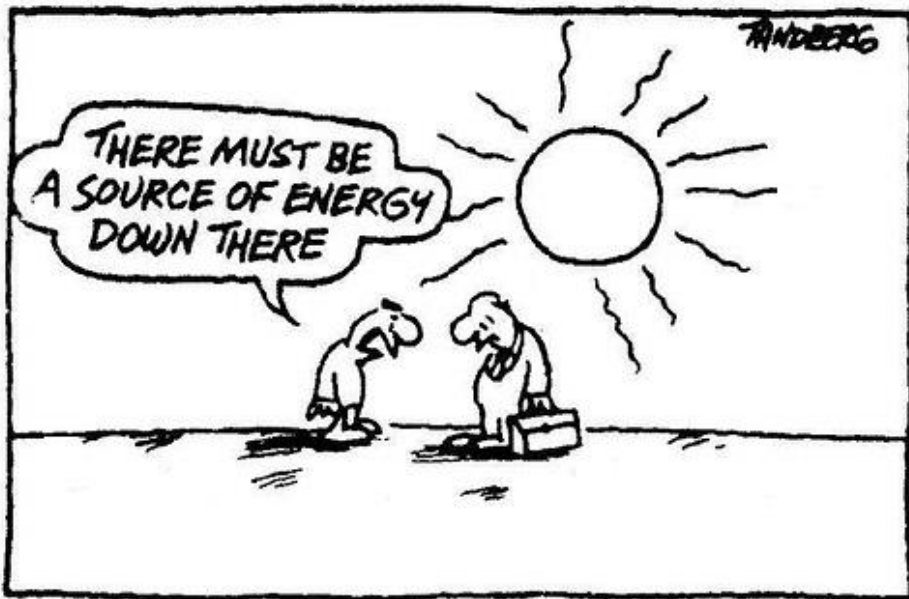Vrije Universiteit Brussel

TABLE OF CONTENTS

Chapter 1

Introduction

Reproduced with permission (copyright Robert Tandberg).

1.1 General introduction

To date, our planet is inhabited by approximately 7.5 billion people and this number keeps on increasing day by day. It is projected that the threshold of 10 billion people will be reached by 2057.[1] Along with the increase of the world population and general welfare, the world's energy demand will also further increase. The main current energy supplies are non-renewable sources like oil, coal, natural gas and uranium. It is difficult to predict within which time-frame these non-renewable energy sources will be depleted, but it is inevitable that they will at a certain moment. Besides their finite supply, they also have a significant negative environmental impact. In the past two decades, significant efforts have been made in the search for sustainable energy. Two main characteristics of sustainable energy are renewability and environmental friendliness. Several natural energy resources like solar, wind, geothermal and hydropower energy clearly demonstrate these aspects. Among them, solar energy is the most attractive one as it is the most abundant and globally accessible energy source. The amount of solar energy that reaches the earth's surface is estimated to be 1500 to 8000 times larger than the global energy demand.[2,3]

Figure 1 illustrates the high potential of solar energy compared to other existing renewable energy technologies and the known reserves of non-renewable energy resources.[4]
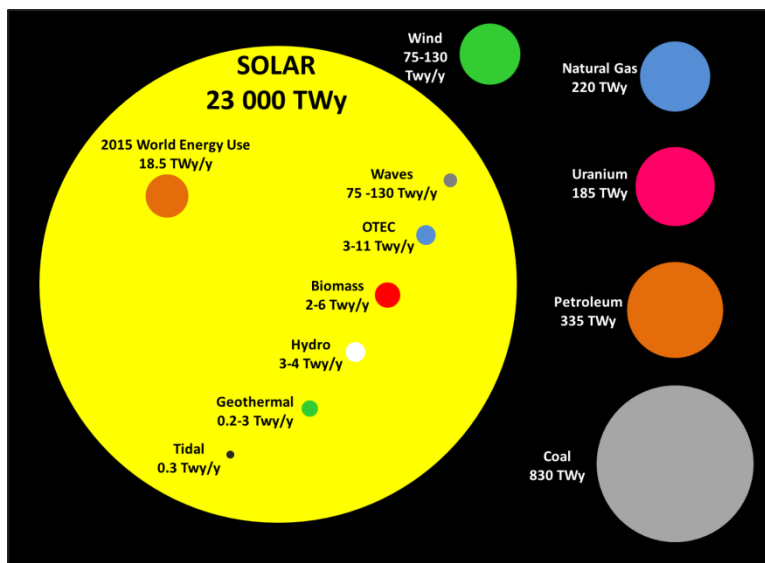

Figure 1. Comparison of the energy capacity of different energy resources (reproduced with permission, copyright 2015 IEA SHC).[4]

Solar energy can be harvested through the conversion of solar irradiation into electrical energy with photovoltaic (PV) technologies, which have experienced a remarkable growth over the past two decades. They cannot only be found in industrial applications but, stimulated by the urge to build new houses as energy neutral as possible, photovoltaic technologies can also readily be found in domestic applications. Although photovoltaics are already an established renewable energy technology for several years, the annual production in one year still increased with 20% in 2015 to 60 GW.[5] Within a timeframe of 15 years, the actual production volume has increased 200-fold. The first steep increase dates back to 2006 and can mainly be contributed to China and Taiwan. Nowadays, the production of photovoltaic technologies has expanded to several other Asian countries. With a total investment of $ 161 billion, solar energy accounted for 56% of all new renewable energy investments in 2016, illustrating the attractiveness and potential of photovoltaic technologies.

The first silicon based solar cells, with a power conversion efficiency (PCE) of 6%, were reported by Chapin *et al*. in 1954.[6] Current PV modules are reaching efficiencies up to 5 times higher (±25%) and can guarantee a continuous energy output over a time span of 25 years. The main part of these PV modules exist out of mono- or polycrystalline silicon, marked as the first generation solar cell technology. Over the years, the production cost of these PV modules has decreased significantly, but it is still considered fairly high. The second generation solar cells can be categorized as thin-film technologies. Their overall cost is significantly lower as they intrinsically have a higher absorption coefficient and therefore significantly smaller material amounts are required. Some examples of second generation PV's are amorphous silicon, Cadmium-Tellurium (CdTe) and Copper-Indium-Gallium-Selenide (CIGS) based solar cells. One of the main issues hindering their global application is the limited scalability of these technologies. In order to overcome this, a third generation of solar cell technologies was developed, based on organic and hybrid organic/inorganic materials, reaching efficiencies up to 11.9% (Sharp Corporation), 11.5% (HKUST) and 13.1% for dye-sensitized (DSSC), single junction polymer-fullerene and single junction polymer-small molecule solar cells, respectively.[7,8] This latest generation of organic solar cells is particularly interesting as it exhibits specific desirable properties such as simple preparation, novel aesthetic possibilities, reduced weight and mechanical flexibility, semi-transparency, production by large scale printing technologies and better performance in diffuse light. Finally, the latest solar cell technology utilizes a light harvesting material with a perovskite crystal structure (generally $CH_3NH_3MX_3$, with M a metal cation and X an oxide or halide anion). The current record efficiency for these materials is 21.02%.[9]

Figure 2 illustrates the roadmaps of the different types of solar cell technologies over the past 4 decades.[7] The curve for organic photovoltaics (OPV) only starts in 2002, with the certification of a solar cell with an efficiency of 2.5%. Within a

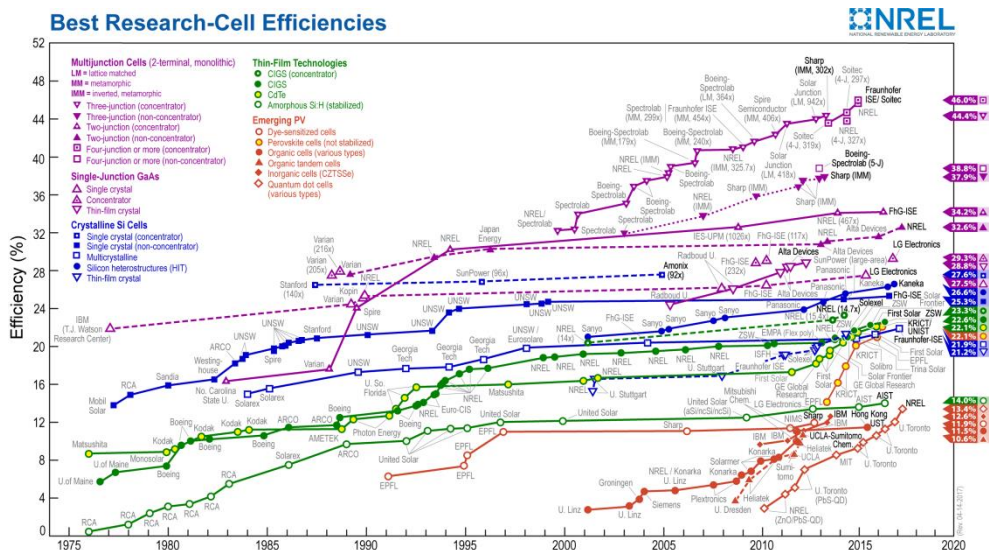timeframe of 15 years, this technology has shown a steady growth, with PCE's nowadays reaching over 12%.

Figure 2. Evolution of the best research-cell efficiencies over the past 4 decades for the different solar cell technologies (source: NREL, version May 2017).[7]

1.2 Organic photovoltaics

1.2.1 Historical overview

The birth of organic semiconductors dates back to the 1970's, with the discovery of the high conductivity of doped polyacetylene by Heeger, MacDiarmid and Shirakawa. This material approached the conductivity of copper and silver (10^5 and 10^8 S/m, respectively) and the impact of the research was so substantial that these researchers were awarded with the Nobel Prize for Chemistry.[10–12] This event coincided with the start of a quest for efficient organic solar cells. The first reasonably efficient organic solar cells (±1%) consisted out of a bilayer of photoactive organic materials, sandwiched between two electrodes, wherein an n-type material was evaporated on top of a p-type material. By combining a perylenetetracarboxylic acid derivative (n-type) with a Cu-phthalocyanine (p-type), Tang *et al.* established organic solar cells with PCE's up to 1%.[13] Although people found these results extremely exciting and promising, the field needed two more kick-starting discoveries before it really advanced. The first was the discovery by Sariciftci *et al.* of the photoinduced electron transfer of conducting polymers to buckministerfulllerenes, which generated the widely applied concept of polymer-fullerene solar cells.[14] The second discovery resolved a fundamental problem of the initial device architecture. As light strikes the donor polymer

material, electron-hole pairs – 'excitons' - are generated. These excitons need to diffuse to the donor-acceptor interface, where they can dissociate (*vide infra*). The excitons have binding energies ranging from 0.4 to 0.5 eV, which intrinsically limits the distance they can travel to approximately 5 to 10 nm, commonly referred to as the exciton diffusion length. Further diffusion is limited as the excitons will undergo radiative or non-radiative recombination.[15] Within the initial bilayer architecture, the thickness of the polymer donor material was limited. To enhance the exciton dissociation, the interfacial area between the donor and acceptor material had to be increased. A solution came up in 1995, with the synthesis of a more soluble methanofullerene derivative, [6,6]-phenyl-C_{61}-butyric acid methyl ester, by Hummelen and Wudl.[16,17] This discovery lead to the concept of the bulk heterojunction (BHJ) solar cell, in which the two organic materials are blended together in solution and an interpenetrating network of both components is formed upon film formation. The intermixing between the two components occurs at the length scale of the exciton diffusion length and thereby generates a significantly larger portion of exciton dissociation events. Today, this BHJ active layer structure is almost solemnly used. The fullerene derivatives are still the predominantly used acceptors, but as they have a limited absorption and solubility and they are rather expensive, the field also started focussing on alternative acceptor materials. Recently the efficiency of non-fullerene organic solar cells has surpassed that of the conventional fullerene-based OPV's (13.1% v. 11.5%).[7,8]

Although organic photovoltaics had a slow start, they developed into a very popular research topic, with almost 5000 publications in 2016 (Figure 3).[18] Besides a rising number of publications each year, OPV technology has also attracted the attention of multiple large industrial companies like BASF, Solvay, Merck, Belectric, Heliatek and ThyssenKrupp.
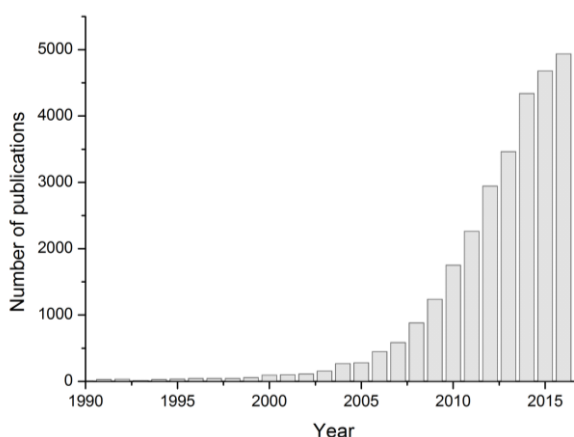

Figure 3. Number of publications per year on the research topic 'organic photovoltaics' (Web of Science).[18]

1.3 Free charge carrier generation in BHJ organic solar cells

While in conventional inorganic solar cells optical absorption results immediately in the formation of free charge carriers, light absorption in organic solar cells will first generate a spatially localized electron-hole pair, which is electrically neutral and is often referred to as 'exciton'. The overall operation mechanism of an organic solar cell can be divided in five steps: i) exciton formation, ii) exciton migration, iii) exciton dissociation, iv) free charge carrier migration toward the respective electrodes and v) charge collection. The photo-induced charge-carrier formation mechanism can be described with the simplified electronic state diagram depicted in Figure 4. In a first step, an incident photon beam excites an electron from the singlet ground state (S_0) of either the donor or acceptor which, after relaxation of the π-system to the bottom of the potential energy surface, generates a singlet exciton (S_1). As stated in the previous paragraph, not every generated exciton will reach the interface between the donor and acceptor material, as the exciton lifetime is limited due to possible radiative and non-radiative decays back to the ground state. Excitons that reach the donor-acceptor interface can undergo intermolecular charge transfer, generating so called charge-transfer (CT) states, where the hole can be found on the donor molecule and the electron is located on the acceptor molecule. In a final state, called the charge separation (CS) state, the electron and hole can be considered free from each other. This transfer from CT tot CS state is still in competition with relaxation toward the ground state. Once the charge carriers are considered free, they will need to move toward their respective electrodes and the efficiency of this process depends on the charge carrier mobility of the materials. The final step is the actual charge collection, which is dependent on the alignment of the frontier energy levels of the active layer materials with the Fermi levels (E_F) of the respective electrodes.[19-24]
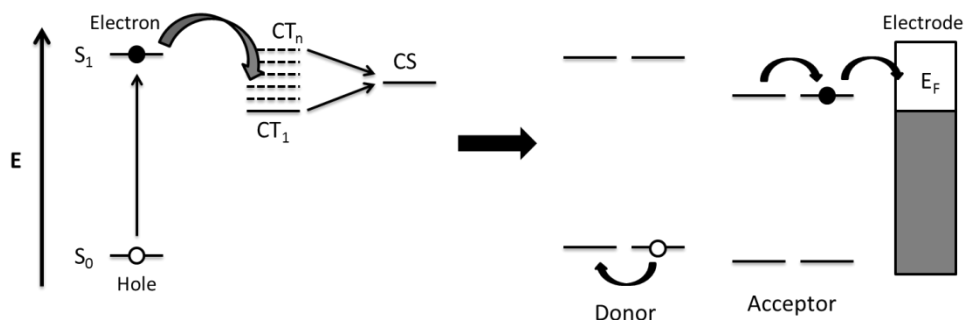

Figure 4. Simplified electronic state diagram of the free charge carrier formation process.[24]

1.4 Solar cell architecture and performance parameters

A standard solar cell stack is built up starting from a transparent glass substrate (Figure 5) which is coated with a high work function (WF) anode material like indium tin oxide (ITO, WF = ± 4.6 eV). The next layer, referred to as the hole conducting layer, ensures a proper ohmic contact between the anode material and the photoactive layer. This layer both smoothens out the surface of the anode material and provides a good wettability of the photoactive layer. The most commonly used material for this purpose is poly(3,4-ethylenedioxythiophene):poly(styrenesulfonate) (PEDOT:PSS). The next layer is the intimate blend of donor and acceptor, which is deposited from solution and forms the actual photoactive heart of the device. Deposition of this photoactive layer can be achieved in various ways, such as spin coating, inkjet printing, blade coating, spray coating or screen printing. Selection of the deposition method depends on the nature of the material components and the production scale. The final layer on top of the device consists out of a low work function cathode material, e.g. a combination of calcium (Ca) and aluminium (Al), and is deposited through thermal evaporation.

A second device architecture is commonly referred to as the inverted solar cell architecture and is generally more stable than the conventional one (Figure 5). The build-up of this stack starts again with ITO, which now acts as the low work function electrode. The next two layers exist out of an electron transporting layer like zinc oxide and the active layer blend. The stack is topped off with a thin layer of molybdenum oxide and a high work function top electrode material, e.g. silver (Ag). In this inverted architecture there is no PEDOT:PSS or calcium present. The first is known for extracting indium atoms out of the ITO layer and the second is prone to oxidation. The presence of these two components could hinder the long-term application of OPV devices. In terms of stability, the inverted stack is hence favoured.
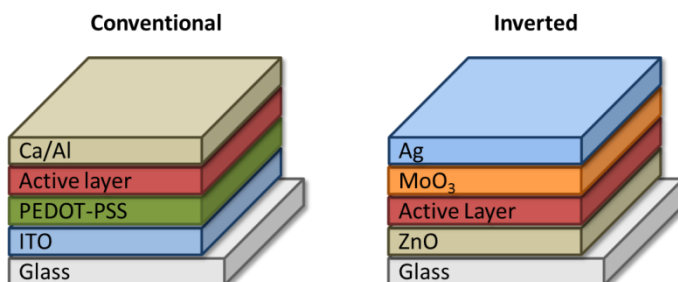

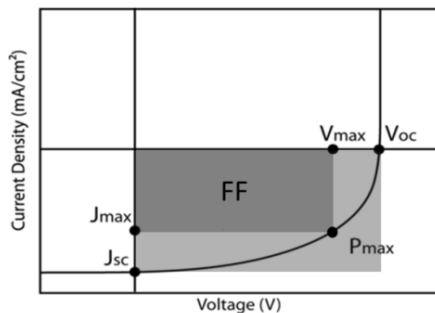**Figure 5.** Generally applied architectures for organic solar cells.

Figure 6. Example of a *J-V* measurement illustrating the parameters J_{sc}, V_{oc}, FF and P_{max}.

There are four main parameters that are used to evaluate the solar cell performance: the short-circuit current density (J_{sc}), the open-circuit voltage (V_{oc}), the fill factor (FF) and the power conversion efficiency. These parameters can be determined by performing *J-V* measurements and plotting the current density as a function of the applied voltage (Figure 6). The J_{sc} is the maximum current the device can deliver and is the current that flows through the device when it is being illuminated and a 0 V bias is being applied. The overlap of the absorption spectrum of the photoactive layer and the solar spectrum has a significant influence on this current. The absorption spectrum is dependent on the intrinsic bandgap of the active layer materials. Additional aspects influencing the current are the solar intensity, the charge collection efficiency and the layer thickness. The second parameter is the V_{oc}, which is the maximum achievable voltage of the illuminated device when there is no current flowing. Purely based on the active layer materials, the upper limit of the V_{oc} can roughly be estimated by evaluating the energy level alignment of the HOMO of the donor and the LUMO of the acceptor.[25,26] Similar as for the J_{sc}, there are additional factor influencing the V_{oc}, like non-optimal contacts between the different layers of the solar cell, the presence of impurities and deviations of the optimal morphology (too large or too little phase separation between the donor and acceptor materials to obtain the right intimately mixed BHJ). The next parameter is the FF, which is a quantification of the solar cell's maximum power output (P_{max}) versus the theoretical maximum achievable power ($P_{Theor\ max}$) based on the product of the J_{sc} and V_{oc}. P_{max} is calculated by multiplying the corresponding J_{max} and V_{max} at the maximum power point. The $P_{Theor\ max}$ can graphically be determined by constructing a rectangle in the fourth quadrant of the *J-V* curve starting from J_{sc} and V_{oc}. Combination of P_{max} and $P_{Theor\ max}$ allows calculation of the FF by the following equation:

$$FF = \frac{P_{max}}{P_{Theor\ max}} = \frac{J_{max} \times V_{max}}{J_{sc} \times V_{oc}} \quad (1)$$

Devices with high FF's are mostly recognised by a low charge carrier recombination rate, a very efficient extraction of charges and a low series resistance.

The final parameter, expressing the performance of the solar cell, is the power conversion efficiency (PCE or η), which is the ratio of the maximum power generated by the device versus the total power input of photon irradiation. The PCE can be calculated using the following equation:

$$PCE = \frac{P_{max}}{P_{in}} = \frac{(J_{max} \times V_{max})}{P_{in}} = FF \times \frac{J_{sc} \times V_{oc}}{P_{in}} \quad (2)$$

To compare solar cell results between the different laboratories around the world, it is imperative that all solar cells are measured under the same illumination conditions. The standard conditions are a measurement temperature of 25 °C and an irradiation of 1000 W/m² with an air mass 1.5 spectrum (AM 1.5 G). The AM 1.5 G spectrum is equivalent to the solar irradiation at an angle of 45° with respect to the horizon.

1.5 State of the art OPV active layer materials

The current global interest for OPV research was triggered by the development of a third generation donor materials, as the first and second generation only showed poor to moderate efficiencies (e.g. for P3HT ±5%)[27,28] due to their inherently limited absorption (coming from a relatively large band gap of ±1.9 eV). This latest generation focussed on effectively lowering the HOMO-LUMO gap of the donor polymer to reduce the bandgap while keeping a deep HOMO level to optimize the V_{oc}. The reduced bandgap generates an increased light absorption, which should lead to higher efficiency devices. These materials generally belong to the class of donor-acceptor (push-pull) copolymers, which effectively lower the bandgap below 2 eV. The polymer backbone exists out of an alternation of electron-rich (donor) and electron-poor (acceptor) units. The library of possible donor and acceptor units, mainly of heterocyclic nature (Figure 7), has become very extensive and the number of combinations is nearly endless. The field has done tremendous efforts in the search for combinations delivering high-performance OPV materials. As it is not only the combination of donor and acceptor units that determines the overall efficiency of the devices, also great efforts have been done in the fine-tuning of the established polymer materials, mainly by adapting the side chains, to optimize their performance.
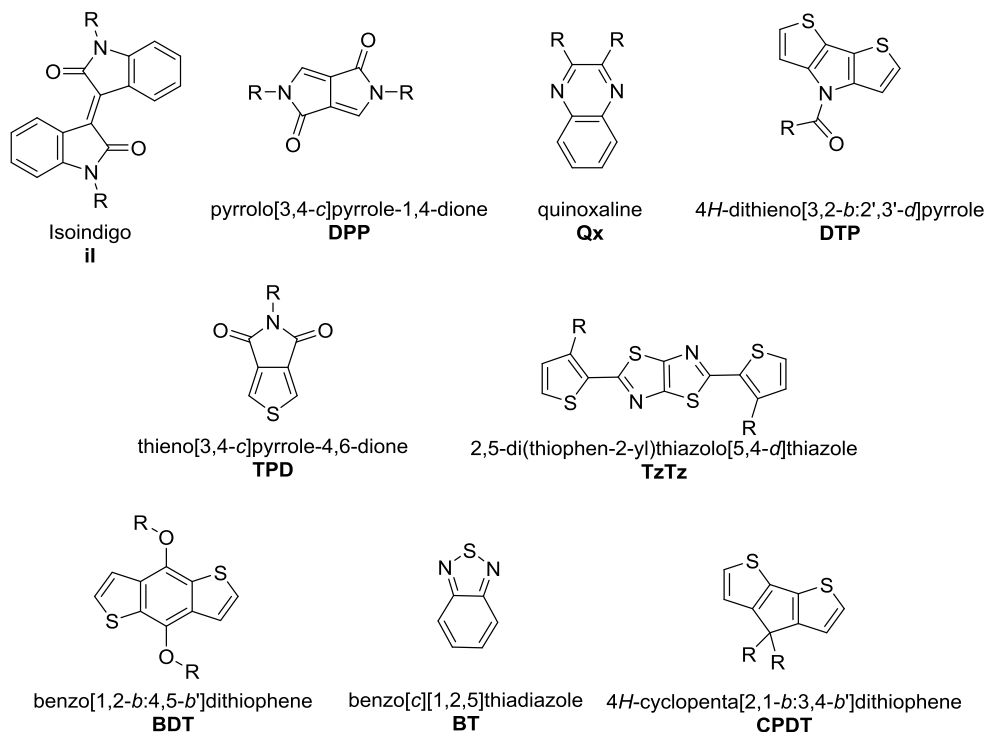
Figure 7. A number of donor and acceptor building blocks for OPV low bandgap polymers (R = alkyl).

Currently, the highest performing low bandgap copolymers can roughly be divided into three categories: benzodithiophene polymers, oligothiophene polymers and all other polymers with a performance above 8%.[29] Polymers based on the benzo[1,2-*b*:4,5-*b'*]dithiophene (BDT) unit belong without any doubt to the most successful polymers in OPV research. In both single and tandem devices, efficiencies above 10% have been reached.[30–32] Its success can mainly be attributed to the rigid planar structure of the fused ring system. The highly delocalized π-system assures proper hole transportation and effectively lowers the bandgap of the polymer. The BDT unit is also easily functionalized in the 4 and 8 positions on the central benzene ring. The first generation of BDT-based polymers, which were functionalized with either alkoxy or alkyl side chains, already afforded efficiencies ranging from 7.3 to 9.2% (Figure 8).[33–35]

A further increase in efficiency was established with a second generation of BDT-based polymers, in which the BDT unit was functionalized with alkylthienyl groups. This functionalization causes a lowering of the HOMO level of the polymer and thereby increases the V_{oc}. Another important effect is the increased π-π stacking ability of the polymers, which leads to higher hole mobilities and a reduction of the optical bandgap. With this new generation, efficiencies up to

10.7% were achieved in combination with the conventionally used $PC_{71}BM$ acceptor (Figure 8).[36] The current record of 11.2% for BDT-based polymers, and OPV in general, was achieved by alternation with the benzodithiophenedione unit and in combination with the non-fullerene acceptor ITIC (Figure 8).[8]

PBDTTPD

PTB7

PTB7-Th

PBDTBDD
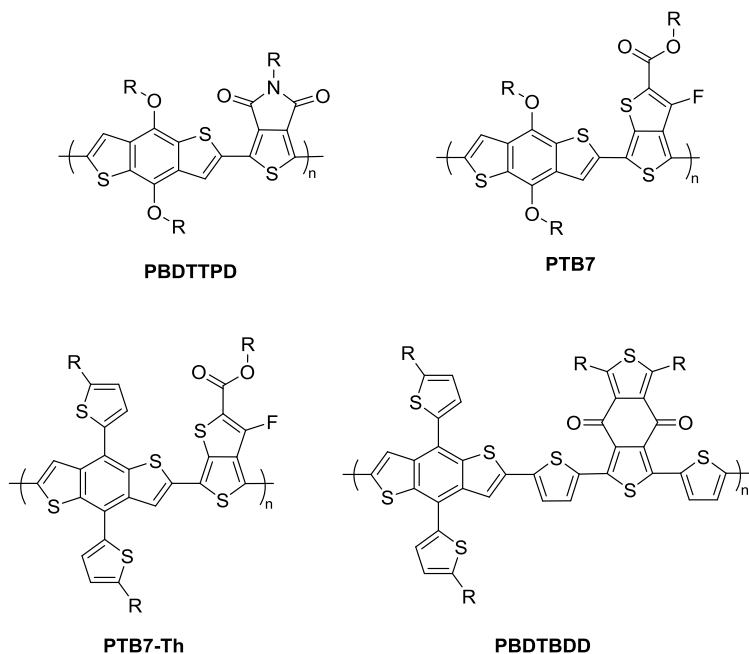
Figure 4. Examples of high-performance BDT-based low bandgap polymers (R = alkyl).

The second group of high-performance materials exists out of oligothiophene based polymers. The implementation of oligothiophene segments (bi-, ter- and quarterthiophenes) was inspired by the second generation workhorse material poly(3-hexylthiophene) (P3HT), which was capable of affording efficiencies around 5% due to its formation of highly ordered lamellae and its π-π stacking ability. Higher efficiencies were not accessible with P3HT due to the limited absorption. Combination of oligothiophene segments with appropriate acceptors allows sufficient lowering of the bandgap to increase the absorption and can preserve the aggregation behaviour. The probably most remarkable contribution to this category, with three donor polymers delivering efficiencies above 10% in combination with different fullerenes, comes from H. Yan and coworkers (Figure 9).[37] The strong temperature dependent aggregation behaviour of all three polymers was identified as the main characteristic generating the high efficiencies. These polymers already partially aggregate in solution, which enhances the formation of very pure and crystalline domains during the film formation process.[38–40] The highly ordered but small domains contribute to a high hole mobility ($1.5\text{-}3 \times 10^{-2}$ V^{-1} s^{-1}) and a minimum of charge recombination

events. These materials have a remarkably high FF for significantly thick films of ~300 nm compared to other donor polymers (mostly around 100-150 nm). Their applicability as thick films makes them strong candidates for industrial application because of the ease of deposition and great roughness tolerance.
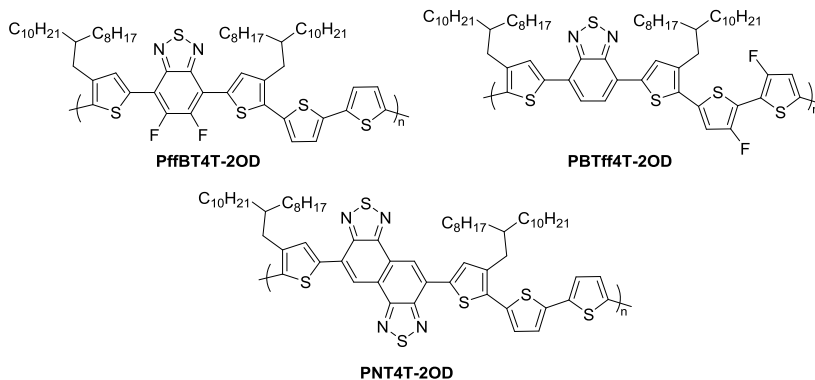
Figure 5. Three cases of >10% PCE oligothiophene based polymers.[37]
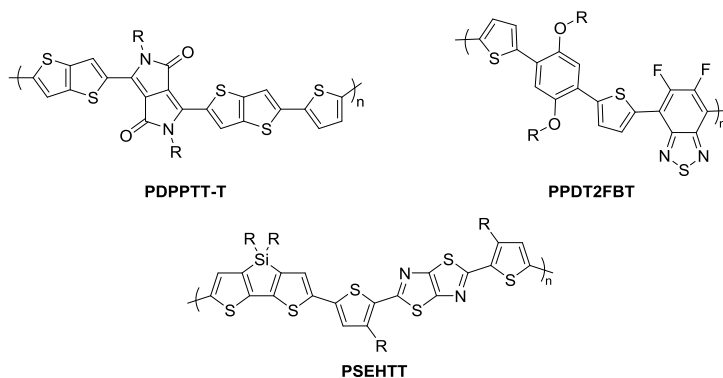
Figure 6. A few examples of >8% PCE low bandgap polymers from the third category (R = alkyl).[29]

The third class gathers all other low bandgap polymers with a OPV performance above 8%. As different building blocks are used for these polymers, an elaboration on the origin of their individual high performance will not be given at this point. A few examples affording efficiencies ranging from 8.1 to 9.4 % are shown in Figure 10.

1.6 OPV applications

One of the main questions which always rises in material research is if it will turn out to be an economically viable technology. In 2004, Brabec proposed three pillars to which OPV has to answer to become a competitive player on the PV market: cost, efficiency and stability.[19] A fourth pillar, based on the synthetic complexity of the material, was added in 2015 by Pelligrino *et al*.[41] Even if the materials can be produced with a low cost and high efficiency, a lack of long term stability diminishes the attractiveness for industrial applications. In order for OPV to make a competitive market entrance, all of these aspects need to be addressed. Within the field, there is a common consensus that OPV will not be able to replace the widely applied silicon solar panels. This statement does, however, not imply that OPV has little market value. OPV has a large number of appealing properties, such as an intrinsic low material cost, aesthetic attractiveness, flexibility and low weight. Especially its flexibility and low weight allow OPV to be applied on surfaces which are not accessible for conventional PV technologies.
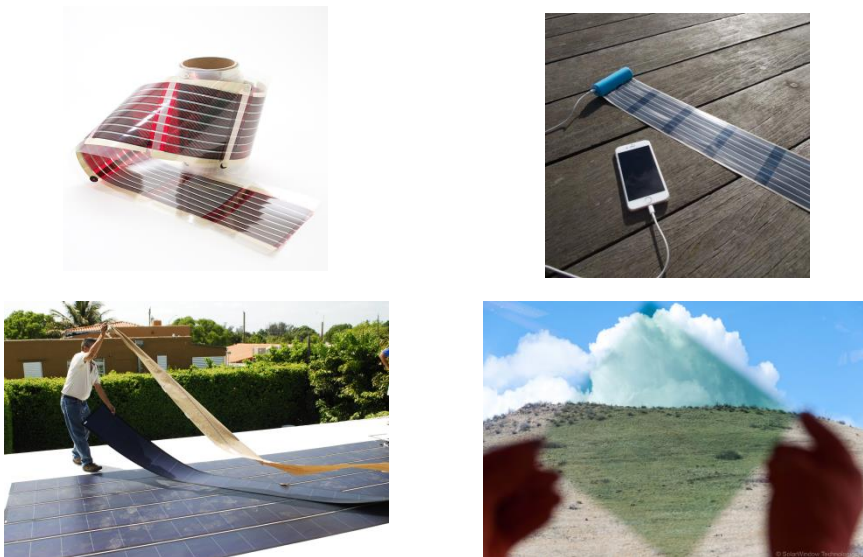
Figure 7. Multiple applications showing the diverse applicability of OPVs. Reproduced with permission, copyright InfinityPV, Uni-Solar Ovonic and SolarWindow Technologies.[42–45]

The organic solar cells can be adapted to e.g. tents, canopies, clothing, lamella, backpacks, etc., and thereby a wide niche market can be addressed (Figure 11). OPV also has the capability to work properly in diffuse light and can therefore be applied in places where no perpendicular sunlight is accessible. As OPV has a low production and transportation cost, it is also a very suitable technology for

providing electricity in third world countries. These low costs identify OPV as a PV technology for everyone.

1.7 Continuous flow chemistry

The chemical industry is constantly developing new technologies to increase the ease of syntheses and their up-scaling, driven by the urge to decrease production costs. In the past decade, continuous flow chemistry has emerged as a powerful complementary material production technique, partly satisfying the general trend for faster, cheaper and cleaner.[46–50] Many chemical companies (in particular the pharmaceutical ones and material providers) have been exploring the potential of flow methods and have implemented them in their research and production facilities, as a lot of processes can strongly benefit from (micro/milli)flow reactor technology.

It has been stated that 40–60% of all organic reactions may profit from flow conditions.[48] Among the major advantages of flow technologies are faster and safer reactions (smaller intrinsic reaction volumes), quick reaction optimization, easy scale-up, high reproducibility, reduced waste production and lower (energy/solvent) costs. Continuous flow procedures can lead to higher selectivities, improved yields and increased purities of the desired products as contact times can be precisely controlled. The use of flow technology can speed up material development and up-scaling in an efficient way. Reagents are continuously pumped into the flow reactor, resulting in a constant stream of product leaving the system. In small scale continuous (micro)flow experiments, reaction conditions (T, p, residence time, reactor type, reactant stoichiometry) can accurately be controlled and easily be adjusted.

The optimal conditions obtained on a small scale can then easily be transferred to larger scale flow systems without the need for substantial further optimization, in strong contrast to the up-scaling of batch processes. In continuous flow chemistry, the upscaling process is frequently approached by scaling out the reactor instead of scaling up one reactor in size.[51-57] The scaling out process involves parallelization of multiple identical flow setups. The reactor conditions that were found during the screening process can be applied to each system and thereby no re-optimization is required upon increasing the production scale. Moreover, reactions that cannot be carried out by conventional batch (i.e. in-flask) processes sometimes become accessible via continuous flow reactors, as extreme temperatures (with an almost isothermal distribution) and pressures can be applied while (diffusional) mixing and heat transfer are more effective. In addition, toxic, corrosive or explosive reagents which are normally forbidden in industry can become acceptable because of the precise operating conditions and smaller intrinsic reaction volumes in flow. In conclusion, it can be stated that flow systems can close the gap between bench chemistry and chemical engineering by mimicking large-scale production facilities on a

laboratory scale, while providing additional benefits in terms of reaction selectivity, safety, cost and waste production.

Although flow chemistry clearly has many advantages over conventional batch processes, there are some drawbacks as well. On transferring in-flask processes to continuous flow systems, some particular points should be considered. Heterogeneous reactions and reagent and/or (by)product precipitation have to be avoided, as this might block the flow (in particular for microreactors). The same holds for reactions resulting in a large increase in viscosity (e.g. certain polymerizations).
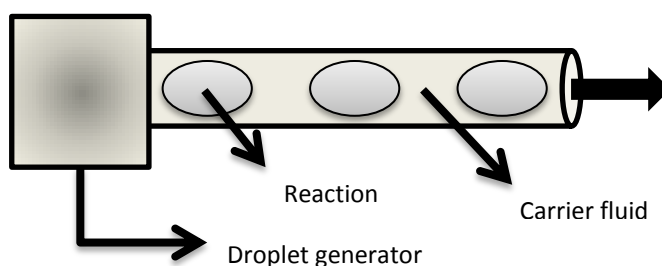
Figure 12. Schematic representation of droplet flow.

For both issues some solutions exist. Reactions which are heterogeneous in the reagents they use, but homogeneous based on the starting and end product, can be conducted by immobilizing the reagents on solid-phase scavengers. These immobilized reagents have the advantage that they do not have to be removed from the reaction mixture afterwards, which simplifies purification and can allow multi-step synthesis without intermediate purification steps. The problem of precipitation of the end product from the reaction mixture as well as the increased viscosity issue can be resolved by the application of droplet-based microfluidics. With this method, the reaction mixture is injected into a continuous stream of a perfluorinated carrier fluid. The perfluorinated solvent will preferentially wet the tubing wall (for tubings derived from teflon) and thereby keeps droplets of the reaction mixture away from the tubing wall (Figure 12). In case of precipitate formation, this will be contained inside the droplet and blockage of the flow reactor can be avoided. For polymerizations, the reaction mixture, for which the viscosity rises with increasing molecular weight, is also kept away from the tubing wall and the overall viscosity inside the flow reactor is only determined by the carrier fluid. Applicability of this method can, however, be limited as even with a proper droplet formation, the reagents might be partially soluble in the perfluorinated solvent.

1.8 Continuous flow chemistry and OPV

In the past decade, OPV research has mainly been focusing on increasing the efficiency and stability of the solar cells, but the aspect of cost has mostly been neglected. OPV has the intrinsic property of being a low-cost PV technology as very thin layers are employed and 'cheap' organic materials are used. Unfortunately, OPV photoactive materials are currently only produced on a very small scale in individual research labs or provided by small and medium-sized enterprises (SME's) on an on-demand basis. This lack of a common materials source results in considerable batch-to-batch variations, in turn impacting ink formulation, device processing and the final photovoltaic parameters,[58] which substantially complicates comparison and benchmarking. Due to this lack of a large scale synthesis process and the insufficient reproducibility of the current methods, OPV is by far not as cheap as it is projected. The development of effective and scalable polymer synthesis processes i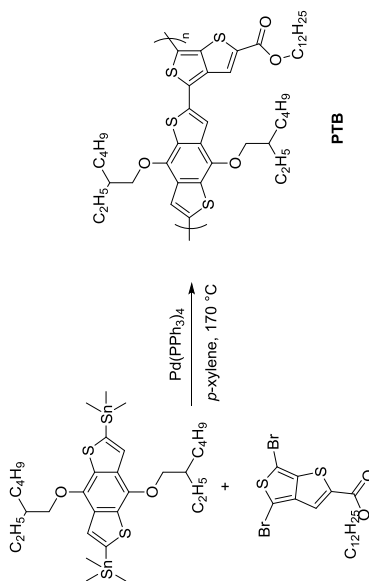s therefore crucial toward economic success.[59] As pointed out in the previous section, continuous flow chemistry has several advantages over conventional batch chemistry. As it is easily scalable and has a very high control over the reaction conditions, it is an interesting technology for large scale OPV material production with reproducible properties.

The initial start of the use of continuous flow chemistry for the synthesis of conjugated polymers dates back to 2012, with a first report from Wong and coworkers.[60] Three polymerization methods, applied for OPV benchmark materials, were translated from batch to flow. The first one is the generally applied Suzuki polycondensation reaction, which involves the palladium catalyzed cross-coupling between a bromoaryl compound and an aryl boronic acid. Both for the homopolymer PFO and the copolymer PCDHTBT (Scheme 1a), the flow based Suzuki polycondensation afforded similar molecular weights and slightly higher yields than the batch process. Most of the current OPV high-performance donor polymers are synthesized by Stille polycondensations, involving the palladium catalysed cross-coupling reaction between a brominated and a stannylated hetero(aryl) monomer. Wong and coworkers also investigated the Stille polycondensation in flow of the popular benzodithiophene based polymer PTB. The flow polymerization, conducted at a temperature of 170 °C, again delivered similar molecular weights as the batch polymerization process, but with a slightly lower polydispersity (Scheme 1b). Finally, the translation from batch to flow was also established for the Gilch polymerization process. This method was applied for synthesizing MEH-PPV (Scheme 1c), one of the first generation OPV materials. Conduction of the polymerization in flow afforded slightly lower molecular weights than the batch process, but this was mainly attributed to the lower concentration used.Higher molecular weights for MEH-PPV were not envisaged as this would lead to a strong viscosity increase, which can cause blockage of the reactor.

a) Suzuki polycondensation

PFO

PCDHTBT

Pd(PPh₃)₄
Et₄NOH (aq.)
toluene, 90 °C

Pd(PPh₃)₄
Et₄NOH (aq.)
toluene, 90 °C

b) Stille polycondensation

PTB

Pd(PPh₃)₄
p-xylene, 170 °C

c) Gilch polymerization

MEH-PPV

Initiator

KOtBu
THF, 25 °C
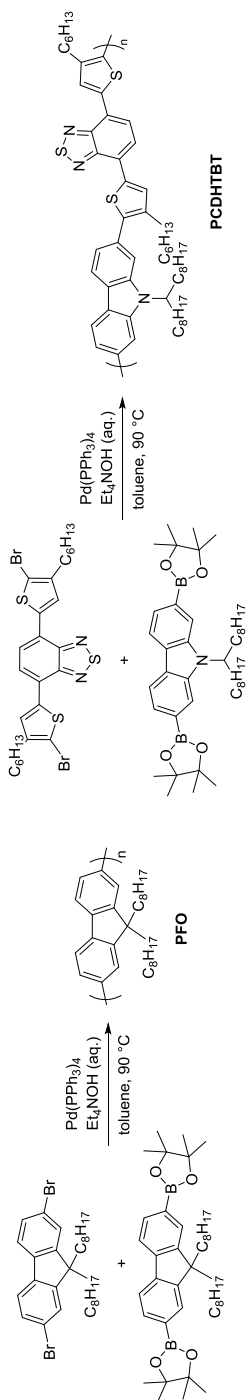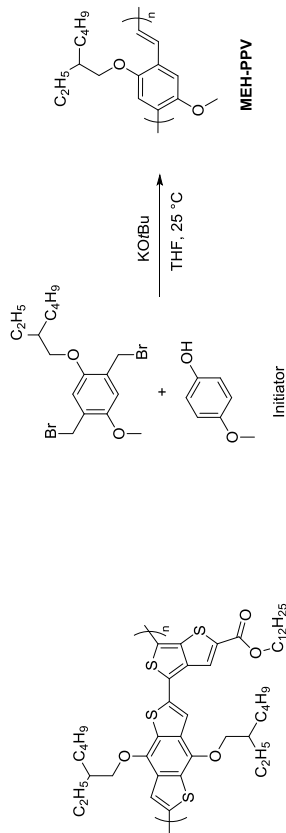
Scheme 1. Multiple polycondensation reactions which were translated from batch to flow by Wong et al.[60]

In summary, three polymerization methods were efficiently transferred from batch to flow, delivering similar molecular weights. The main additional advantages of the flow based protocols are the easily scalable character and a significantly reduced reaction time.

In 2013, two reports were published on the flow synthesis of the widely studied P3HT. Both flow polymerization processes employed an adaptation of the batch Kumada catalyst transfer polymerization (KCTP) route from McCullough et al.[61] The first publication by Wong et al. nicely demonstrated that P3HT can be successfully synthesized with a benchtop commercially available flow reactor, delivering molecular weights up to 41 kg/mol and with a similar regioselectivity as conventional batch protocols.[62] Precise control over the polymerization could simply be achieved by the adjustment of the monomer and initiator feed rate. Rather than using a single phase flow reactor, De Mello et al. utilized a droplet-based flow reactor.[53] As outlined in the previous section, the carrier fluid keeps the droplets, containing the reaction mixture, away from the tubing wall and therefore greatly diminishes the chance of reactor blockage due to precipitation or viscosity increases. Besides looking at a single flow reactor, the authors also developed a five-channel flow reactor (Figure 13), which nicely demonstrates the effectiveness of scaling out for continuous flow reactors. P3HT was successfully synthesized with molecular weights up to 92 kg/mol, a regioregularity above 98% and a daily production rate up to 60 gram.
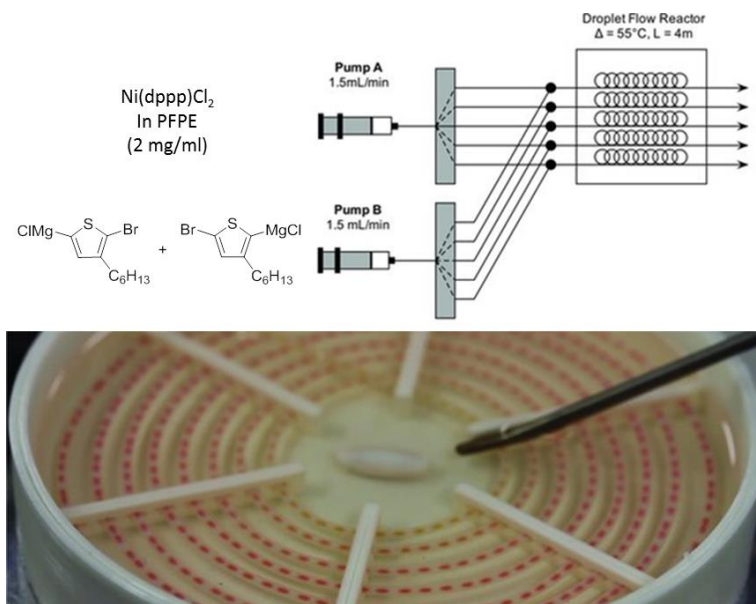
Figure 13. Scaling out the droplet-based flow polymerization using a passive-flow divider. Reproduced with permission (copyright John Wiley and Sons).[53]

The ease of upscaling with continuous flow chemistry was also reported in 2015 by Krebs and coworkers.[63] The large scale synthesis (10 g) of PBDTTTz-4 by Stille polycondensation was achieved with a custom made flow setup consisting of a high performance liquid chromatography (HPLC) pump and a pressurized 40 mL coiled stainless steel reactor. The reaction was performed in o-xylene at 200 °C with Pd_2dba_3/P(o-tol)$_3$ as the catalytic system. With a residence time of approximately 10 minutes, a molecular weight of 16 kg/mol was achieved, which delivered an average device performance of 3.7% with roll-to-roll (R2R) printing technology.

The applicability of continuous flow chemistry for the synthesis of conjugated polymers was further expanded by Wong and Leclerc.[64] Their report involved the use of Direct (Hetero)Arylation Polymerization (DHAP) in flow for the synthesis of PiIEDOT (Scheme 2). DHAP has received increased attention as it avoids the use of toxic chemicals for the generation of intermediates (unlike the tin-based stannylated compounds that are used for conventional Stille cross-coupling).[65–67] DHAP was established by pumping the monomers and the soluble catalyst through a solid-phase reactor which was charged with cesium carbonate and pivalic acid. Molecular weights up to 42 kg/mol were achieved. Although the molecular weight was significantly lower than in batch, the flow-synthesized polymer delivered a similar (low) performance in organic solar cells (1.8%).
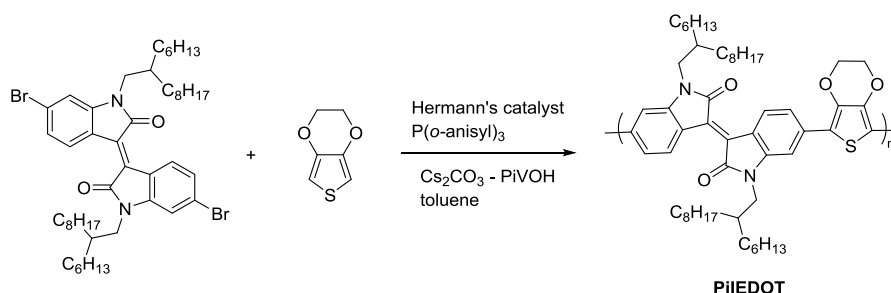
Scheme 2. Direct (Hetero)Arylation Polymerization of isoindigo and 3,4-ethylenedioxythiophene.[64]

Continuous flow chemistry for the synthesis of conjugated polymers might be a relatively new field, but it has already proven to be a successful complementary technique to the conventional batch methods. Continuous flow is mainly attractive because of its ease of upscaling, precise control over reagent addition and the accessibility of a wide temperature range, even above the boiling point of the reaction solvent. Reaction conditions can easily be screened as multiple reactions can be performed from the same stock solutions, while temperature, residence time and the stoichiometry of the reaction mixture can be easily adjusted.

1.9 Homocoupling defects

Within OPV research, cross-coupling reactions are frequently used to form carbon-carbon bonds between two different building blocks. Each type of building block bares a different functional group in order to establish selective couplings of the type AB. A commonly observed side reaction is the coupling between two building blocks of the same type, resulting in AA or BB side products, which is referred to as homocoupling. As polymer purification is limited, a strong impact of this synthesis-based defect can be expected in the material properties of the conjugated polymers used for organic electronic applications. Because of the high similarity between the Stille and Suzuki-Miyaura cross-coupling reactions, only the homocoupling pathways for Stille are outlined below. In direct arylation reactions, homocoupling is also frequently observed for either the arylhalogen compound or the C-H activated aryl.[68–72] Detailed mechanistic studies on the origin of the homocoupling defects in direct arylations are still to be published, but are presumable similar to Stille and Suzuki-Miyaura reactions.[68]

The homocoupling side reaction can occur either for the organostannane (or organoboron for Suzuki-Miyaura) or the organohalide reaction partner. These side reactions originate from reaction pathways competing with the desired cross-coupling cycle. The presence of oxidative impurities can induce oxidation of Pd(0) to Pd(II). These oxidized palladium species will reduce themselves again to Pd(0) by a double transmetallation step with the aryltin species, which is subsequently followed by a reductive elimination step yielding a homocoupled biaryl species (Scheme 3). Within their laboratories, experimental scientists try to conduct the Stille cross-coupling reactions very carefully under nitrogen or argon atmosphere to avoid the presence of these oxidizing impurities, in order to inhibit this pathway. Even when the reaction is hypothetically conducted free of oxidizing impurities, homocoupling can still be observed. The origin of this effect can be found in one of the homocoupling pathways of the arylhalogen species. After the oxidative addition step, the Ar-Pd(II)-Br species can undergo an aryl group exchange with another palladium aryl species instead of undergoing the transmetallation step with the aryltin compound (Scheme 3).[73–76] A disproportionation step will then yield the homocoupled arylhalogen species, a regenerated Pd(0) entity and a Pd(II) species. It is this generation of the Pd(II) species which opens up the above described homocoupling pathway of the aryltin species. Whenever the reaction system is forming homocoupled arylhalogen derivatives via this route, this will inevitably lead to the formation of homocoupled aryl tin species too.
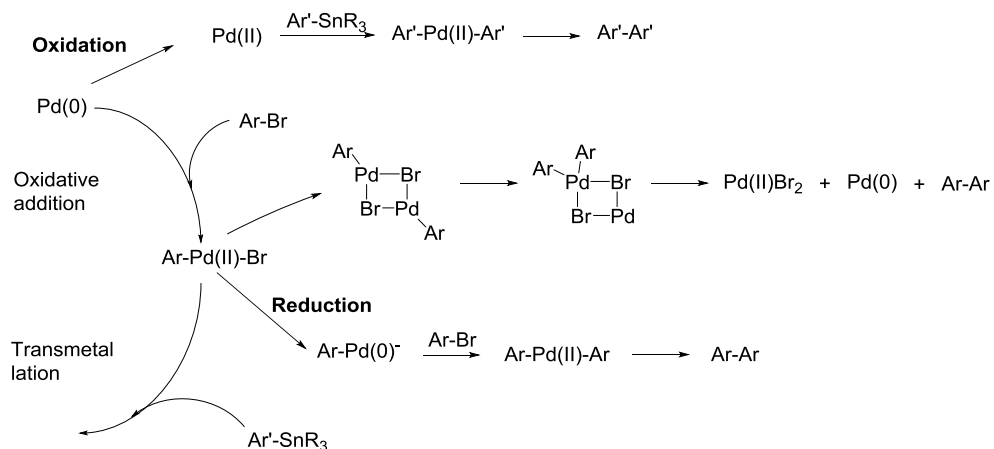
Scheme 3. Additional pathways in palladium catalyzed cross-coupling reactions leading to homocoupling.[68]

Another possible pathway for the generation of arylhalogen homocoupling occurs when there are reducing impurities present in the reaction mixture. These reducing agents will reduce Ar-Pd(II)-Br complexes to Ar-Pd(0)⁻, which will undergo oxidative addition of another arylhalogen species. The Ar-Pd(II)-Ar complex will then undergo reductive elimination, forming the homocoupled Ar-Ar species and regeneration of Pd(0).[77]

Although homocoupling defects are a widespread phenomenon, there are only a limited number of reports on its effect on the photovoltaic performance of organic solar cells. One of the first reports which specifically focussed on homocoupling defects was published by Janssen *et al.* in 2014.[78] By synthesizing PDPPTPT under different conditions, they identified that the homocoupling side reaction can largely be suppressed, but unfortunately not completely, by choosing the optimal palladium to ligand ratio. The presence of homocoupling defects of the polymer donor unit caused a red-shift in the absorption spectrum. It was further emphasized that homocoupling defects can lead to low-lying energy trap sites and effectively increase the HOMO level and decrease the LUMO level of the polymer. The main effects on the solar cell parameters were identified as a decrease in photocurrent and a significantly lower PCE.

Another polymer investigated for homocoupling defects is the popular PTB7 (Figure 8). Vangerven *et al*. investigated several commercial batches of PTB7 by Gel Permeation Chromatography (GPC) and Matrix Assisted Laser Desorption Ionisation mass spectrometry (MALDI).[79] The lower molecular weight batches clearly showed a bimodal molecular weight distribution. Analysis by MALDI revealed that homocoupling occurs for both the brominated and stannylated monomer (Figure 14). Similar to what was observed by Janssen *et al*.,

homocoupling caused a clear red-shift in the absorption spectra. The large differences in the PCE's of the different samples was mainly caused by a strong fluctuation in the short-circuit current and the FF. Besides altering the HOMO and LUMO levels of the polymer, homocoupling can also cause changes in the aggregation behaviour of the polymer upon film formation. As outlined before, an optimal morphology is highly important for achieving high efficiencies.

Also in 2015, Yu *et al*. reported the same effects of homocoupling on the performance of PTB7.[80] Additionally, it was identified that homocoupling leads to increased bimolecular recombination within the solar cells. Similar to Janssen *et al.*, increased trap-assisted recombination due to the presence of homocoupling was reported.
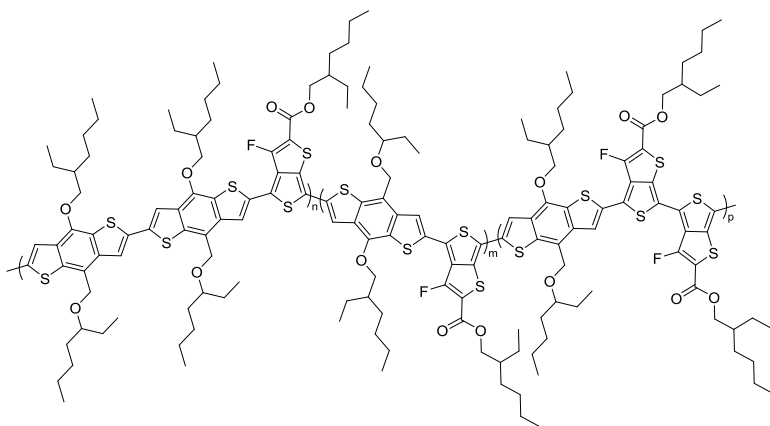
Figure 8. Example of the structure of PTB7 with homocoupling defects in both the BDT donor unit and the TT acceptor unit.[79]

Although the reports are limited, the presence of homocoupling in the donor polymer clearly has a strong influence on the photovoltaic performance. Characterization of the effect of homocoupling remains, however, a difficult task as it does not influence one parameter solely and the extent to which homocoupling occurs can differ from batch to batch. It also remains difficult to precisely quantify the specific amount of homocoupling that is present in the donor polymer. Therefore, there is a need to further analyse the effects of homocoupling, preferentially for cases which allow proper characterization of the extent of homocoupling.

1.10 Thesis outline

As stated above, for OPV to become an economically viable technology, certain requirements have to be fulfilled. Great steps have been taken with respect to solar cell efficiency and stability, but there is still a missing platform for OPV material production on a large scale and with reproducible properties. Continuous flow chemistry has a great potential for providing a synthesis method that is applicable on a small scale for reproducible properties and can easily be transformed into a large production tool without significant alteration of the reaction conditions.

The main goal of this thesis was thus to implement continuous flow chemistry in OPV research for the production of low bandgap conjugated polymers in a reproducible way and affording straightforward upscaling. The next chapter focusses on the use of different continuous flow technology methods for the synthesis of monomers, in order to demonstrate the wide versatility of this synthesis technique. The subsequent two chapters then deal with the actual production of device-grade donor polymers by continuous flow. Reproducibility, scalability and the influence of different flow parameters are assessed. The final chapter focusses on the influence of the extent of homocoupling defects along the polymer chain on the photovoltaic performance. The presence of homocoupling greatly affects the reproducibility of OPV donor polymers and it is therefore important that this effect is thoroughly investigated.

Chapter 2: In order to address the issue of a limited material availability, it is important to evaluate the entire synthesis process from the monomer building blocks up to the polymer formation. As monomer synthesis requires several different reaction steps with different reagents, it is a good starting point to demonstrate the power and versatility of continuous flow chemistry to the OPV research community. The isoindigo building block, which has been frequently used in OPV research, forms a suitable candidate to evaluate the transformation process from a batch to flow procedure. The synthetic pathways toward isoindigo, symmetrically or asymmetrically substituted, generally consists of three different reactions: an alkylation, a reduction and a condensation step. All reactions are translated from batch to flow by making use of the modular Syrris Asia flow system employing glass chip reactors, PFA tubular reactors and a solid-phase reactor.

Chapter 3: During monomer preparation several different purification steps can be implemented. For the final product, the conjugated polymer used as a component of the active layer, purification is rather difficult. Therefore the final polymerization reaction itself is highly important, as the efficiency of the reaction determines the properties of the product. For conventional batch reactions, batch-to-batch variations are often seen and scalability is an issue. Therefore, this chapter focusses on the evaluation of a continuous flow based polymerization, for which the high-performance donor polymer PBDTTPD is

used. The reproducibility of the material quality is evaluated by comparing the photovoltaic performances of materials synthesized in different flow experiments and fractionating the output of the continuous flow setup to evaluate if production by flow can truly deliver a constant stream of device-grade polymer material. In a final step, the flow protocol is scaled up by continuous operation for 8 hours, yielding 1.5 grams of material with a similar OPV performance as achieved in the small scale experiments.

Chapter 4: With an established scalable flow protocol for Stille polycondensations, yielding polymers with highly reproducible properties, the next step consists of an evaluation of the tunability of this process. A flow protocol on a custom made continuous flow setup is formulated for one of the best performing polymers in the field, PffBT4T-2OD, yielding solar cell efficiencies >10%. The influence of different reaction parameters during the flow synthesis is evaluated, with a specific attention for the influence on the final molecular weight of the polymer. The performance of PffBT4T-2OD in organic solar cells is strongly dependent on the molecular weight as this greatly influences the aggregation behaviour during film formation. The main parameters under investigation are temperature, concentration, injection volume and residence time. The photovoltaic performance of the flow synthesized polymer is compared to PffBT4T-2OD from commercial sources.

Chapter 5: Previous chapters focused on the technological aspect of the synthesis. However, there are also other factors which can influence the reproducibility. One of them is the occurrence of homocoupling along the polymer chain, formed by an undesired side reaction of the Stille cross-coupling. Although it is commonly known that this side reaction occurs, little is known about its actual effect on the photovoltaic performance and it is rather difficult to detect it. Therefore, this final chapter focusses on the influence of homocoupling on the photovoltaic performance of the highly soluble PDTSQx$_{ff}$ polymer, allowing careful characterization. A deliberately homocoupled acceptor monomer is synthesized and different percentages of this material are added during the polymerization reaction, yielding a series of PDTSQx$_{ff}$ polymers with a homocoupling percentage of 0, 5, 25, 50, 75 and 100%. Successful built-in of the deliberately homocoupled monomer is verified by GPC, NMR and MALDI-TOF analysis. The influence of homocoupling on the physical properties of the polymers is evaluated by performing UV-VIS and CV measurements and testing their performance in organic solar cells.

To end, a general summary of the thesis is presented and the research is put in a broader context to clarify its impact on the field of organic photovoltaics, also providing a vision on the future use of continuous flow chemistry.

1.11 References

(1)   United Nations: Department of Economic and Social affairs; https://esa.un.org/unpd/wpp/ (accessed May 16, 2017).

(2)   R. Perez, M. Perez, *SHC Solar Update* **2009**, 50, 2.

(3)   C. Philibert, *IEA* **2005**, 1.

(4)   IEA. *SHC Solar Update* **2015**, 4.

(5)   A. Jäger-waldau, *PV Status Report* October 2016.

(6)   D. M. Chapin, C. S. Fuller, G. L. Pearson, *J. Appl. Phys.* **1954**, 25, 676.

(7)   National Renewable Energy Laboratory (NREL);

        https://www.energy.gov/eere/sunshot/photovoltaics-research-and-development (accessed May 17, 2017).

(8)   W. Zhao, S. Li, H. Yao, S. Zhang, Y. Zhang, B. Yang, J. Hou, *J. Am. Chem. Soc.* **2017**, 139, 7148.

(9)   M. Saliba, T. Matsui, J.-Y. Seo, K. Domanski, J.-B. Correa-Baena, M. Khaja Nazeeruddin, S. M. Zakeeruddin, W. Tress, A. Antonio, A. Hagfelt, M. Grätzel, *Energy Environ. Sci.* **2016**, 9, 1989.

(10)   H. Shirakawa, E. J. Louis, A. G. MacDiarmid, C. K. Chiang, A. J. Heeger, *J. Chem. Soc. Chem. Commun.* **1977**, 578.

(11)   C. K. Chiang, C. R. Fischer, Y. W. Park, A. J. Heeger, H. Shirakawa, E. J. Louis, S. C. Gau, A. G. MacDiarmid, *Phys. Rev. Lett.* **1977**, 39, 1098.

(12)   H. Shirakawa, *Nobel Lecture Chemistry* 1996-2000; 2003.

(13)   C. W. Tang, *Appl. Phys. Lett.* **1986**, 48, 183.

(14)   N. S. Sariciftci, L. Smilowitz, A. J. Heeger, F. Wudl, *Science* **1992**, 258, 1474.

(15)   R. Kroon, M. Lenes, J. C. Hummelen, P. W. M. Blom, B de Boer., *Polym. Rev.* **2008**, 48, 531.

(16)   F.Wudl, *Acc. Chem. Res.* **1992**, 25, 15716.

(17)   J. C. Hummelen, B. W. Knight, F. Lepeq, F. Wudl, J. Yao, C. L. Wilkins, *J. Org. Chem.* **1995**, 60, 532.

(18)   Thomson Reuters; http://webofscience.com (accessed May 17, 2017).

(19)   C. J. Brabec, *Sol. Energy Mater. Sol. Cells* **2004**, 83, 273.

(20)   J. Xue, *Polym. Rev.* **2010**, 50, 411.

(21)   M. Helgesen, R. Sondergaard, F. C. Krebs, *J. Mater. Chem.* **2010**, 20, 36.

(22)   P.-L. T. Boudreault, A. Najari, M. Leclerc, *Chem. Mater.* **2011**, 23, 456.

(23)   A. Hübler, B. Trnovec, T. Zillger, M. Ali, N. Wetzold, M. Mingebach, A. Wagenpfahl, C. Deibel, V. Dyakonov, *Adv. Energy Mater.* **2011**, 1, 1018.

(24) J.-L. Brédas, J. E. Norton, J. Cornil, V. Coropceanu, *Acc. Chem. Res.* **2009**, 42, 1691.

(25) C. J. Brabec, A. Cravino, D. Meissner, N. S. Sariciftci, T. Fromherz, L. Sanchez, J. C. Hummelen, *Adv. Funct. Mater.* **2001**, 11, 374.

(26) M. C. Scharber, D. Mülbacher, M. Koppe, P. Denk, C. Waldauf, A. J. Heeger, C. J. Brabec, *Adv. Mater.* **2006**, 18, 789.

(27) B. W. Ma, C. Yang, X. Gong, K. Lee, A. J. Heeger, *Adv. Funct. Mater.* **2005**, 15, 1617.

(28) W. Ma, J. R. Tumbleston, M. Wang, E. Gann, F. Huang, H. Ade, *Adv. Energy Mater.* **2013**, 3, 864.

(29) S. Holliday, Y. Li, C. K. Luscombe, *Prog. Polym. Sci.* **2017**, DOI: 10.1016/j.progpolymsci.2017.03.0.

(30) L. Lu, L. Yu, *Adv. Mater.* **2014**, 26, 4413.

(31) H. Yao, L. Ye, L. Zhang, J. Hou, *Chem. Rev.* **2016**, 116, 7397.

(32) S. Zhang, L. Ye, J. Hou, *Adv. Energy Mater.* **2016**, 6, 1502529.

(33) C. Cabanetos, A. El Labban, J. A. Bartelt, J. D. Douglas, W. R. Mateker, J. M. J. Fréchet, M. D. McGehee, P. M. Beaujuge, *J. Am. Chem. Soc.* **2013**, 135, 4656.

(34) B. Y. Liang, Z. Xu, J. Xia, S. Tsai, Y. Wu, G. Li, C. Ray, L. Yu, *Adv. Energy Mater.* **2010**, 22, 135.

(35) Z. He, C. Zhong, S. Su, M. Xu, H. Wu, Y. Cao, *Nat. Photonics* **2012**, 6, 593.

(36) S. Nam, J. Seo, S. Woo, W. H. Kim, H. Kim, D. D. C. Bradley, Y. Kim, *Nat. Commun.* **2015**, 6, 8929.

(37) Y. Liu, J. Zhao, Z. Li, C. Mu, W. Ma, H. Hu, K. Jiang, H. Lin, H. Ade, H. Yan, *Nat. Commun.* **2014**, 5, 5293.

(38) Z. Chen, P. Cai, J. Chen, X. Liu, L. Zhang, L. Lan, J. Peng, Y. Ma, Y. Cao, *Adv. Mater.* **2014**, 26, 2586.

(39) I. Osaka, M. Shimawaki, H. Mori, I. Doi, E. Miyazaki, T. Koganezawa, K. Takimiya, *J. Am. Chem. Soc.* **2012**, 134, 3498.

(40) Y. Wang, X. Xin, Y. Lu, T. Xiao, X. Xu, N. Zhao, X. Hu, S. Ong, S. C. Ng, *Macromolecules* **2013**, 46, 9587.

(41) R. Po, G. Bianchi, C. Carbonera, A. Pellegrino, *Macromolecules* **2015**, 48, 453.

(42) InfinityPV; https://infinitypv.com/ (accessed May 19, 2017).

(43) Ken Fields - Uni-Solar Ovonic; https://commons.wikimedia.org/wiki/File:Thin_Film_Flexible_Solar_PV_Installation_2.JPG (accessed August 25, 2017).

(44) K. Walker, *AZO Cleantech* **2016**, 580.

(45) SolarWindow Technologies Inc.; https://solarwindow.com/technology/ (accessed August 28, 2017).

(46) G. Jas, A. Kirschning, *Chem. Eur. J.* **2003**, 9, 5708.

(47) P. Watts, S.J. Haswell, *Chem. Soc. Rev.* **2005**, 34, 235.

(48) T. R. Dietrich, Microchemical Engineering in Practice; John Wiley & Sons, Inc., 2009.

(49) C. Wiles, P. Watts, *Green Chem.* **2012**, 14, 38.

(50) S. G. Newman, K. F. Jensen, *Green Chem.* **2013**, 15, 1456.

(51) F. Ullah, T. Samarakoon, A. Rolfe, R. D. Kurtz, P. R. Hanson, M. G. Organ, *Chem. Eur. J.* **2010**, 16, 10959.

(52) N. Jongen, M. Donnet, P. Bowen, J. Lemaître, H. Hofmann, R. Schenk, C. Hofmann, M. Aoun-Habbache, S. Guillemet-Fritsch, J. Sarrias, A. Rousset, M. Viviani, M. T. Buscaglia, V. Buscaglia, P. Nanni, A. Testino, J. R. Herguijuela, *Chem. Eng. Technol.* **2003**, 26, 303.

(53) J. H. Bannock, S. H. Krishnadasan, A. M. Nightingale, C. P. Yau, K. Khaw, D. Burkitt, J. J. M. Halls, M. Heeney, J. C. De Mello, *Adv. Funct. Mater.* **2013**, 23, 2123.

(54) P. Styring, A. I. R. Parracho, *Beilstein J. Org. Chem.* **2009**, 5, 29.

(55) P. V. Snytnikov, D. I. Potemkin, E. V. Rebrov, V. A. Sobyanin, V. Hessel, J. C. Schouten, *Chem. Eng. J.* **2010**, 160, 923.

(56) J. D. Moseley, E. K. Woodman, *Org. Process Res. Dev.* **2008**, 12, 967.

(57) P. Löb, H. Löwe, V. Hessel, *J. Fluor. Chem.* **2004**, 125, 1677.

(58) T. Vangerven, P. Verstappen, N. Patil, J. D'Haen, I. Cardinaletti, J. Benduhn, N. Van den Brande, M. Defour, V. Lemaur, D. Beljonne, R. Lazzaroni, B. Champagne, K. Vandewal, J. W. Andreasen, P. Adriaensens, D. W. Breiby, B. Van Mele, D. Vanderzande, W. Maes, J. Manca, *Chem. Mater.* **2016**, 28, 9088.

(59) S. Lizin, S. Van Passel, E. De Schepper, W. Maes, L. Lutsen, J. Manca, D. Vanderzande, *Energy Environ. Sci.* **2013**, 6, 3136.

(60) H. Seyler, D. J. Jones, A. B. Holmes, W. W. H. Wong, *Chem. Commun.* **2012**, 48, 1598.

(61) B. R. S. Loewe, S. M. Khersonsky, R. D. McCullough, *Adv. Mater.* **1999**, 11, 250.

(62) H. Seyler, J. Subbiah, D. J. Jones, A. B. Holmes, W. W. H. Wong, *Beilstein J. Org. Chem.* **2013**, 9, 1492.

(63) M. Helgesen, J. E. Carlé, G. A. dos Reis Benatto, R. R. Søndergaard, M. Jørgensen, E. Bundgaard, F. C. Krebs, *Adv. Energy Mater.* **2015**, 5, 1401996.

(64) F. Grenier, B. R. Aich, Y. Lai, M. Guérette, A. B. Holmes, Y. Tao, W. W. H. Wong, Leclerc, M. *Chem. Mater.* **2015**, 27, 2137.

(65) L. Ackermann, *Chem. Rev.* **2011**, 111, 1315.

(66) J.-R. Pouliot, F. Grenier, J. T. Blaskovits, S. Beaupré, M. Leclerc, *Chem. Rev.* **2016**, 116, 14225.

(67) T. W. Lyons, M. S. Sanford, *Chem. Rev.* **2010**, 110, 1147.

(68) A. E. Rudenko, B. C. Thompson, *J. Polym. Sci. Part A Polym. Chem.* **2015**, 53, 135.

(69) M. Wakioka, Y. Nakamura, M. Montgomery, F. Ozawa, *Organometallics* **2015**, 34, 198.

(70) E. Iizuka, M. Wakioka, F. Ozawa, *Macromolecules* **2016**, 49, 3310.

(71) F. Lombeck, H. Komber, S. I. Gorelsky, M. Sommer, *ACS Macro Lett.* **2014**, 3, 819.

(72) S. Kowalski, S. Allard, U. Scherf, *Macromol. Rapid Commun.* **2015**, 36, 1061.

(73) V. V. Grushin, W. J. Marshall, *J. Am. Chem. Soc.* **2009**, 131, 918.

(74) T. Yagyu, M. Hamada, K. Osakada, T. Yamamoto, *Organometallics* **2001**, 20, 1087.

(75) M. S. Remy, T. R. Cundari, M. S. Sanford, *Organometallics* **2010**, 29, 1522.

(76) Y. Suzaki, K. Osakada, *Organometallics* **2003**, 22, 2193.

(77) V. Calò, A. Nacci, A. Monopoli, P. Cotugno, *Chem. Eur. J.* **2009**, 15, 1272.

(78) K. H. Hendriks, W. Li, G. H. L. Heintges, G. W. P. Van Pruissen, M. M. Wienk, R. A. J. Janssen, *J. Am. Chem. Soc.* **2014**, 136, 11128.

(79) T. Vangerven, P. Verstappen, J. Drijkoningen, W. Dierckx, S. Himmelberger, A. Salleo, D. Vanderzande, W. Maes, J. Manca, *Chem. Mater.* **2015**, 27, 3726.

(80) L. Lu, T. Zheng, T. Xu, D. Zhao, L. Yu, *Chem. Mater.* **2015**, 27, 537.

Chapter 2

Synthesis of
N,N'-dialkyl-6,6'-dibromoisoindigo
derivatives by continuous flow
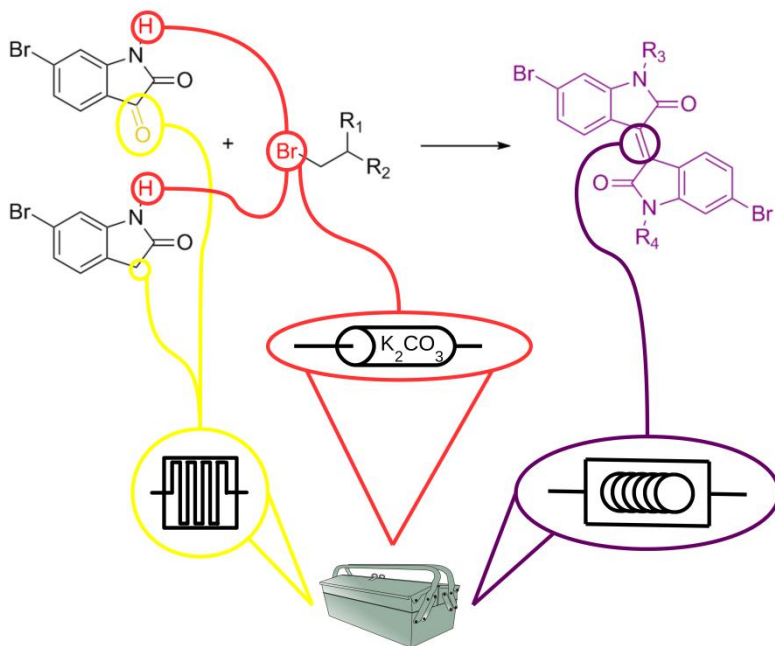
Abstract

In this work, the synthesis of N,N'-dialkyl-6,6'-dibromoisoindigo derivatives by continuous flow chemistry is explored as a means to enhance material availability and structural diversity, in particular toward the application of isoindigo-based semiconductors in high-performance organic photovoltaic devices. The individual steps in the conventional batch synthesis protocol are evaluated and, when needed, adapted to flow reactors. To overcome the low solubility of non-alkylated 6,6'-dibromoisoindigo in common organic solvents, the flow condensation reaction between the 6-bromo-isatin and 6-bromo-oxindole precursors is evaluated in polar aprotic solvents. Dialkylation of 6,6'-dibromoisoindigo is readily performed in flow using a solid-phase reactor packed with potassium carbonate. In an alternative strategy, solubility is ensured by first introducing the N-alkyl side chains on 6-bromo-isatin and 6-bromo-oxindole (accessible via a high-yielding flow reduction of alkylated 6-bromo-isatin), followed by condensation using the conventional method in acetic/hydrochloric acid medium. The N,N'-dialkylated 6,6'-dibromoisoindigo derivatives indeed show enhanced solubility in the hot reaction mixture compared to the non-alkylated material, but eventually precipitate when the reaction mixture is cooled down. Nevertheless, the condensation between both alkylated starting materials is achieved in flow without any blockages by keeping the outlet from the reactor heated and as short as possible. The latter strategy allows the preparation of both symmetrically and asymmetrically N-substituted isoindigo compounds.

Contribution to the publication

Minor part of the batch and flow experiments for completion of the manuscript, manuscript corrections, final formatting and revision of the manuscript.

2.1 Introduction

Over the last decades, multiple types of solar cell technologies have been developed to aid to renewable energy production. Among those, the class of organic photovoltaics (OPV) has particular advantages in terms of aesthetics, flexibility and cost, and mainly aims at portable or wearable consumer goods and building/automotive integration.[1–5] OPV device efficiencies have recently made a huge leap forward, reaching ~10% for polymer and small molecule based solution-processed bulk (single) heterojunction devices.[6–17] Nevertheless, some issues concerning cost, efficiency and reliability still need to be resolved for OPV to become an economically viable technology. There is an obvious need for improved material availability with a low production cost, in high quality and, most importantly, with reproducible properties, for example toward device optimization in large area roll-to-roll printing processes.[18] As most of the synthetic processes are nowadays still performed in (academic) research labs, there is a need for reaction optimization and translation from lab to pilot-scale.

The chemical industry is constantly developing new technologies to increase the ease of syntheses and their up-scaling, driven by the urge to decrease production costs and the increased awareness of process safety and environmental impact. Continuous flow chemistry has been developed into a powerful complementary material production technique, partly satisfying the general trend toward faster, cheaper and cleaner processes.[19–23] Many chemical companies, in particular the pharmaceutical ones and material providers, have been exploring the potential of flow methods and have implemented them in their research and production facilities, as a lot of processes can benefit from (micro/milli)flow reactor technology. Among the major advantages of flow technologies are faster and safer reactions (smaller intrinsic reaction volumes), quick reaction screening, easy scale-up, high reproducibility, reduced waste production and lower (energy/solvent) costs. Additionally, continuous flow procedures can also lead to higher reaction selectivities, improved yields and increased purities of the desired products as contact times can be precisely controlled. Based on these intrinsic properties, it has been stated that 40–60% of all organic reactions may profit from flow conditions.[21] Although flow chemistry clearly has many advantages over conventional batch processes, there are some drawbacks as well. On transferring in-flask processes to continuous flow systems, some particular points have to be considered. Heterogeneous reactions and reagent and/or (by)product precipitation have to be avoided whenever possible, as they tend to block the flow (in particular for micro-reactors). The same holds for reactions resulting in a large increase in viscosity (e.g. certain polymerizations).

Continuous flow chemistry can be a versatile tool to close the gap between OPV material discovery and device (processing) optimization by translating and carefully optimizing synthesis protocols for state of the art low bandgap

(precursor) materials from batch-to-flow, in this way paving the way for efficient scalability and low-cost OPV.[24–31] In contrast to the past generations of photoactive (electron donor) conjugated polymer materials, poly(p-phenylene vinylene)s and poly(3-alkylthiophene)s, there is not a single workhorse material anymore that is widely used and studied by all (non-synthetic) researchers active in the domain. Most of the top research groups and industrial players focus on their own home-made materials, which are therefore scarcely available to others.

Isoindigo was already synthesized in 1988, but it took over two decades before it was recognized as a versatile component of OPV materials.[32–34] The isoindigo core contains two fused lactam rings, inducing a strong electron-deficient character and therefore rendering it attractive as an acceptor component in push-pull type organic semiconductors. Nowadays, isoindigo has become a widely applied building block, with over 100 publications on its characteristics and use in polymer and molecular solar cells.[35–41] Power conversion efficiencies (PCE's) of 3.7 and 7.3%, respectively, have been reached for small molecule and polymer solar cells based on photoactive isoindigo-containing light-harvesting materials.[40,41] N-functionalized isoindigo derivatives are typically synthesized via a two-step strategy (Scheme 1).[33] In the first step, an acid-catalyzed condensation reaction between (commercially available) 6-bromo-oxindole (**1**) and 6-bromo-isatin (**2**) is performed, followed by the N-alkylation of the obtained 6,6'-dibromoisoindigo (**3**). During the condensation reaction at elevated temperature (100–120 °C in AcOH/HCl), 6,6'-dibromoisoindigo (**3**) precipitates out of the hot reaction mixture. The subsequent alkylation step uses a barely soluble base (K_2CO_3 in DMF), resulting in a heterogeneous reaction mixture. As such, both steps are difficult to perform in a continuous flow reactor. The synthetic strategy therefore needs some adaptations to allow the use of flow processes. The main issues to deal with are the low solubility of the pristine 6,6'-dibromoisoindigo core in common organic solvents and the use of the inorganic base K_2CO_3. On the other hand, 6,6'-dibromoisoindigo dissolves rather well in polar aprotic solvents such as DMSO and DMF, and the solubility improves drastically by introducing alkyl substituents on the lactam nitrogen atoms. This explorative study follows both approaches toward the desired N,N'-dialkyl-6,6'-dibromoisoindigo derivatives.
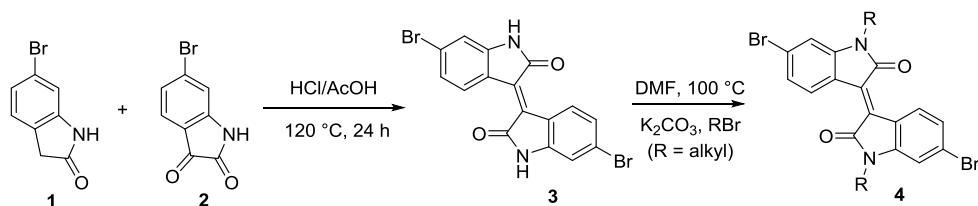
Scheme 1. Conventional batch procedure for the synthesis of N,N´-dialkylated-6,6'-dibromoisoindigo derivatives **4**.[33]

2.2 Results and discussion

All continuous flow experiments were conducted on a Syrris Asia 320 system (Figure S1), consisting of a pressurized solvent/reagent input store under N_2 atmosphere, a corrosion resistant dual syringe pump, a heater module with an adaptor for a tubular or glass chip reactor and an adaptor for a solid-phase (SP) reactor, a 5–10 mL PTFE (polytetrafluoroethylene) loop reagent injector, and a corrosion resistant back pressure regulator (BPR). Different synthetic methods toward N,N′-dialkyl-6,6′-dibromoisoindigo derivatives **4** have been evaluated, as outlined in Scheme 2. *Routes A*, *B*, and *C* are based on the idea to improve the solubility of the precursor compounds in the standard solvent used for the condensation reaction, acetic acid (AcOH), by first introducing N-alkyl side chains on the starting materials. *Route D* is motivated by the fact that both starting and end products dissolve well in polar aprotic solvents such as DMF and DMSO, implying that the condensation reaction between non-alkylated 6-Br-isatin and 6-Br-oxindole can be performed in these solvents without precipitation of pristine 6,6′-dibromoisoindigo (**3**).

2.2.1 N-alkylation

We started our explorative study with the N-alkylation reaction, which is required for all synthetic routes depicted in Scheme 2 and is a general reaction to afford solution-processable semiconducting materials. Since the conventional N-alkylation reaction of 6,6′-dibromoisoindigo (**3**) (Scheme 1) uses a heterogeneous base-solvent system, K_2CO_3 in DMF, it was necessary to evaluate this procedure and possibly adapt it to work under continuous flow conditions.

Initially, a wide variety of reaction conditions, in standard batch settings or applying microwave irradiation,[42] has been screened for the N-alkylation of 6-Br-isatin (**2**) (Table S1). The first idea was to change K_2CO_3 by a more soluble organic base. However, none of the conditions examined turned out to be efficacious. All attempts to perform the N-alkylation in a biphasic system in combination with the phase transfer catalyst TBAB (tetrabutylammonium bromide) were not successful either,[43] since this resulted in the opening of the 5-membered ring of the 6-Br-isatin starting compound. The use of the more soluble base KOtBu was screened in THF as well as in 1,4-dioxane, under high dilution conditions (due to the poor solubility of 6-Br-isatin in these solvents). In this case, conversion to the N-alkylated 6-Br-isatin **2a** was only observed when 18-crown-6 was added to the reaction mixture. Dioxane was not a good choice because it resulted in a viscous reaction mixture which is disadvantageous in flow. After all attempts to keep the reaction mixture homogeneous, it turned out that none of the screened conditions actually afforded a good alternative for the classical heterogeneous N-alkylation reaction. Therefore it was decided to stay with K_2CO_3 as the preferred base. The best results in batch were obtained when the reaction was done in the presence of a catalytic amount of KI in acetonitrile at reflux or DMF at temperatures between 130 and 150 °C. These conditions
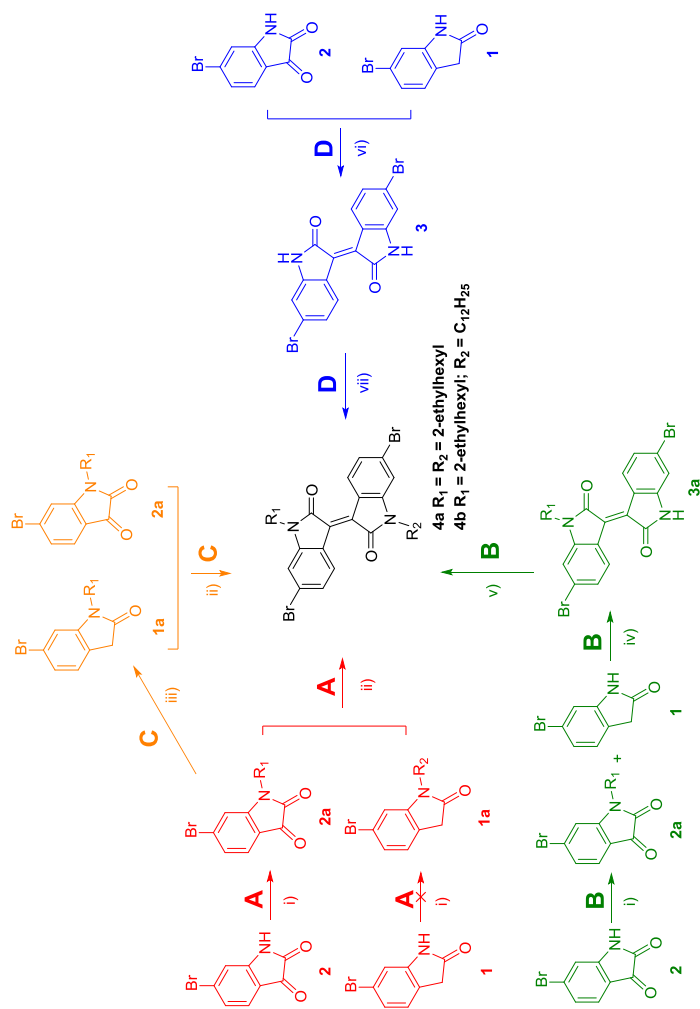
Scheme 2. Overview of the synthetic strategies applied toward the flow synthesis of N,N′-dialkyl-6,6′-dibromoisoindigo derivatives **4**: i) solid-phase reactor filled with K$_2$CO$_3$, DMF, 2-ethylhexyl bromide (1.2 equiv), 120 °C, 100−135 µL/min (50−70 mm path length), 4 bar, H$_2$O quench); ii) AcOH/HCl, 110 °C, 80 min, 3 bar; iii) hydrazine hydrate, DMF, 180 °C, 20 min, 4 bar; iv) AcOH/HCl, 110 °C, 80 min; v) solid-phase reactor filled with K$_2$CO$_3$, DMF, dodecyl bromide (1.2 equiv), 120 °C, 135 µL/min; vi) **1** (1.5 equiv), TEOF (7 equiv), DMF, 12 M HCl (7 equiv) in DMF, 120 °C, 80 min; vii) solid-phase reactor filled with K$_2$CO$_3$ (70 mm path length), DMF, 2-ethylhexyl bromide (2.1 equiv), 120 °C, 135 µL/min.

resulted in 96% conversion to the desired N-alkylated 6-Br-isatin (analysis via ^{1}H NMR). Having at hand a set of optimized batch reaction conditions for the N-alkylation of 6-Br-isatin, we then moved to a continuous flow process, on a small scale as well as on a larger scale (Table S2). For this purpose, a high temperature glass solid-phase reactor (Omnifit®) was filled with K_2CO_3 and a stream of the reagent solution was sent through this packed bed with a typical overall flow rate of 100−135 µL/min (average residence time of 40 min) and a post-slug volume of 3 mL (necessary for collecting the entire reaction mixture since the product tends to stick to the solid K_2CO_3). A solution of 6-Br-isatin (**2**) and 1.2 equivalents of 2-ethylhexyl bromide in DMF (20–44 mM) was passed through the solid-phase reactor filled with K_2CO_3 (3–3.5 g; 50–70 mm path length) heated to 120 °C, as shown in Figure S2. Typically, 100–200 mg of 6-Br-isatin were used for the small scale screening, whereas for the larger scale reaction 2.0 g of starting material was used. In the first case, the reagents were injected into small injector loops (5–10 mL), whereas in the latter case the reagents were put in a solvent bottle and pumped as such. Important to note is that, despite being a good solvent in batch, acetonitrile was not the most suitable solvent in the flow experiments since it resulted in an irregular movement of the solvent front through the solid packing (Figure S3). To obtain a smooth flow pattern and to avoid the formation of bubbles inside the solid-phase reactor, a BPR was inserted into the fluidic set-up after the solid-phase reactor, maintaining the system at a constant pressure of 4 bar. To prevent blockages inside the BPR and pressure build-up during the entire run, a stream of water was inserted between the outlet of the solid-phase reactor and the BPR via a T-piece to remove any solid K_2CO_3 (partially solubilized or precipitated/deposited inside the BPR or the connecting tubing). The most suitable fluidic set-ups for the small and larger scale N-alkylation reactions are depicted in Figure 1. The product was collected manually in a flask containing toluene, and a post-slug volume of 3 mL was set to ensure the complete elution of the compound from the packed-bed reactor. After removal of the solvent and drying, the crude reaction mixture was analyzed by ^{1}H NMR. In both cases, 92% (^{1}H NMR, Figure S4) conversion could be obtained. The remaining 8% corresponded to the starting material. The product could be successfully isolated from the reaction mixture by consecutive hexane extractions. To be able to determine the conversions by ^{1}H NMR, the crude mixture was extracted with diethyl ether, since both 6-Br-isatin (**2**) and *N*-2-ethylhexyl-6-Br-isatin (**2a**) dissolve in diethyl ether. Purification by column chromatography finally resulted in *N*-2-ethylhexyl-6-Br-isatin in high purity in 80% yield (Figure S5).
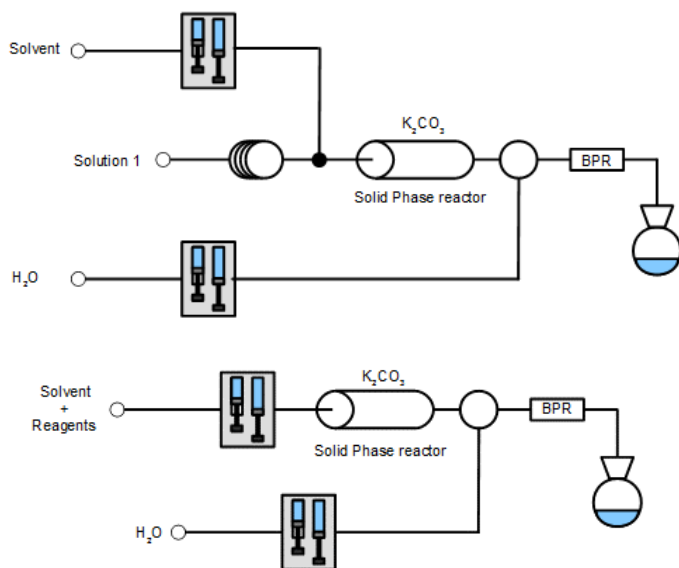
Figure 1. Fluidic set-ups for the N-alkylation of 6-Br-isatin (**2**) in flow on a small (100–200 mg) (top) and larger (2.0 g) scale (bottom).

Based on literature procedures, N-alkylation of 6-Br-isatin was also attempted utilizing solid-supported KF/alumina (Table S2, entry 4).[44,45] Good conversion to the desired alkylated compound could be obtained (87%), but problems arose with blockages caused by the solid support passing through the filter of the solid-phase reactor, leading to it settling down inside the BPR. Since this problem could not be solved by just adding a water quench between the solid-phase reactor and the BPR, it was decided to not further pursue this method, because it would anyway hamper upscaling of the reaction.

The optimized procedures, in batch and in the flow reactor, were then also applied for the N-alkylation of 6-Br-oxindole (**1**). It turned out, though, that it was not possible to alkylate 6-Br-oxindole in a regioselective way. All trials resulted in the formation of a mixture of mono-, di-, and tri-alkylated materials (through the occurrence of carbonyl α-substitution), each time in a more or less 1:1:1 ratio (according to GC/MS). This finding forced us to find an alternative approach to synthesize N-alkylated 6-Br-oxindole (*vide infra*).

On the other hand, the optimized flow alkylation method did work properly for both the N-alkylation of mono-alkylated isoindigo **3a** (*vide infra*) and for the double N-alkylation of 6,6′-dibromoisoindigo (**3**) (Scheme 2). The double alkylation could be performed without any difficulties and with acceptable yield (63%) and high purity (98%) after column chromatography. For the N-alkylation of monosubstituted isoindigo derivative **3a** (R_1 = 2-ethylhexyl), some precipitation was observed at the outlet of the reactor, resulting in loss of

product. The desired asymmetrically substituted isoindigo compound **4b** (R_1 = 2-ethylhexyl, R_2 = dodecyl) was obtained in 41% yield after purification. These flow experiments were performed without BPR and without the water quench to avoid blockages in the set-up due to product precipitation (Figure 2).
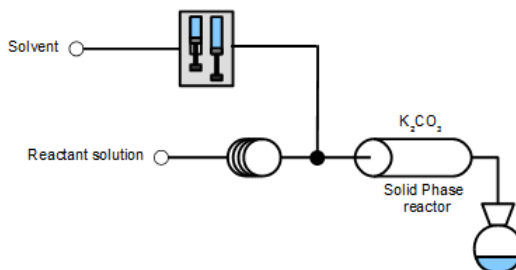
Figure 2. Fluidic set-up for the N,N'-dialkylation reaction of 6,6'-dibromoisoindigo (**3**) in flow.

From the conducted experiments it can be concluded that a similar conversion ratio could be obtained for the N-alkylation reaction of 6-Br-isatin in flow and batch (92 and 96%, respectively), while the reaction time could significantly be reduced (from 20 h to only 40 min) in the flow protocol. Moreover, the reaction was scaled up without difficulties and less impurities were formed during the reaction in flow, resulting in higher net yields after purification. Furthermore, the optimized flow protocol was also successfully applied for isoindigo dialkylation.

2.2.2 Reduction of 6-Br-isatin (Route C)

The failure of the (regioselective) N-alkylation reaction of 6-Br-oxindole (**1**) prompted us to find an alternative method to synthesize *N*-2-ethylhexyl-6-Br-oxindole (**1a**) (Scheme 2). According to literature, this can be achieved through reduction of the respective isatin derivative with hydrazine hydrate in polar solvents (DMF, ethylene glycol, *i*-PrOH or MeOH) without the addition of a base, through conventional heating or via microwave irradiation.[46,47] First of all, this approach was evaluated on 6-Br-isatin (**2**) in ethylene glycol and in *i*-PrOH in the microwave (30 W, 5 min at 180 or 150 °C, respectively), affording full conversion of the starting material with formation of up to 98% of 6-Br-oxindole (**1**) (as analyzed by GC/MS). Unfortunately, ethylene glycol and *i*-PrOH are not so suitable for the reduction of 6-Br-isatin in the flow reactor, since the solubility of the starting compound in these solvents is low. Therefore, we moved to the more suitable solvent DMF for a standard batch reaction, and the reaction progress was monitored with a ReactIR probe (Figure S6). After 2 hours of reaction at 150 °C, a (GC/MS) conversion of 94% was obtained, with 6% of hydrazone still remaining in the reaction mixture (Table 1, entry 1). Based on this experience, we then moved to the flow reactor. The fluidic set-up applied for the reduction reaction is shown in Figure 3. Different reaction conditions

(residence time and temperature) in DMF and *i*-PrOH have been evaluated (Table S3). The experiments showed that DMF is the most suitable solvent and temperatures higher than 150 °C are required to convert the hydrazone intermediate to the desired 6-Br-oxindole. When the reaction was performed at 150 °C, only limited conversion (up to 55%) was observed. Increasing the temperature to 180 °C resulted in full conversion to 6-Br-oxindole within 10 minutes.
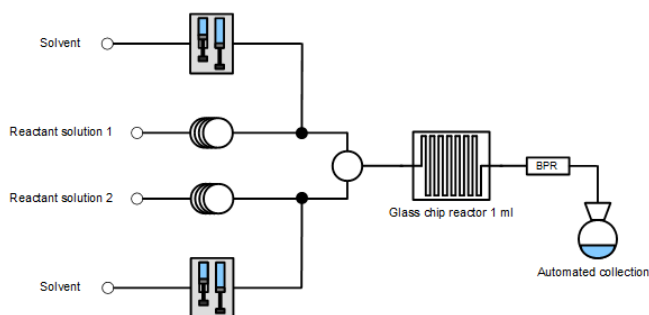
Figure 3. Fluidic set-up for the flow reduction of 6-Br-isatin (**2**) and *N*-2-ethylhexyl-6-Br-isatin (**2a**).

Next, a variety of conditions were also screened for the reduction of *N*-2-ethylhexyl-6-Br-isatin (**2a**) in batch, in the microwave and in the flow reactor (Figure 3, Table S4). In contrast to what was observed for non-alkylated 6-Br-isatin, the flow reduction of *N*-2-ethylhexyl-6-Br-isatin afforded the best results in *i*-PrOH as a solvent. An overview of the best conditions for both 6-Br-isatin and *N*-2-ethylhexyl-6-Br-isatin reduction is provided in Table 1.

In general, it can be concluded that it is possible to convert N-alkylated 6-Br-isatin to the corresponding N-alkylated 6-Br-oxindole in flow without noticeable difficulties and with a good conversion. The optimum solvent turned out to be *i*-PrOH and a conversion of 99% to the desired oxindole compound was achieved, which is slightly better as compared to the batch and microwave procedures. Higher temperatures are required to convert the intermediate hydrazone to the final oxindole derivative and it is important to note that, when DMF is used as a solvent, residence times in the reactor should not exceed 25 minutes, as prolonged exposure to high temperature in this solvent results in partial loss of the bromine moiety and the formation of other impurities.

Table 1. Comparison of the optimum reaction conditions and reaction outcome for the reduction of 6-Br-isatin (**2**) and *N*-2-ethylhexyl-6-Br-isatin (**2a**) in batch, in the microwave (MW) and in the flow reactor (1 mL glass chip).

Entry	Synthetic procedure	Starting material	Solvent	Conc. (M)	T (°C)	Time (min)	GC/MS
1	batch	**2**	DMF	0.1	130	120	94% **1** 6% hydrazone
2	batch	**2a**	DMF	0.2	150	180	90% **1a** 10% **1a** - Br [a]
3	MW (30 W)	**2**	ethylene glycol (or *i*-PrOH)	0.22	180 (or 150)	5	98% **1**
4	MW (50 W)	**2a**	DMF	0.12	150	10	84% **1a** 3% hydrazone 14% **1a** - Br [a]
5	MW (100 W)	**2a**	*i*-PrOH	0.12	150	10	90% **1a** 5% **2a** 5% hydrazone
6	flow	**2**	DMF	0.05	180	10	100% **1**
7	flow	**2a**	DMF	0.05	180	20	84% **1a** 4% **2a** 8% **2a** - Br [a] 4% other side products
8	flow	**2a**	*i*-PrOH	0.06	170	35	99% **1a** 1% **1a** - Br [a]

[a] Loss of the bromine group has been observed in some cases while reducing *N*-2-ethylhexyl-6-Br-isatin (**2a**).

Condensation

Having both alkylated starting materials successfully prepared in flow, we moved to the condensation reaction. In a first attempt, condensation of *N*-2-ethylhexyl-6-Br-isatin (**2a**) and 6-Br-oxindole (**1**) (*route B*) or *N*-2-ethylhexyl-6-Br-oxindole (**1a**) (*routes A,C*) was performed in batch according to the conventional method in AcOH/HCl medium at elevated temperatures (Scheme 1 and 2). The corresponding mono- and dialkylated 6,6'-dibromoisoindigo products (**3a** and **4a**, respectively) showed a reasonable solubility in the hot reaction mixture, but they started to precipitate immediately upon cooling down the reaction medium. Nevertheless, this method was transferred to the flow reactor. Two separate solutions, one containing *N*-2-ethylhexyl-6-Br-isatin (**2a**) and 6-Br-oxindole (**1**) (or *N*-2-ethylhexyl-6-Br-oxindole (**1a**)) in AcOH and the other one containing 12 M HCl in AcOH, were prepared and introduced into two injection loops, and then connected with two pumps delivering AcOH to the fluidic set-up (Figure 4). Both solutions were mixed via a Teflon T-piece mixer before entering the preheated 4 mL tubular reactor (110 °C). The residence time in the tubular reactor was set to 80 min. To avoid precipitation, the outlet of the reactor was kept heated and as short as possible. For this reason, the reaction was also carried out without BPR. For the condensation between both N-alkylated starting materials, a conversion of about 75% to the desired isoindigo derivative **4a** was obtained when using equimolar amounts of both starting materials. When using an excess (2 equiv) of *N*-2-ethylhexyl-6-Br-oxindole (**1a**), it was possible to consume the isatin derivative completely. For the condensation of *N*-2-ethylhexyl-6-Br-isatin (**2a**) with unsubstituted 6-Br-oxindole (**1**), an excess of the oxindole (1.5 equiv) was used. This resulted in a reaction mixture containing 71% of the desired isoindigo compound **3a** and 29% of remaining *N*-2-ethylhexyl-6-Br-isatin (according to ^{1}H NMR, Figure S7). The desired compound **3a** could be obtained in 60% yield by crystallization from the crude reaction mixture.
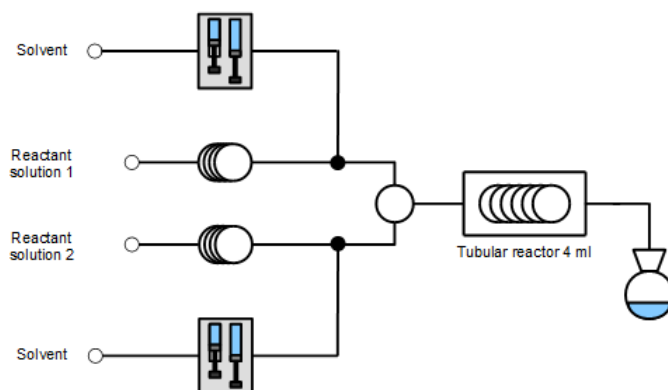

Figure 4. Fluidic set-up for the condensation reactions in the tubular flow reactor.

In the meantime, the condensation reaction between the unsubstituted precursors, 6-Br-oxindole (**1**) and 6-Br-isatin (**2**), was also evaluated in batch in polar aprotic solvents (DMSO and DMF) in the presence of HCl (*route D*). Since the idea was to keep the synthesized isoindigo in solution, it was expected that it could be more difficult to drive the reaction to completion. For this reason, the water scavenger triethyl orthoformate (TEOF) was added to the reaction mixture. When the condensation reaction was carried out in DMSO, no reproducible results and poor conversions and yields were obtained. The ^{1}H NMR spectrum of the crude reaction mixture indicated the absence of the signals corresponding to 6-Br-oxindole (**1**), whereas the signals corresponding to the desired isoindigo **3** and 6-Br-isatin (**2**) were clearly visible. The spectrum showed, however, also the presence of new signals, more in particular in the alkene region (at 4.7 and 4.9 ppm) (Figure S8). These findings made us to suggest that 6-Br-oxindole reacts with DMSO in a type of condensation reaction.[48] When the condensation was performed in deuterated DMSO, the signals around 4.7 and 4.9 ppm were absent, indicating the participation of DMSO in the reaction.

Before changing to DMF as an alternative solvent for the condensation, the stability of 6-Br-oxindole (**1**) was tested under the applied reaction conditions (DMF, HCl, TEOF, 120 °C, 120 min). After 2 hours of stirring, the ^{1}H NMR spectrum showed only the signals corresponding to 6-Br-oxindole (Figure S9). The condensation reaction was investigated in DMF and in mixtures of DMF and AcOH, changing the reaction temperature, reaction time, and the number of equivalents of HCl and TEOF. When DMF and AcOH were used in a 3:1 ratio, no precipitation was formed, but when going to 2:1 and 1:1 mixtures, the isoindigo product precipitated from the hot reaction mixture. The best result in batch was obtained when the reaction was performed in DMF (0.1 M) during 2 hours at 120 °C with equimolar amounts of starting materials, 7 to 15 equivalents of HCl and 7 equivalents of TEOF. This resulted in the formation of the desired isoindigo compound **3** in 70% yield (after work-up). Isoindigo **3** remained in solution and even upon cooling down no precipitate was formed. This method was then transferred to the flow reactor and it was shown that it is indeed possible to synthesize alkyl-free 6,6′-dibromoisoindigo **3** in this way. Although good conversions were obtained in batch using equimolar amounts of both starting materials, an excess of 6-Br-oxindole (**1**) (1.5–2 equiv) was required in flow to achieve comparable conversions (Table 2). For the flow condensation reactions (Figure 4), the reagents were injected into two 5 mL injector loops (Soln 1 and Soln 2), each inlet being connected to a syringe pump delivering the solvent. The reaction was accomplished in a 4 mL tubular reactor heated to 120 °C. The residence time for the condensation reactions was typically set to 80 min.

Table 2. Overview of the screened reaction conditions for the condensation between 6-Br-oxindole (**1**) and 6-Br-isatin (**2**) in flow in DMF.

Entry	Injector solution 1	Injector solution 2	Reactor	T (°C)	Time (min)	NMR (mol %)
1	0.073 M **2** + HCl 0.05 M	0.073 M **1** + TEOF (1 equiv)	tubular 4 mL	120	80	**A: 43** B: 24 C: 33 D: 0
2[a]	0.086 M **2** + HCl 0.24 M	0.088 M **1**	tubular 4 mL	120	80	**A: 46** B: 17 C: 37 D: 0
3	0.070 M **2** + HCl 0.52 M	0.070 M **1** + TEOF (7 equiv)	tubular 4 mL	120	80	**A: 43** B: 38 C: 19 D: 0
4	0.070 M **2** + HCl 0.52 M	0.102 M **1** + TEOF (7 equiv)	tubular 4 mL	120	80	**A: 74** B: 0 C: 3 D: 0 Unknown: 23
5	0.070 M **2** + HCl 0.52 M	0.140 M **1** + TEOF (7 equiv)	tubular 4 mL	120	40	**A: 28** B: 0 C: 33 D: 39
6	0.070 M **2** + HCl 0.52 M	0.140 M **1** + TEOF (7 equiv)	tubular 4 mL	120	80	**A: 69** B: 0 C: 31 D: 0
7	0.070 M **2** 0.102 M **1** TEOF (7 equiv)	12 M HCl in DMF 0.52 M	tubular 4 mL	120	80	**A: 74** B: 0 C: 26 D: 0
8	0.070 M **2** 0.070 M **1** TEOF (7 equiv)	12 M HCl in DMF 0.57 M	tubular 4 mL	120	80	**A: 54** B: 22 C: 24 D: 0
9[b]	0.070 M **2** 0.102 M **1**	TFA/Ac$_2$O in DMF	tubular 4 mL	120	80	**A: 73** B: 25 C: 3

[a] The solvent used was a mixture DMF/AcOH 3:1. A = isoindigo **3**; B = 6-Br-isatin (**2**); C = alcohol precursor; D = 6-Br-oxindole (**1**). [b] Precipitation occurred in the last part of the reactor.

During the reaction screening in DMF, it was observed that in a many cases the reaction mixture still contained a significant amount of the intermediate alcohol derivative (i.e. the hydrated isoindigo analogue). For this reason, the flow condensation was also performed in flow using a mixture of TFA and acetic anhydride in DMF (in the tubular reactor), using the same conditions as before (120 °C for 80 min) (Table 2, entry 9). ^{1}H NMR analysis of the crude reaction mixture showed an acceptable conversion to the desired isoindigo compound (73%) and only a minor amount of the alcohol precursor. However, the isoindigo material started to precipitate in the last part of the reactor, hampering the scale-up of the reaction using these conditions.

Summarizing, the condensation of pristine 6-Br-isatin and 6-Br-oxindole could be achieved in a tubular flow reactor using DMF as a solvent to keep the formed 6,6′-dibromoisoindigo in solution. After optimization of the reaction conditions the desired isoindigo compound was synthesized in 70% yield with a good purity after precipitation. N-alkylation of both 6-Br-isatin and 6-Br-oxindole resulted in increased solubility of the isoindigo compound and in this way the conventional batch strategy using AcOH/HCl could be used for the condensation reaction in a tubular flow reactor without blocking the reactor.

2.3 Conclusions

In conclusion, both symmetrically and asymmetrically N,N′-dialkylated 6,6′-dibromoisoindigo derivatives were efficiently synthesized using continuous flow technology. All individual steps in the different possible synthetic routes were carefully optimized and transferred to flow. The main issues to solve were the low solubility of the unsubstituted 6,6′-dibromoisoindigo core in common organic solvents and the heterogeneous reaction mixture in the N-alkylation reaction. In a first strategy, the condensation reaction between 6-Br-isatin and 6-Br-oxindole was performed in DMF, avoiding precipitation of pristine 6,6′-dibromoisoindigo. Subsequent dialkylation using a packed-bed reactor filled with K_2CO_3 resulted in the N,N-disubstituted isoindigo derivative in a good yield and high purity. In a second strategy, 6-Br-isatin was first N-alkylated in flow using the same solid-phase alkylation procedure, with a similar conversion ratio as in batch, an increased yield after purification and a significantly reduced reaction time. This N-alkylated 6-Br-isatin was readily reduced in flow to the corresponding N-alkyl-6-Br-oxindole using hydrazine hydrate in *i*-PrOH upon optimizing the residence time. Both N-alkylated starting materials were then combined in flow using the conventional AcOH/HCl conditions at 110 °C affording the desired N,N′-dialkylated 6,6′-dibromoisoindigo compounds. Reactor fouling by precipitation was avoided by keeping the outlet from the reactor heated. The latter strategy also allowed the synthesis of an unprecedented asymmetrically dialkylated isoindigo derivative. The N,N′-dialkyl-6,6′-dibromoisoindigo flow synthesis

protocol reported here represents the first real example of an important OPV building block prepared by continuous flow. Further efforts in this direction are considered relevant to increase material availability – with an emphasis on purity and reproducible material properties – and thereby foster further technological progress in the OPV field.

2.4 Experimental section

Materials and instrumentation

Unless stated otherwise, all reagents and chemicals were obtained from commercial sources and used without further purification. Solvents were dried by a solvent purification system (MBraun, MB-SPS-800). ^{1}H NMR chemical shifts (δ, in ppm) were determined relative to the residual solvent signals (2.50 ppm for DMSO-d_6, 2.05 ppm for $(CD_3)_2CO$, and 7.26 ppm for $CDCl_3$). Gas chromatography/mass spectrometry (GC/MS) analyses were carried out on a Finnigan TSQ-7000 Thermoquest, with a 30 m DB5-MS 0.25 mm ID, 0.25 μm FT column. ESI-MS was performed using an LTQ orbitrap velos pro mass spectrometer (ThermoFischer Scientific) equipped with an atmospheric pressure ionization source operating in the nebulizer assisted electro spray mode. The instrument was calibrated in the m/z range 220-2000 using a standard solution containing caffeine, MRFA and Ultramark 1621. A constant spray voltage of 5 kV was used and nitrogen at a dimensionless sheath gas flow-rate of 7 was applied. Capillary temperature was set to 275°C. HPLC grade methanol was used as solvent. Spectra were analyzed in Thermo Xcalibur Qual Browser software. The flow experiments were conducted on a Syrris Asia 320 system. The applied solid-phase reactor is a glass (10 mm ID) Omnifit column. The used FT-IR probe is a ReactIR15 from Mettler-Toledo with a liquid N_2 MCT detector, an AgX 6 mm x 2 m fiber, a probe tip comprised of diamond (DiComp), and an integrated thermal device (RTD) temperature sensor. The system is controlled, and the raw data are collected and analyzed by the iC-IR software. Reactions under microwave irradiation were performed in a CEM Discover Explorer Hybrid12 microwave, controlled by the Synergy Application Software.

N-Alkylation in flow

* N-Alkylation of 6-Br-isatin (**2**) - Synthesis of 6-bromo-1-(2-ethylhexyl)indoline-2,3-dione (*N*-2-ethylhexyl-6-Br-isatin) (**2a**) (*route A*)[49]

Small scale synthesis (fluidic set-up in Figure 1 - top)

6-Br-isatin (**2**) (0.050 g, 0.22 mmol) and 2-ethylhexyl bromide (0.051 g, 0.265 mmol, 1.2 equiv) were dissolved in dry DMF (11 mL) and this solution was injected into a 10 mL injection loop. The Omnifit® glass solid-phase reactor

(path length 50–70 mm) was filled with anhydrous K_2CO_3 (2.5 g) and the mixed starting product solution was pumped through the preheated reactor (120 °C). The flow rate of the water stream (at the reactor outlet) was kept fixed at 50 μL/min and the BPR was set at 4 bar. The reaction mixture leaving the flow reactor was collected over toluene. At the end of the experiment, the solvent was removed under reduced pressure by co-evaporation with toluene. The crude compound was diluted with water and extracted with *n*-hexane. The combined organic phase was dried over $MgSO_4$, filtered, and the solvent was removed under reduced pressure. The crude compound was purified by column chromatography (eluent diethyl ether:petroleum ether, 8:2), which resulted in a pure orange solid (0.046 g, 62%). ^{1}H NMR (400 MHz, DMSO-d_6) δ 7.47 (d, *J* = 7.9 Hz, 1H), 7.41 (d, *J* = 1.5 Hz, 1H), 7.32 (dd, *J* = 7.9, 1.6 Hz, 1H), 3.54 (d, *J* = 7.4 Hz, 2H), 1.46–1.10 (m, 9H), 0.91–0.81 (m, 6H).[49]

Upscaling (fluidic set-up in Figure 1 - bottom)

6-Br-isatin (**2**) (2.00 g, 8.84 mmol) and 2-ethylhexyl bromide (2.05 g, 10.61 mmol, 1.2 equiv) were dissolved in dry DMF (200 mL), together with KI (0.146 g, 0.88 mmol, 0.1 equiv), and this solution was collected in a solvent reagent bottle. The Omnifit® glass solid-phase reactor (path length 50–70 mm) was filled with anhydrous K_2CO_3 (3.2 g) and the mixed starting product solution was pumped through the preheated reactor (120 °C). The flow rate of the water stream (at the reactor outlet) was kept fixed at 50 μL/min and the BPR was set at 4 bar. The reaction stream exiting the flow reactor was collected over toluene. At the end of the experiment, the solvent was removed under reduced pressure by co-evaporation with toluene. The crude compound was diluted with water and extracted with *n*-hexane. The combined organic phase was dried over $MgSO_4$, filtered, and the solvent was removed under reduced pressure. The crude compound was purified by column chromatography (eluent hexanes:CH_2Cl_2, 8:2), affording the pure product in 80% (2.39 g) yield.

* N-Monoalkylation of *N*-2-ethylhexyl-6,6'-dibromoisoindigo - Synthesis of (*E*)-6,6'-dibromo-1-dodecyl-1'-(2-ethylhexyl)-[3,3'-biindolinylidene]-2,2'-dione (**4b**) (*route B*)[33]

A solution of *N*-2-ethylhexyl-6,6'-dibromoisoindigo (**3a**) (0.070 g, 0.132 mmol) and 1-dodecyl bromide (0.039 g, 0.158 mmol, 1.2 equiv) in dry DMF (5 mL) was introduced into a 5 mL injector loop connected with a syringe pump to pump DMF through the fluidic set-up. The Omnifit® glass solid-phase reactor (path length 70 mm) was filled with anhydrous K_2CO_3 (3.5 g) and the mixed starting product solution was pumped through the preheated reactor (120 °C) with a flow rate of 135 μL/min and a post-slug volume of 3 mL. The reaction stream exiting the flow reactor was collected over toluene. At the end of the experiment, the solvent was removed under reduced pressure by co-evaporation with toluene. The crude compound was diluted with water and extracted with

diethyl ether. The combined organic phase was dried over MgSO$_4$, filtered, and the solvent was removed under reduced pressure. The crude compound was purified by flash column chromatography (petroleum ether:CH$_2$Cl$_2$ eluent gradient) and obtained as a pure red solid (0.038 g, 41%). ^{1}H NMR (300 MHz, CDCl$_3$) δ 9.05 (ddd, J = 8.6, 4.9, 2.1 Hz, 2H), 7.15 (dd, J = 8.6, 1.9 Hz, 2H), 6.91 (d, J = 1.8 Hz, 1H), 6.89 (d, J = 1.8 Hz, 1H), 3.71 (t, J = 7.4 Hz, 2H), 3.66–3.62 (m, 2H), 1.64–1.02 (m, 25H), 0.92–0.80 (m, 9H); ^{13}C NMR (100 MHz, CDCl$_3$) δ 168.5, 168.1, 146.6, 146.2, 133.04, 133.00, 131.6, 131.4, 127.15, 127.11, 125.6, 125.2, 120.82, 120.78, 112.0, 111.7, 44.8, 40.7, 37.8, 32.3, 31.0, 30.1, 30.03, 29.97, 29.91, 29.75, 29.69, 29.0, 27.8, 27.4, 24.4, 23.5, 23.1, 14.6, 14.5, 11.1; MS (ESI) calcd for C$_{36}$H$_{48}$Br$_2$N$_2$O$_2$Na [M+Na]$^+$ m/z 721.19; found 721.14.

* N,N'-Dialkylation of 6,6'-dibromoisoindigo - Synthesis of (*E*)-6,6'-dibromo-1,1'-bis(2-ethylhexyl)-[3,3'-biindolinylidene]-2,2'-dione (**4a**) (*route D; fluidic set-up in Figure 2*)[33]

A solution of 6,6'-dibromoisoindigo (**3**) (0.150 g, 0.357 mmol) and 2-ethylhexyl bromide (0.152 g, 0.786 mmol, 2.2 equiv) in DMF (10 mL) was introduced into a 10 mL injector loop connected with a syringe pump to pump DMF through the fluidic set-up. The Omnifit® glass solid-phase reactor (path length 70 mm) was filled with anhydrous K$_2$CO$_3$ (3.5 g) and the mixed starting product solution was pumped through the preheated reactor (120 °C) with a flow rate of 135 µL/min and a post-slug volume of 3 mL. The reaction stream exiting the flow reactor was collected over toluene. At the end of the experiment, the solvent was removed under reduced pressure by co-evaporation with toluene. The crude compound was diluted with water and extracted with diethyl ether. The combined organic phase was dried over MgSO$_4$, filtered, and the solvent was removed under reduced pressure. The crude compound (82% yield) was purified by flash column chromatography (eluent *n*-hexane:CH$_2$Cl$_2$, 8:2) and obtained as a pure red solid (0.145 g, 63%). ^{1}H NMR (300 MHz, acetone-d_6) δ 9.19 (d, J = 8.6 Hz, 2H), 7.25 (dd, J = 8.6, 1.9 Hz, 2H), 7.21 (d, J = 1.8 Hz, 2H), 3.76 (d, J = 7.6 Hz, 4H), 1.50–1.24 (m, 18H), 1.00–0.82 (m, 12H).[33]

Reduction of N-2-ethylhexyl-6-Br-isatin (in MW and flow) (route C)[49]

* Microwave synthesis of 6-bromo-1-(2-ethylhexyl)indolin-2-one (*N*-2-ethylhexyl-6-Br-oxindole) (**1a**)

N-2-ethylhexyl-6-Br-isatin (**2a**) (0.200 g, 0.592 mmol) was dissolved in DMF (4 mL) in a 10 mL MW vial and hydrazine hydrate (51% v/v; 0.160 mL) was added to this solution. The vial was inserted into the CEM® microwave reactor and irradiated for 10 min at 150 °C (50 W). The reaction mixture was poured on ice, neutralized with 1 N HCl (aq) and extracted with diethyl ether. The crude product was purified by flash column chromatography (petroleum ether:CH$_2$Cl$_2$ eluent gradient, from 99 to 10% petroleum ether) and obtained as a white solid

in 77% yield (0.140 g). ^{1}H NMR (300 MHz, DMSO-d_6) δ 7.27–7.08 (m, 3H), 3.53 (s + d, J = 8.0 Hz, 4H), 1.39–1.12 (m, 9H), 0.93–0.75 (m, 6H).[49]

* Flow synthesis of 6-bromo-1-(2-ethylhexyl)indolin-2-one (N-2-ethylhexyl-6-Br-oxindole) (**1a**) (*fluidic set-up in Figure 3*)

Two separate solutions were prepared, one containing N-2-ethylhexyl-6-Br-isatin (**2a**) (0.100 g, 0.30 mmol) in iPrOH (5 mL; 0.06 M) and the other one containing hydrazine hydrate (51% v/v, 0.08 mL) in iPrOH (5 mL). Both solutions were injected into 5 mL injection loops and passed through the 1 mL glass chip reactor, heated to 170 °C, with a residence time of 35 min. The BPR was set to 7 bar. The The reaction stream exiting the flow reactor was collected on ice, neutralized with 1 N HCl and extracted with diethyl ether. The crude compound was purified by flash column chromatography (petroleum ether:CH_2Cl_2 eluent gradient) and obtained as an off-white solid in 70% yield (67 mg).

Condensation reaction in flow (fluidic set-up in Figure 4)

* Condensation between 6-Br-oxindole (**1**) and 6-Br-isatin (**2**) - Synthesis of 6,6'-dibromoisoindigo (**3**) (*route D*)

Two separate solutions were prepared, one (solution 1) containing 6-Br-isatin (**2**) (0.100 g, 0.44 mmol) and 6-Br-oxindole (**1**) (0.140 g, 0.66 mmol, 1.5 equiv) together with TEOF (0.5 mL) in DMF (6 mL), and the other one (solution 2) containing HCl (12 M; 0.3 mL) in DMF (6 mL). Of those solutions, 5 mL was injected into injector loops A and B, respectively. Both pump A (connected with the inlet of injector loop A) and pump B (connected with the inlet of injector loop B) provide DMF from the solvent bottle reservoir to the fluidic set-up. Solutions 1 and 2 were mixed together in a teflon T-piece before entering into the 4 mL tubular reactor, which was preheated to reach a liquid temperature of 120 °C. The residence time in the reactor was set to 80 min. The reaction stream exiting the flow reactor was concentrated by evaporation under reduced pressure, and diluted with water and acetic acid. The formed precipitate was filtered off and washed with water and acetic acid. The residue was dissolved in DMF, the solvent was removed under reduced pressure, and the compound was dried under high vacuum, affording 82% (0.105 g) of pure isoindigo **3**. ^{1}H NMR (300 MHz, DMSO-d_6) δ 11.11 (s, 2H), 8.99 (d, J = 8.7 Hz, 2H), 7.19 (dd, J = 8.7, 2.0 Hz, 2H), 7.00 (d, J = 2.0 Hz, 2H).[33]

* Condensation between 6-Br-oxindole (**1**) and N-2-ethylhexyl-6-Br-isatin (**2a**) - Synthesis of (E)-6,6'-dibromo-1-(2-ethylhexyl)-[3,3'-biindolinylidene]-2,2'-dione (N-2-ethylhexyl-6,6'-dibromoisoindigo (**3a**)) (*route C*)[33]

Two separate solutions were prepared, one (solution 1) containing N-2-ethylhexyl-6-Br-isatin (**2a**) (0.100 g, 0.30 mmol) and 6-Br-oxindole (**1**) (0.095

g, 0.45 mmol, 1.5 equiv) in AcOH (5 mL), and the other one (solution 2) containing HCl (12 M; 0.5 mL) in AcOH (5 mL). Of those solutions, 5 mL was injected into the 5 mL injector loops A and B, respectively. Both pump A (connected with the inlet of injector loop A) and pump B (connected with the inlet of injector loop B) pump AcOH from the solvent bottle reservoir into the fluidic set-up. Solutions A and B were mixed together in a teflon T-piece before entering into the 4 mL tubular reactor, which was preheated to reach a liquid temperature of 110 °C. The residence time in the reactor was set to 80 min. The outlet of the reactor was kept as short as possible to avoid precipitation and blockage. The reaction stream exiting the flow reactor was diluted with water, neutralized with NaHCO$_3$ (aq) and extracted with diethyl ether. The crude compound was crystallized from hot ethanol, resulting in isoindigo **3a** in 60% yield (0.086 g) (still containing a little bit of starting material). ^{1}H NMR (400 MHz, CDCl$_3$) δ 9.04 (d, J = 8.7 Hz, 1H), 8.97 (d, J = 8.6 Hz, 1H), 7.61 (br s, 1H), 7.18–7.16 (m, 1H), 7.16–7.14 (m, 1H), 6.97 (d, J = 1.8 Hz, 1H), 6.89 (d, J = 1.8 Hz, 1H), 3.64–3.59 (m, 2H), 1.85–1.76 (m, 1H), 1.38–1.24 (m, 8H), 0.95–0.85 (m, 6H); ^{13}C NMR (100 MHz, CDCl$_3$) δ 168.6, 167.3, 145.9, 145.5, 133.08, 133.05, 131.3, 130.9, 130.4, 125.9, 124.4, 123.9, 120.6, 119.7, 112.4, 111.7, 43.4, 36.6, 29.6, 27.7, 23.2, 22.4, 13.8, 10.3; HRMS (ESI) calcd for C$_{24}$H$_{24}$Br$_2$N$_2$O$_2$Na [M+Na]$^+$ m/z 553.0105; found 553.0043.

* Condensation between N-2-ethylhexyl-6-Br-oxindole (**1a**) and N-2-ethylhexyl-6-Br-isatin (**2a**) - Synthesis of N,N'-bis(2-ethylhexyl)-6,6'-dibromoisoindigo (**4a**) (*route A*)[50]

Two separate solutions were prepared, one (solution 1) containing N-2-ethylhexyl-6-Br-isatin (**2a**) (0.087 g, 0.258 mmol) and N-2-ethylhexyl-6-Br-oxindole (**1a**) (0.167 g, 0.561 mmol, 2 equiv) in AcOH (5 mL), and the other one (solution 2) containing HCl (12 M; 0.5 mL) in AcOH (5 mL). Of those solutions, 5 mL was injected into the 5 mL injector loops A and B, respectively. Both pump A (connected with the inlet of injector loop A) and pump B (connected with the inlet of injector loop B) pump AcOH from the solvent bottle reservoir into the fluidic set-up. Solutions A and B were mixed together in a teflon T-piece before entering into the 4 mL tubular reactor, which was preheated to reach a liquid temperature of 110 °C. The residence time in the reactor was set to 80 min. The outlet of the reactor was kept as short as possible to avoid precipitation and blockage. The reaction stream exiting the flow reactor was diluted with water and extracted with chloroform. The crude compound was purified by column chromatography (n-hexane:CH$_2$Cl$_2$ eluent gradient) to afford isoindigo **4a** in pure form (because the reactor cracked during the run, the yield could not exactly be determined). ^{1}H NMR (400 MHz, acetone-d_6) δ 9.17 (d, J = 8.6 Hz, 2H), 7.23 (dd, J = 8.6, 1.9 Hz, 2H), 7.19 (d, J = 1.9 Hz, 2H), 3.77–3.72 (m, 4H), 1.44–1.24 (m, 18H), 1.00–0.89 (m, 12H).

2.5 Supporting information

Figure S1. Syrris Asia 320 system: 1. Pressurized solvent/reagent input store; 2. Dual pair syringe pump; 3. Reagent injector with 5 or 10 mL PTFE loops; 4. Glass chip heater (0.25–1 mL glass chips; temperature up to 150 °C); 5. Back pressure regulator (BPR); 6. Heater module with adaptor for a) tubular or stainless steel reactor (4–16 mL) and b) solid-phase reactor.
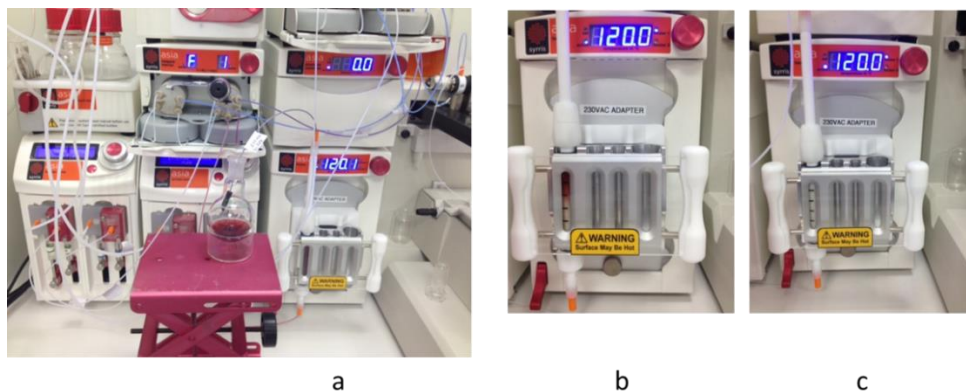
Figure S2. Reactor set-up (a) for the N-alkylation reaction: heated solid-phase reactor filled with K_2CO_3 during the experiment (b), and after washing with DMF (post-slug volume) (c).

Figure S3. Bad elution of the reagents through the solid-phase reactor when using CH$_3$CN or THF as a solvent for the N-alkylation reaction of 6-Br-isatin (**2**).
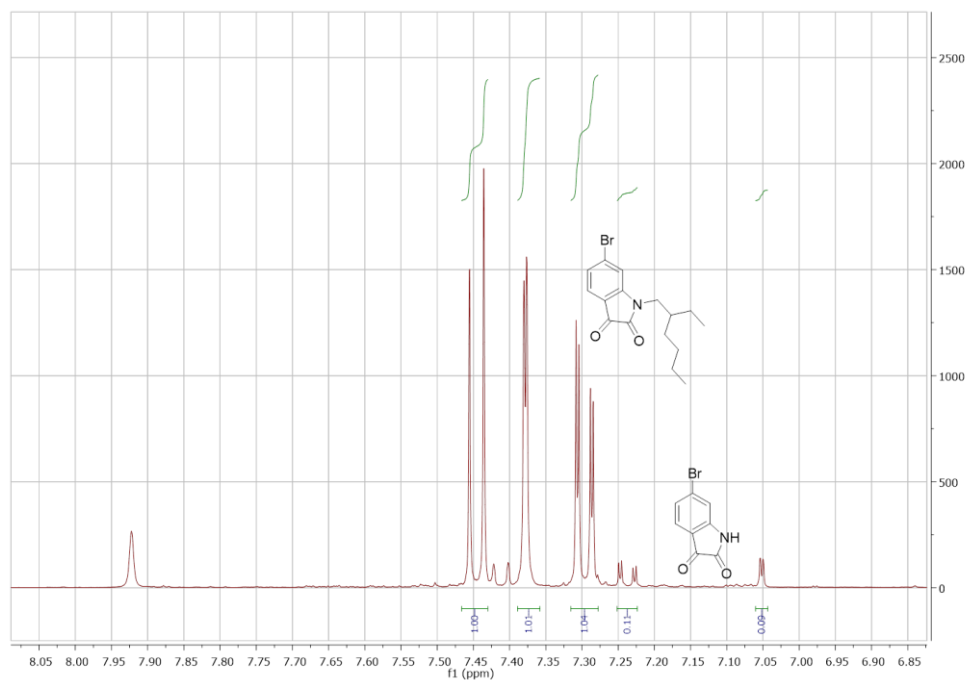
Figure S4. ^{1}H NMR spectrum (in DMSO-d_6; aromatic region) of the crude reaction mixture after N-alkylation of 6-Br-isatin in the flow reactor, showing both *N*-2-ethylhexyl-6-Br-isatin (**2a**) (92%) and unreacted 6-Br-isatin (**2**) (8%).
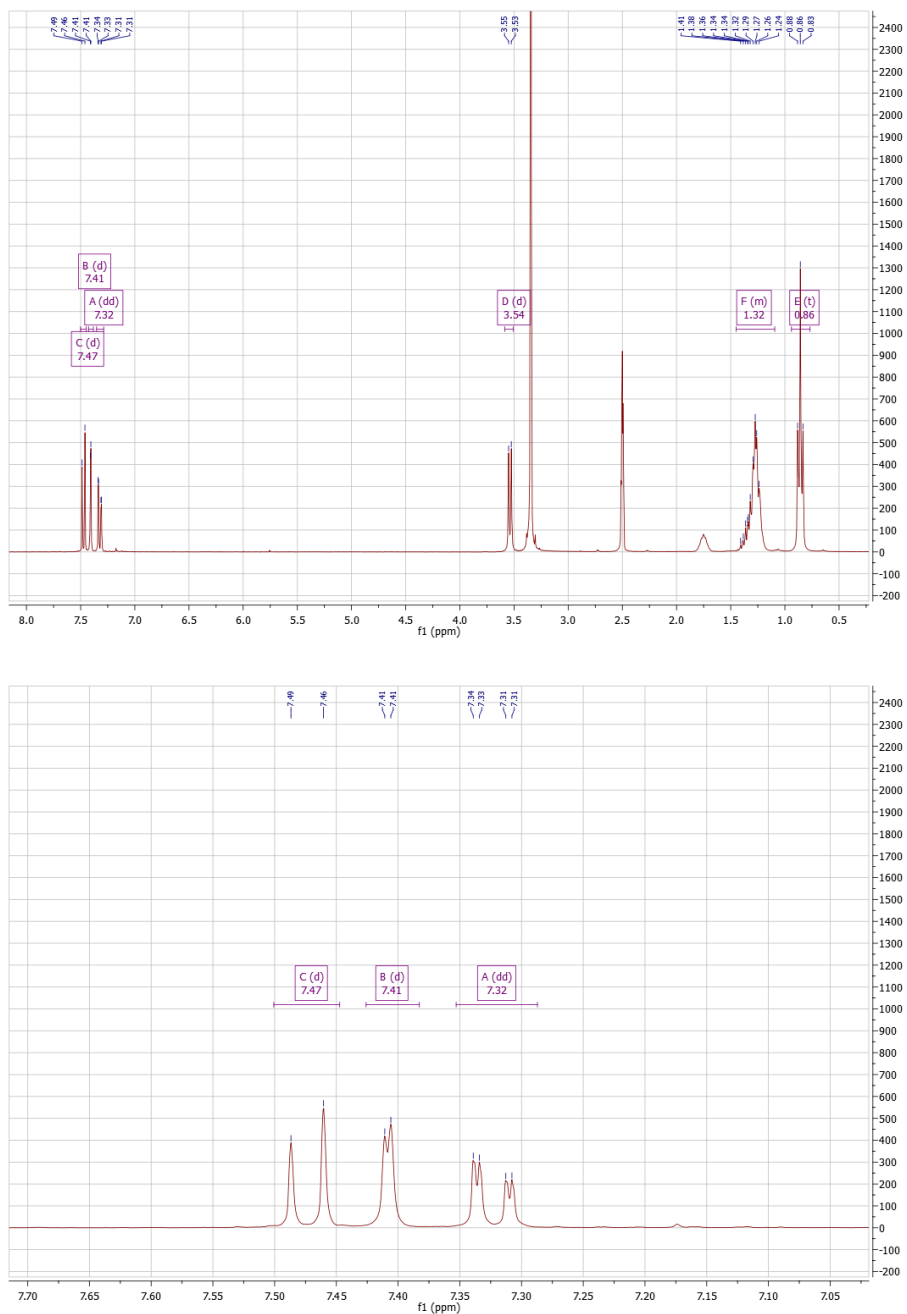
Figure S5. ^{1}H NMR spectrum (in DMSO-d_6) of *N*-2-ethylhexyl-6-Br-isatin (**2a**) after synthesis in flow and subsequent purification by column chromatography.
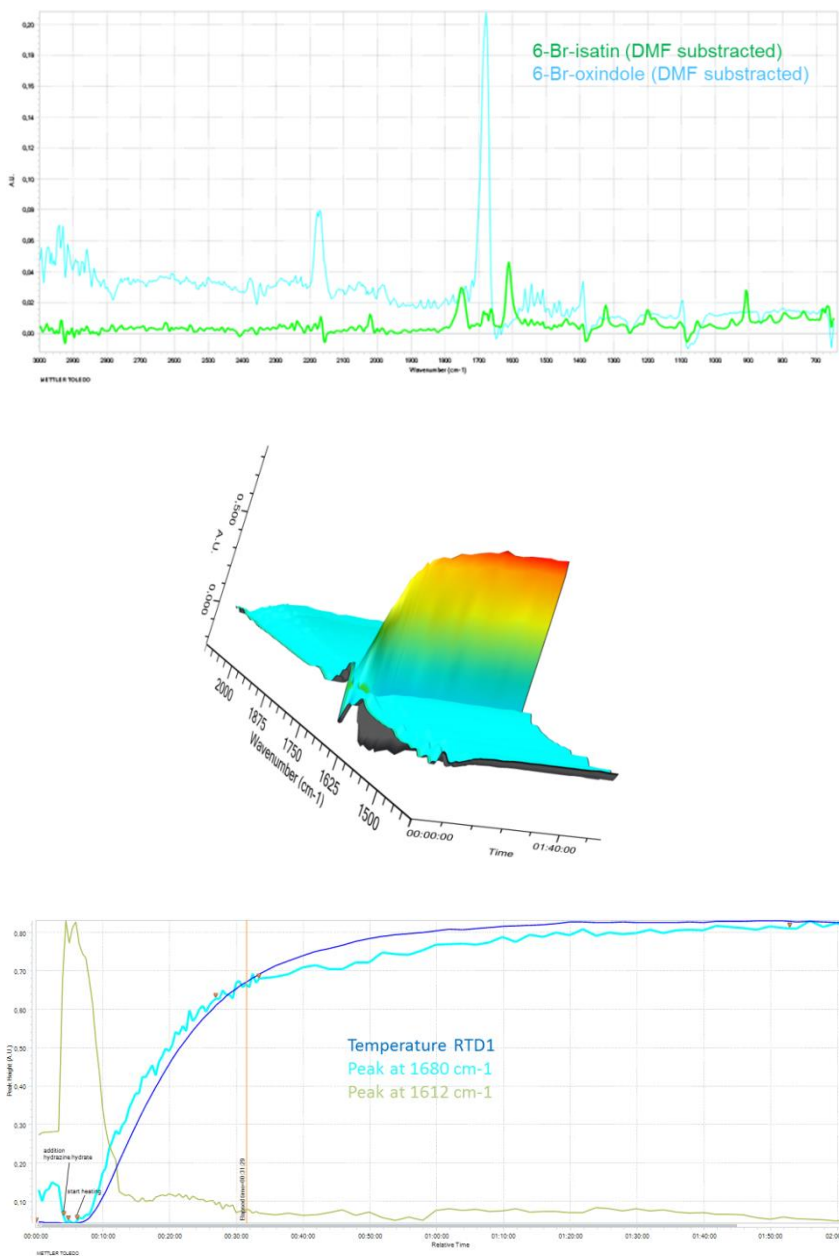
Figure S6. Reaction monitoring by the ReactIR15 probe during the reduction of 6-Br-isatin (**2**) to 6-Br-oxindole (**1**) in batch: IR spectra of **1** and **2** (top), 3D view (middle), and the trends in function of reaction time of the vibrations at 1680 (illustrative for 6-Br-oxindole formation) and 1612 cm^{-1} (illustrative for 6-Br-isatin disappearance).
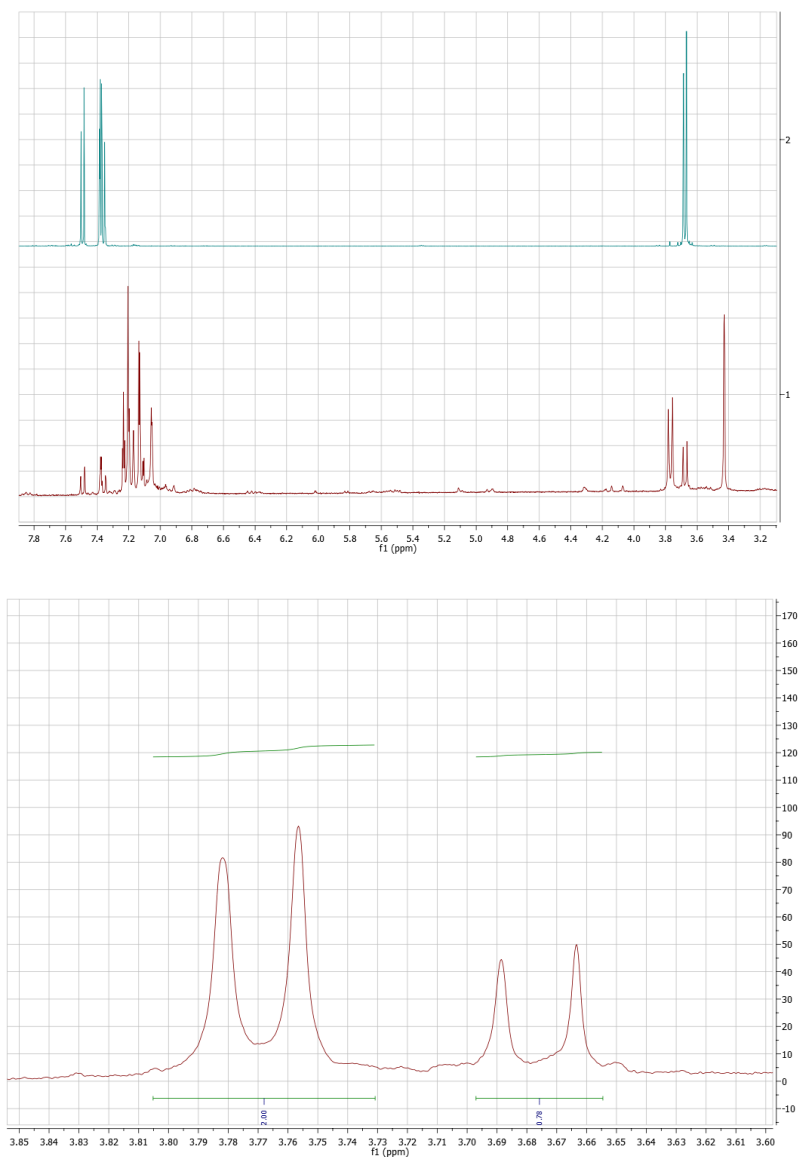
Figure S7. ^{1}H NMR spectra (in acetone-d_6) of *N*-2-ethylhexyl-6-Br-isatin (**2a**) (blue) and the crude reaction mixture after condensation between *N*-2-ethylhexyl-6-Br-isatin and 6-Br-oxindole (**1**) in flow (red) (top). Zoom of the 3.5–4 ppm region of the ^{1}H NMR spectrum of the crude reaction mixture after the condensation (bottom) (71% desired isoindigo **3a**, 29% starting compound **2a**).
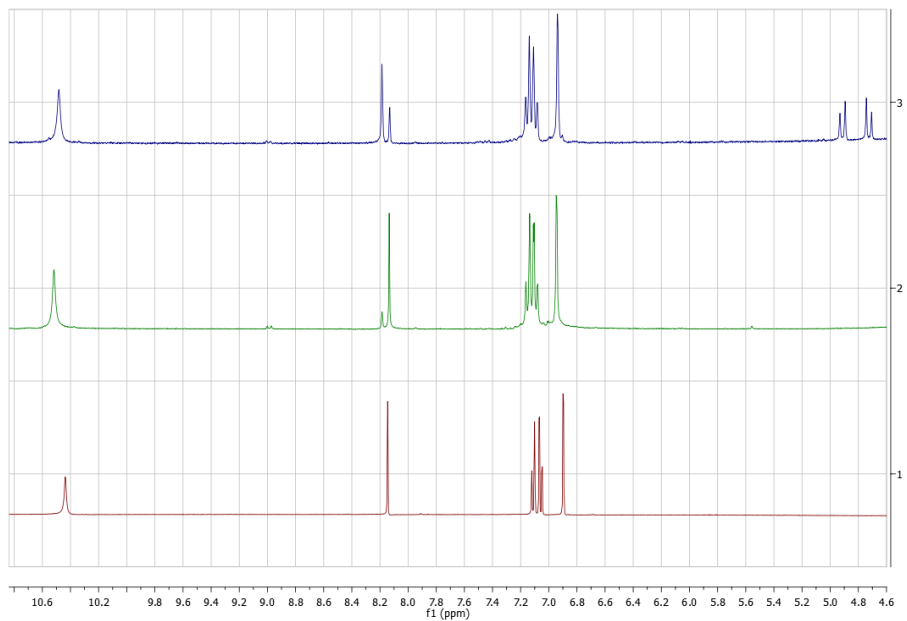
Figure S8. ^{1}H NMR spectra of pure 6-Br-oxindole (**1**) (red), 6-Br-oxindole under the reaction conditions (HCl, TEOF) applied for the condensation reaction in DMSO (after 2 h at 120 °C) (blue), and 6-Br-oxindole under the reaction conditions (HCl, TEOF) applied for the condensation reaction in DMSO-d_6 (after 80 min at 120 °C) (green).
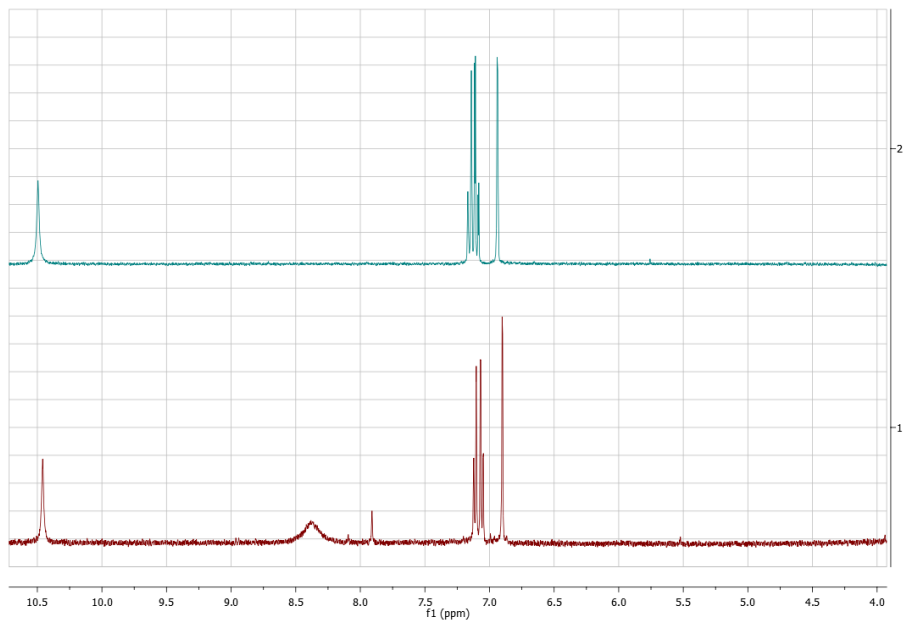
Figure S9. ^{1}H NMR spectra (in DMSO-d_6) of pure 6-Br-oxindole (**1**) (blue) and 6-Br-oxindole under the reaction conditions applied for the condensation reaction (HCl, TEOF) in DMF after 2 h at 120 °C (red).
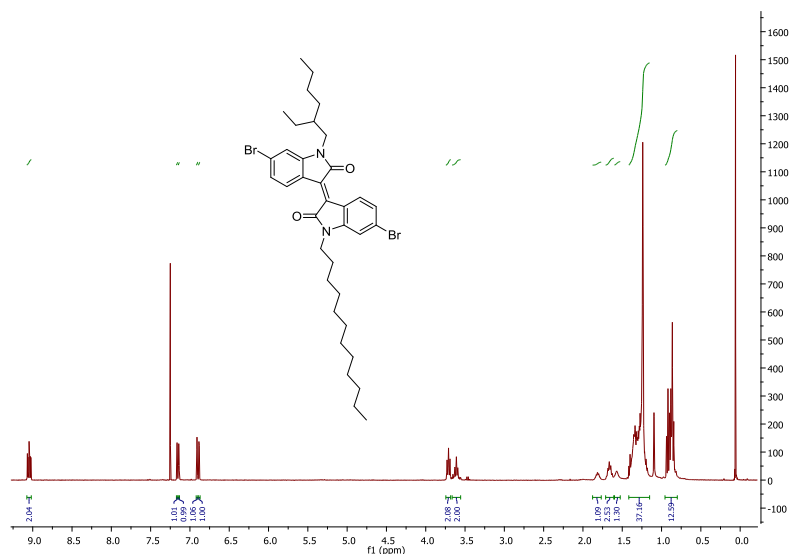
Figure S10. ^{1}H NMR spectrum (in CDCl$_3$) of (*E*)-6,6'-dibromo-1-dodecyl-1'-(2-ethylhexyl)-[3,3'-biindolinylidene]-2,2'-dione (**4b**).

55
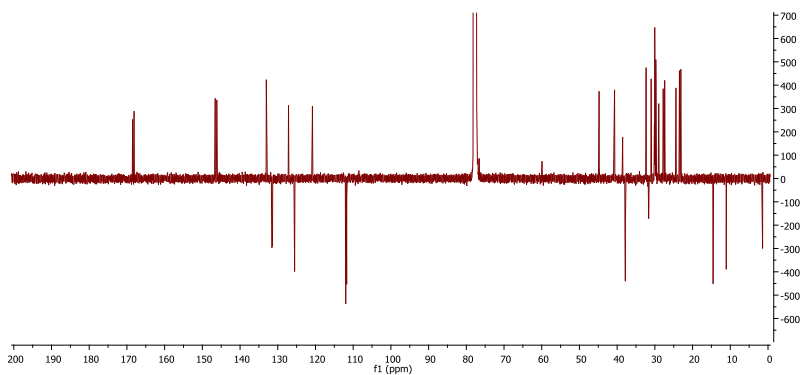
Figure S11. ^{13}C-APT NMR spectrum (in CDCl$_3$) of (*E*)-6,6'-dibromo-1-dodecyl-1'-(2-ethylhexyl)-[3,3'-biindolinylidene]-2,2'-dione (**4b**).
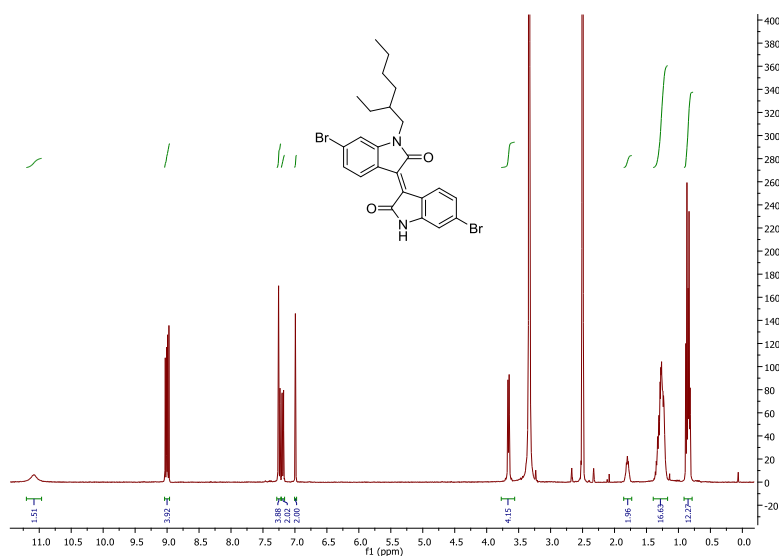
Figure S12. ^{1}H NMR spectrum (in DMSO-*d$_6$*) of (*E*)-6,6'-dibromo-1-(2-ethylhexyl)-[3,3'-biindolinylidene]-2,2'-dione (**3a**).
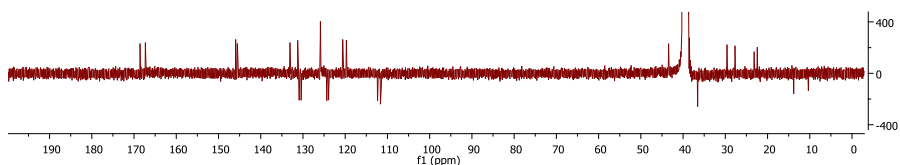
Figure S13. ^{13}C-APT NMR spectrum (in DMSO-*d$_6$*) of (*E*)-6,6'-dibromo-1-(2-ethylhexyl)-[3,3'-biindolinylidene]-2,2'-dione (**3a**).

Table S1. Overview of the different reaction conditions applied for the N-alkylation of 6-Br-isatin (**2**) with 2-ethylhexyl bromide (to afford *N*-2-ethylhexyl-6-Br-isatin (**2a**)) in batch. Molar ratios were determined by ^{1}H NMR (in DMSO-d_6).

Entry	Solvent	Reaction time (h)	T (°C)	Base/ Additive	NMR (mol %)
1	CH$_3$CN	20	reflux	K$_2$CO$_3$	82% **2a** 18% **2**
2	CH$_3$CN	20	reflux	DBU	-
3	THF	24	reflux	K$_2$CO$_3$	-
4	THF	2	reflux	KO*t*Bu	-
5	THF	24	reflux	KO*t*Bu	-
6	dioxane	24	reflux	KO*t*Bu	-
7	THF	20	reflux	K$_2$CO$_3$	50% **2a** 50% **2**
8	THF	20	reflux	KO*t*Bu/ 18-crown-6	-
9	dioxane	20	reflux	KO*t*Bu/ 18-crown-6	-
10	DMF	20	reflux	pyridine	-
11	DMF	20	130	DBU	-
12	DMF	20	130	K$_2$CO$_3$/ KI	96% **2a** 4% **2**
13	CH$_2$Cl$_2$/H$_2$O	20	reflux	K$_2$CO$_3$/ TBAB	-

Table S2. Overview of the different reaction conditions applied for the N-alkylation of 6-Br-isatin (**2**) with 2-ethylhexyl bromide (to afford *N*-2-ethylhexyl-6-Br-isatin (**2a**)) in flow. Molar ratios were determined by ^{1}H NMR (in DMSO-d_6).

Entry	Solvent [conc. **2**]	T (°C)	Base/ Additive	Overall flow rate (μl/min)	Residence time (min)	NMR (mol %)
1	CH$_3$CN [6 mM]	100	K$_2$CO$_3$	550	10	20% **2a** 80% **2**
				275	20	24% **2a** 76% **2**
2	DMF [10 mM]	100	K$_2$CO$_3$	550	10	64% **2a** 36% **2**
				275	20	84% **2a** 16% **2**
3	DMF [10 mM]	50	K$_2$CO$_3$	275	20	100% **2**
4	DMF [20 mM]	120	KF/Al$_2$O$_3$	138	40	87% **2a** 13% **2**
5	DMF [20 mM]	120	K$_2$CO$_3$	138	40	90% **2a** 10% **2**
6	DMF [0.044 M]	120	K$_2$CO$_3$/KI	138	40	92% **2a** 8% **2**

Table S3. Overview of the different reaction conditions applied in flow (1 mL glass chip reactor) for the reduction of 6-Br-isatin (**2**) to 6-Br-oxindole (**1**). In each experiment, hydrazine hydrate (51% v/v) was used as the reducing agent. Conversions are based on GC/MS analysis of the reaction mixture (after extraction).

Entry	Conc. **2** (mM)	Solvent	Overall flow rate (μl/min)	Residence time (min)	T (°C)	**2**	**1**	Hydrazone
1	5	*i*-PrOH	200	5	150	95%	5%	-
2	5	*i*-PrOH	100	10	150	95%	5%	-
3	5	*i*-PrOH	50	20	150	92%	8%	-
4	8	DMF	200	5	150	20%	55%	25%
5	8	DMF	100	10	150	17%	29%	54%
6	0.05	DMF	100	10	180	-	86%	-
7	0.05	DMF	50	20	180	-	89%	-

Table S4. Overview of the different reaction conditions applied in flow (1 mL glass chip reactor) for the reduction of *N*-2-ethylhexyl-6-Br-isatin (**2a**) to *N*-2-ethylhexyl-6-Br-oxindole (**1a**). In each experiment, hydrazine hydrate (51% v/v) was used as the reducing agent. Conversions are based on GC/MS analysis of the reaction mixture (after extraction). Other compounds formed during the reaction: A = *N*-2-ethylhexyl-6-Br-oxindole product with loss of bromine; B = *N*-2-ethylhexyl-6-Br-isatin with loss of bromine; C = hydrazone with loss of bromine; D = unknown.

[2a]	Solvent	Overall flow rate (µl/min)	t_r (min)	T (°C)	2a	1a	Hydrazone	Other
50mM	DMF	200	5	180	5%	53%	27%	A = 2%, B = 5%, C = 8%
50mM	DMF	100	10	180	3%	79%	7%	A = 5%; B = 1%; C = 5%
50mM	DMF	50	20	180	4%	84%	0.5%	A = 8%; B = 0.5%; C = 3%
50mM	DMF	25	40	180	-	71%	-	A = 14%; B = 5%; D = 10%
0.12M	DMF	200	5	100	69%	5%	26%	-
0.12M	DMF	100	10	100	30%	10%	60%	-
0.12M	*i*-PrOH	40	25	100	8%	15%	77%	-
0.12M	*i*-PrOH	33	30	100	1%	12%	87%	-
0.12M	*i*-PrOH	200	5	150	4%	18%	78%	-
0.12M	*i*-PrOH	100	10	150	3%	32%	65%	-
0.12M	*i*-PrOH	40	25	150	-	52%	48%	-
0.12M	*i*-PrOH	33	30	150	-	51%	49%	-
0.06M	*i*-PrOH	50	20	170	-	89%	7%	B = 4%
0.06M	*i*-PrOH	40	25	170	-	97%	-	B = 3%
0.06M	*i*-PrOH	33	30	170	-	95%	-	B = 5%

2.6 References

(1)   L. Dou, J. You, Z. Hong, Z. Xu, G. Li, R.A. Street, Y. Yang, *Adv. Mater.* **2013**, 25, 6642.

(2)   B. Kippelen, J.-L. Brédas, *Energy Environ. Sci.* **2009**, 2, 251.

(3)   Y. Su, S. Lan, K. Wei *Mater. Today* **2012**, 15, 554.

(4)   M. C. Scharber, N.S. Sariciftci, *Prog. Polym. Sci.* **2013**, 38, 1929.

(5)   S. Lizin, S. Van Passel, E. De Schepper, W. Maes, L. Lutsen, J. Manca, D. Vanderzande, *Energy Environ. Sci.* **2013**, 6, 3136.

(6)   Z. He, C. Zhong, S. Su, M. Xu, H. Wu, Y. Cao, *Nat. Photonics* **2012**, 6, 593.

(7)   A. K. K. Kyaw, D. H. Wang, V. Gupta, W. L. Leong, L. Ke, G. C. Bazan, A. J. Heeger, *ACS Nano* **2013**, 7, 4569.

(8)   K. H. Hendriks, G. H. L. Heintges, V. S. Gevaerts, M. M. Wienk, R. A. J. Janssen, *Angew. Chem. Int. Ed.* **2013**, 52, 8341.

(9)   C. Cabanetos, A. El Labban, J. A. Bartelt, J. D. Douglas, W. R. Mateker, J. M. J. Fréchet, M. D. McGehee, P. M. Beaujuge, *J. Am. Chem. Soc.* **2013**, 135, 4656.

(10)   Y. Liu, J. Zhao, Z. Li, C. Mu, W. Ma, H. Hu, K. Jiang, H. Lin, H. Ade, H. Yan, *Nat. Commun.* **2014**, 5, 5293.

(11)   Y. Liu, Y. M. Yang, C.-C. Chen, Q. Chen, L. Dou, Z. Hong, G. Li, Y. Yang, *Adv. Mater.* **2013**, 25, 4657.

(12)   W. Zhang, Y. Wu, Q. Bao, F. Gao, J. Fang, *Adv. Energy Mater.* **2014**, 4, 1400359.

(13)   B. Kan, M. Li, Q. Zhang, F. Liu, X. Wan, Y. Wang, W. Ni, G. Long, X. Yang, H. Feng, Y. Zuo, M. Zhang, F. Huang, Y. Cao, T. P. Russell, Y. Chen, *J. Am. Chem. Soc.* **2015**, 137, 3886.

(14)   J. Kesters, T. Ghoos, H. Penxten, J. Drijkoningen, T. Vangerven, D. M. Lyons, B. Verreet, T. Aernouts, L. Lutsen, D. Vanderzande, J. Manca, W. Maes, *Adv. Energy Mater.* **2013**, 3, 1180.

(15)   K. Gao, L. Li, T. Lai, L. Xiao, Y. Huang, F. Huang, J. Peng, Y. Cao, F. Liu, T. P. Russell, R. A. J. Janssen, X. Peng, *J. Am. Chem. Soc.* **2015**, 137, 7282.

(16)   K. Sun, Z. Xiao, S. Lu, W. Zajaczkowski, W. Pisula, E. Hanssen, J. M. White, R. M. Williamson, J. Subbiah, J. Ouyang, A. B. Holmes, W. W. H. Wong, D. J. Jones, *Nat. Commun.* **2015**, 6, 6013.

(17)   L. K. Jagadamma, M. Al-Senani, A. El-Labban, I. Gereige, G. O. Ngongang Ndjawa, J. C. D. Faria, T. Kim, K. Zhao, F. Cruciani, D. H. Anjum, M. A. McLachlan, P. M. Beaujuge, A. Amassian, *Adv. Energy Mater.* **2015**, 5, 1500204.

(18) R. Søndergaard, M. Hösel, D. Angmo, T. T. Larsen-Olsen, F. C. Krebs, *Mater. Today* **2012**, 15, 36.

(19) G. Jas, A. Kirschning, *Chem. – A Eur. J.* **2003**, 9, 5708.

(20) P. Watts, S. J. Haswell, *Chem. Soc. Rev.* **2005**, 34, 235.

(21) T. R. Dietrich, *Microchemical Engineering in Practice*; John Wiley & Sons, Inc., 2009.

(22) C. Wiles, P. Watts, *Green Chem.* **2012**, 14, 38.

(23) S. G. Newman, K. F. Jensen, *Green Chem.* **2013**, 15, 1456.

(24) J. H. Bannock, S. H. Krishnadasan, A. M. Nightingale, C. P. Yau, K. Khaw, D. Burkitt, J. J. M. Halls, M. Heeney, J. C. de Mello, *Adv. Funct. Mater.* **2013**, 23, 2123.

(25) A. Kumar, J. Hasan, A. Majji, A. Avhale, S. Gopinathan, P. Sharma, D. Tarange, R. Bajpai, A. Kumar, *J. Flow Chem.* **2014**, 4, 206.

(26) H. Seyler, D. J. Jones, A. B. Holmes, W. W. H. Wong, *Chem. Commun.* **2012**, 48, 1598.

(27) F. Grenier, B. R. Aich, Y. Lai, M. Guérette, A. B. Holmes, Y. Tao, W. W. H. Wong, M. Leclerc, *Chem. Mater.* **2015**, 27, 2137.

(28) M. Helgesen, J. E. Carlé, G. A. dos Reis Benatto, R. R. Søndergaard, M. Jørgensen, E. Bundgaard, F. C. Krebs, *Adv. Energy Mater.* **2015**, 5, 1401996.

(29) H. Seyler, W. W. H. Wong, D. J. Jones, A. B. Holmes, *J. Org. Chem.* **2011**, 76, 3551.

(30) E. Rossi, T. Carofiglio, A. Venturi, A. Ndobe, M. Muccini, M. Maggini, *Energy Environ. Sci.* **2011**, 4, 725.

(31) G. Pirotte, J. Kesters, P. Verstappen, S. Govaerts, J. Manca, L. Lutsen, D. Vanderzande, W. Maes, *ChemSusChem* **2015**, 8, 3228.

(32) J.-C. Flores, U. Berens, F. Bienewald, H. J. Kirner, M. G. R. Turbiez, *Ketopyrroles as organic semiconductors.* US20100297405 A1, 2010.

(33) J. Mei, K. R. Graham, R. Stalder, J. R. Reynolds, *Org. Lett.* **2010**, 12, 660.

(34) R. Stalder, J. Mei, K. R. Graham, L. A. Estrada, J. R. Reynolds, *Chem. Mater.* **2014**, 26, 664.

(35) E. Wang, W. Mammo, M. R. Andersson, *Adv. Mater.* **2014**, 26, 1801.

(36) Y. Yang, R. Wu, X. Wang, X. Xu, Z. Li, K. Li, Q. Peng, *Chem. Commun.* **2014**, 50, 439.

(37) Y. Deng, J. Liu, J. Wang, L. Liu, W. Li, H. Tian, X. Zhang, Z. Xie, Y. Geng, F. Wang, *Adv. Mater.* **2014**, 26, 471.

(38) E. H. Jung, W. H. Jo, *Energy Environ. Sci.* **2014**, 7, 650.

(39)   M. Tomassetti, F. Ouhib, A. Wislez, A.-S. Duwez, H. Penxten, W. Dierckx, I. Cardinaletti, R. A. A. Bovee, G. W. P. van Pruissen, C. Jérôme, J. Manca, W. Maes, C. Detrembleur, *Polym. Chem.* **2015**, 6, 6040.

(40)   K. R. Graham, P. M. Wieruszewski, R. Stalder, M. J. Hartel, J. Mei, F. So, J. R. Reynolds, *Adv. Funct. Mater.* **2012**, 22, 4801.

(41)   Z. Ma, D. Dang, Z. Tang, D. Gedefaw, J. Bergqvist, W. Zhu, W. Mammo, M. R. Andersson, O. Inganäs, F. Zhang, E. Wang, *Adv. Energy Mater.* **2014**, 4, 1301455.

(42)   M. S. Shmidt, A. M. Reverdito, L. Kremenchuzky, I. A. Perillo, M. M. Blanco, *Molecules* **2008**, 13, 831.

(43)   B. Reichart, C. Kappe, T. Glasnov, *Synlett* **2013**, 24, 2393.

(44)   K. Haraguchi, H.-J. Li, K. Matsuda, T. Takehisa, E. Elliott, *Macromolecules* **2005**, 38, 3482.

(45)   L. Ers, B. E. Blass, M. Drowns, C. L. Harris, S. Liu, D. E. Portlock, *Tetrahedron Lett.* **1999**, 40, 6545.

(46)   J. F. M. Silva, S. J. Garden, A. C. *J.* Pinto, *Braz. Chem. Soc.* **2001**, 12, 273.

(47)   C. M. Clay, PhD Thesis, *Synthesis of Isatin Derivatives Used for the Inhibition of Pro-Apoptotic Jurkat T Cells*, Wright State University, 2011.

(48)   D. P. Becker, P. M. Finnegan, P. W. Collins, *Tetrahedron Lett.* **1993**, 34, 1889.

(49)   I. Bulut, P. Lévêque, B. Heinrich, T. Heiser, R. Bechara, N. Zimmermann, S. Méry, R. Ziessel, N. Leclerc, *J. Mater. Chem. A* **2015**, 3, 6620.

(50)   G. W. P. Van Pruissen, J. Brebels, K. H. Hendriks, M. M. Wienk, R. A. J. Janssen, *Macromolecules* **2015**, 48, 2435.

Chapter 3

Continuous flow synthesis of PBDTTPD toward highly efficient bulk heterojunction organic solar cells
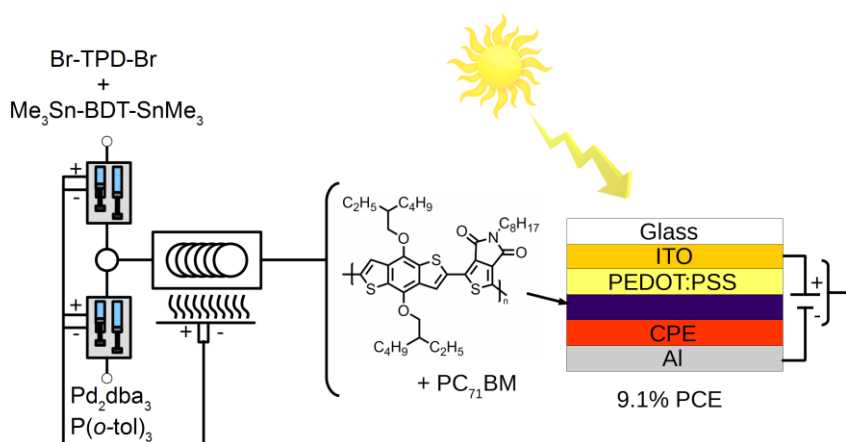
Abstract

Organic photovoltaics (OPV) have attracted great interest as a solar cell technology with appealing mechanical, aesthetical and economies-of-scale features. To drive OPV toward economic viability, low cost-large scale module production has to be realized, combined with increased top-quality material availability with minimal batch-to-batch variations. To this extent, continuous flow chemistry can serve as a powerful tool. In the present contribution, a flow protocol is optimized for the high performance copolymer PBDTTPD and the material quality is probed through systematic solar cell evaluation. A stepwise approach is adopted to turn the batch process into a reproducible and scalable continuous flow procedure. Solar cell devices fabricated from the obtained polymer batches deliver an average power conversion efficiency of 7.2%. Upon incorporation of an ionic polythiophene-based cathodic interlayer, the photovoltaic performance could be enhanced to a maximum efficiency of 9.1%.

Contribution to the publication

Monomer and polymer synthesis, construction continuous flow setup, all flow experiments, manuscript writing and revision.

3.1 Introduction

Organic photovoltaics (OPV) have emerged as an attractive technology complementary to other types of solar cells, mainly aiming at portable and/or wearable consumer goods and building or automotive integration.[1] Despite the recent progress in efficiency, currently over 10% for solution-processed (polymer and small molecule) single junction devices, the cost-efficiency-reliability triangle still needs extra optimization to allow for a competitive market entrance.[2–5] An important bottleneck hindering further progress, in particular toward large area solution processing, module development and real-world applications, is material availability on a reasonable scale (*i.e.* multi-gram to kilogram), in high quality and with reproducible properties. At this moment, the conjugated polymer materials affording highest power conversion efficiencies (PCE's) in bulk heterojunction (BHJ) polymer solar cells are either synthesized on an individual research lab basis or provided by small and medium-sized enterprises (SME's) on an on-demand basis. This lack of a common materials source results in considerable batch-to-batch variations, in turn impacting ink formulation, device processing and the final photovoltaic parameters,[6] which substantially complicates comparison and benchmarking. Even though some SME's strive for real-life OPV products, the development of effective and scalable polymer synthesis processes is crucial toward economic success.[7] This aspect has been largely neglected to date, since most OPV research is conducted in academic labs with a primary focus on novel high performance materials and with limited resources for up-scaling.

Continuous flow chemistry has emerged as a powerful synthetic R&D technique providing an entry to faster, cheaper and cleaner material production.[8–12] Many chemical (*e.g.* pharmaceutical) companies have explored the potential of flow methods and have implemented them in their research and production facilities. The major advantages of flow technologies comprise, among others, faster (high surface to volume ratio, superior heat and mass transfer) and safer reactions (smaller intrinsic reaction volumes and increased reaction control), quick reaction optimization, easy scale-up, high reproducibility, reduced waste production and lower (energy/solvent) costs. Moreover, continuous flow procedures can lead to higher reaction selectivity, improved yield and enhanced product purity due to a more precise control of the reaction conditions and the contact times of the reagents. It has been stated that 40–60% of all organic reactions may profit from flow conditions.[12] Nonetheless, certain aspects have to be considered upon transferring batch processes to continuous flow methods. Especially reagent and/or (by)product precipitation and large viscosity increases should be avoided, since these can cause blockage of the flow.

Flow chemistry has recently also caught attention for the production of semiconducting polymers. Nonetheless, optimized flow protocols remain scarce, in particular with respect to conjugated polymers applicable in polymer

photovoltaics. Effective and scalable flow protocols were developed for the workhorse polymer P3HT (poly(3-hexylthiophene)).[13,14,15] Furthermore, flow synthesis of PPV-type conjugated polymers via the Gilch route was established, whereas low bandgap copolymers were created via Stille and Suzuki cross-coupling continuous flow methods, producing similar molar mass ranges as realized in batch.[16] Simultaneous to the present work, two OPV copolymers were prepared in flow as well, one by direct (hetero)arylation, resulting in OPV devices with a PCE of 1.8%, and another one by Stille cross-coupling polymerization, affording a maximum (roll-to-roll) efficiency of 3.8%.[17,18] On the other hand, the complementary methanofullerene electron acceptor materials, to be combined with the envisaged donor polymers in the BHJ photoactive layer, were also successfully prepared in flow.[19,20] The complete organic material set to be used in OPV devices hence can be prepared by flow techniques, thereby portraying the potential of continuous flow as a versatile tool to close the gap between OPV material discovery, evaluation/optimization in devices and technology take-off. For this purpose, careful batch to flow translation and flow optimization has to be established for state of the art photoactive materials.

Whereas the previous generation of polymer solar cells was mainly based on P3HT, there is no single widely used and studied benchmark material among the novel generation low bandgap (push-pull) copolymers. Most established research groups and industrial players focus on their own type of materials, which are then scarcely available to others. In the present work, PBDTTPD (poly[(benzo[1,2-*b*:4,5-*b*']dithiophene)-*alt*-(4*H*-thieno[3,4-*c*]pyrrole-4,6(5*H*)-dione)], with 2-ethylhexyloxy and octyl side chains on the BDT and TPD units, respectively) is chosen as the target copolymer to be prepared by continuous flow, as it provides high efficiency polymer solar cells, with a reported average PCE of 7.3% (increased to 8.3% by molar mass optimization).[21–23] PBDTTPD is also one of the most promising materials to be used in the high-bandgap cell of tandem solar cells. Additionally, PBDTTPD has been reported to show (dark) thermostability and unexpectedly high photostability, attributed to its alkoxy side chains and well-organized structure mitigating the photodegradation process.[21,24] Moreover, it has recently been classified quite near to P3HT based on the 'synthetic complexity' versus efficiency ratio.[25] As most donor-acceptor copolymers providing high-efficiency devices have a substantially larger synthetic complexity, PBDTTPD has been designated as one of the most suitable materials for highly efficient and scalable organic photovoltaics. Hence, PBDTTPD clearly has the potential to become the next-generation workhorse OPV polymer, pending smooth synthetic access to high quality material on a reasonable scale. To address this issue, we have first developed a small (mg) scale flow procedure for PBDTTPD. Thereafter, inter-run reproducibility tests were carried out and finally a proof-of-concept continuous flow production of 1.5 g of PBDTTPD was performed, probing the constant high polymer quality by standard solar cell tests.

3.2 Results and discussion

3.2.1 PBDTTPD synthesis

To obtain insights on the physicochemical material properties and to provide a means of comparison, the PBDTTPD copolymer was first prepared in batch (**P$_{batch}$**) by Stille polycondensation of the corresponding stannylated and brominated building blocks (Scheme 1). The polymerization reaction was done on a 50 mg scale in chlorobenzene at 110 °C employing the Pd$_2$dba$_3$/P(o-tol)$_3$ catalyst system according to a literature procedure.[22] The two required monomers, [4,8-bis(2-ethylhexyloxy)benzo[1,2-b:4,5-b']dithiophene-2,6-diyl]bis(trimethylstannane) (Me$_3$Sn-BDT-SnMe$_3$) and 1,3-dibromo-5-octyl-4H-thieno[3,4-c]pyrrole-4,6(5H)-dione (Br-TPD-Br) are commercially available or can easily be acquired by a short synthetic pathway.[21]
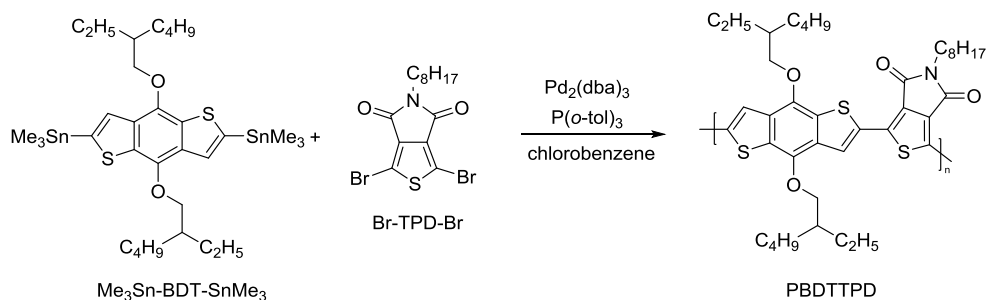
Scheme 1. Stille polycondensation of Me$_3$Sn-BDT-SnMe$_3$ and Br-TPD-Br, yielding the PBDTTPD copolymer.

Unfortunately, smooth analysis of the polymerization efficiency through molar mass determination via size exclusion chromatography (SEC) was complicated by the strong polymer aggregation at the measurement temperature of 60 °C using chlorobenzene as the mobile phase. When measuring on a SEC system at 140 °C with *ortho*-dichlorobenzene as the eluent, this aggregation tendency remained present (see Fig. S1 and S2).[26] Consequently, it was opted to use the resulting solar cell device performance as a material quality analysis tool to compare the polymer batches prepared by the different experimental setups (vide infra). Polymer solar cells are known to be very sensitive to the donor polymer purity, molar mass and molar mass distribution and hence provide a proper measure of semiconducting polymer quality.[6]

Similar to the batch protocol, continuous flow PBDTTPD synthesis was performed in chlorobenzene as a solvent to ensure proper solubility of both the catalytic complex and the monomers. Initial flow experiments were conducted on a modified commercially available Syrris Asia flow system equipped with a home-

made PFA (perfluoroalkyl) 11.6 mL tubular reactor (Fig. 1 and S3). The reactor size was chosen to be sufficiently large to minimize the amount of back and forward diffusion. Due to the rapid cooling outside the reactor (inherent to flow) it was not possible to attach a back-pressure regulator (BPR) to the system since this leads to accumulation of polymer material inside the BPR and inevitable blocking of the reactor. As a result, the reaction temperature was only slightly increased to 116 °C (compared to 110 °C in batch) to stay well below the boiling point of the solvent. To compensate for the large increase in viscosity of the reaction mixture (as observed in batch), the monomer concentration was decreased to 0.055 M, while the catalyst concentration was kept constant at 6 mol%.
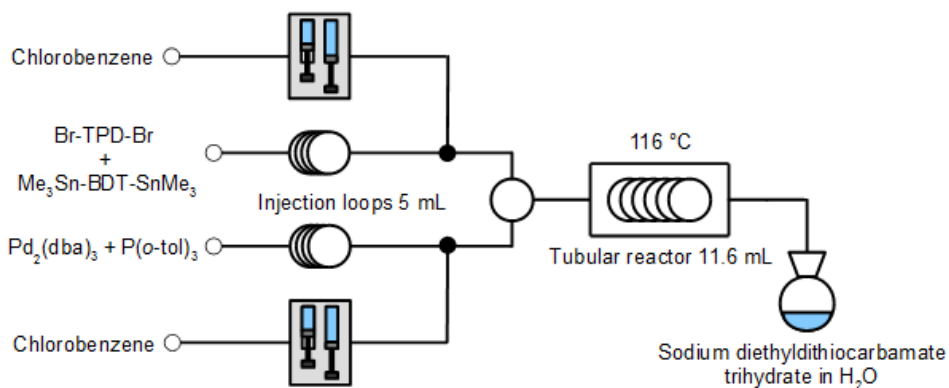
Figure 1. Schematic representation of the small scale fluidic set-up.

Two injectors with a volume of 5 mL were used, one loaded with a solution of the monomers and the other one with the catalyst solution, both in chlorobenzene. The reagents were mixed using a T-piece mixer. It was previously shown that for a Stille polycondensation in flow a residence time of 1 hour is sufficient to produce a polymer of similar molar mass as for a batch reaction running for 24 hours, demonstrating the potential of flow to significantly reduce reaction times.[16] Based on the internal volume of the system, a residence time of 1 hour was achieved by pumping both solutions at a fixed flow rate of 100 µL/min. Mixing the monomer and catalyst solutions results in an orange mixture at room temperature. The color of the mixture changes to red and rapidly to deep purple upon entering the reactor due to the fast increase in temperature and progressing of the reaction (see movie in SI). The product coming out of the reactor was dropped in a heavily stirred aqueous solution of sodium diethyldithiocarbamate (Cupral) to quench the reaction and complex Pd. The synthesized flow polymer was consequently purified by Soxhlet extractions with methanol and dichloromethane and final product collection was performed with chlorobenzene (as in batch). Precipitation in methanol and subsequent

filtration afforded 200 mg of the targeted PBDTTPD (**P_flow**), resulting in an overall polymerization yield of 90% (comparable to the literature batch yield).

The material quality as produced by continuous flow synthesis is expected to be independent on the production scale, since every point inside the reactor is subjected to the same reaction conditions (if the initial concentrations are maintained and neglecting back and forward diffusion). In contrast, batch polymerizations can only be scaled up to a limited extent. Due to the rapidly increasing volume of the batch reactor, the mixing efficiency decreases and heat distribution within the vessel becomes more heterogeneous and higher molar masses can only be obtained by increasing reaction times. To investigate the consistency of the material quality during the flow process, a second experiment was performed (on the same scale) in which the polymer was fractionated in three samples of approximately similar size (at the start, middle and end of the process). This fractionation test yielded 168 mg (78%) of PBDTTPD (**P_flow,F1−3**). The slightly reduced yield can be attributed to the triplicate small scale purification procedure applied.

In a final step, the scalability of the flow polymerization reaction was investigated. For this experiment, the precursor materials were freshly synthesized to rule out strong monomer batch-to-batch dependency. Minor adjustments were made to the fluidic setup to achieve an efficient scale-up without jeopardizing material quality (Fig. 2).
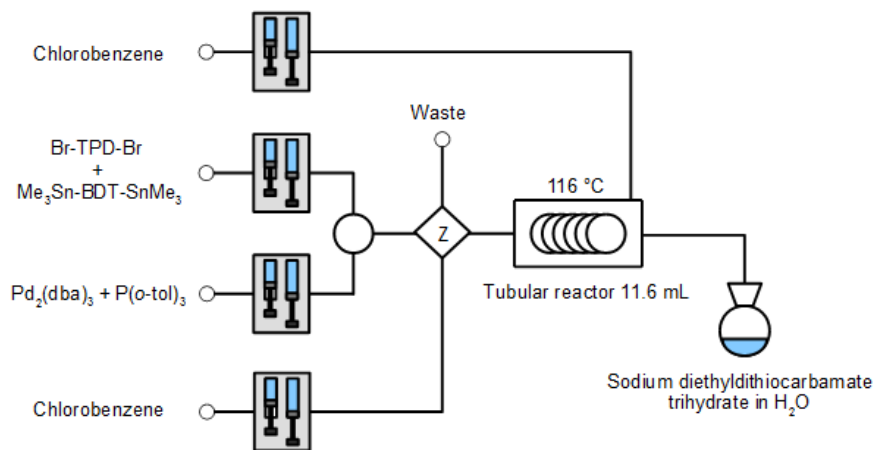

Figure 2. Schematic representation of the fluidic set-up applied for the up-scaling experiment (Z = flow switch).

Instead of using injectors, the monomer and catalyst solutions were pumped directly from solvent bottles (under inert atmosphere) into the system. Similar to the previous flow experiments, monomer and catalyst concentrations were retained at 0.055 M and 6 mol%, respectively. A solvent switch was implemented directly after reagent mixing to empty the reactor at a flow rate of 200 µL/min and as a means to collect all produced polymer, even after the reagent bottles are depleted. The outlet of the reactor was flushed every two hours with a fresh stream of chlorobenzene to remove adhered polymer from the reactors inner walls, caused by the decreased polymer solubility as a result of the lower temperature of the connection line between the reactor and the quenching flask. The final polymer was purified in an identical way as mentioned above. A flow run of 8 hours afforded 1.55 g of PBDTTPD (**P$_{flow,L}$**) in a high overall polymerization yield of 95%.

3.2.2 Photovoltaic properties

The material quality of the various PBDTTPD polymer samples was then evaluated in BHJ OPV devices fabricated using the conventional architecture glass/ITO/PEDOT:PSS/PBDTTPD:PC$_{71}$BM/Ca/Al. The PBDTTPD:PC$_{71}$BM blend solutions were prepared in a 1:1.5 ratio (wt/wt%) with a total concentration of 20 mg/mL and an optimal processing solvent mixture (95% chlorobenzene and 5% 1-chloronaphthalene), according to literature procedures.[22,27]

To guarantee a proper translation from batch to flow, an initial assessment was made for the PBDTTPD polymer samples made by the small scale flow and batch experiments (**P$_{flow}$** and **P$_{batch}$**). As can be seen in Table 1 (entries 1–3) and Fig. 3, minor fluctuations for all *I-V* parameters were observed and an average PCE (7.0%) in the range of the literature value was obtained. Nonetheless, comparison with literature values shows minor deviations (a slightly lower short-circuit current (J_{sc}), compensated by a small increase in fill factor (FF)), which are tentatively ascribed to small differences in the device processing procedure and facilities.

In a next step, the consistency of the material quality over the flow synthesis timescale was investigated by analyzing the three different fractions (**P$_{flow,F1}$**, **P$_{flow,F2}$** and **P$_{flow,F3}$**) obtained at different stages during the flow process. Again, similar device performances were achieved for the three fractions (Table 1, entries 4–6). For either the average or best PCE results, standard deviations of less than 0.25 were obtained for the three fractions, nicely demonstrating that the material quality is satisfactorily consistent during the whole flow production process and that it is not likely to diminish upon up-scaling. Comparison of the *I-V* characteristics for the two small scale flow syntheses also reveals a high run-to-run reproducibility (Table 1).

Table 1. Photovoltaic performances of the BHJ polymer solar cells based on batch and flow-synthesized PBDTTPD (in combination with $PC_{71}BM$ in a 1:1.5 ratio; spin-coating from chlorobenzene + 5% 1-chloronaphthalene).

Entry	Polymer	V_{oc} [V]	J_{sc} [mA/cm^2]	FF	Aver. PCE [%][b]	Best PCE [%]
1	**P**[lit.](a)	0.93	12.5	0.65	7.3	7.5
2	**P**batch	0.94	10.4	0.71	6.9	7.9
3	**P**flow	0.92	11.3	0.69	7.1	7.6
4	**P**flow,F1	0.92	11.6	0.70	7.4	7.6
5	**P**flow,F2	0.92	11.2	0.70	7.2	7.2
6	**P**flow,F3	0.92	11.8	0.69	7.5	7.7
7	**P**flow,L	0.92	11.4	0.67	7.0	7.5
8[c]	**P**flow	0.93	12.5	0.71	8.2	9.1

[a] Values according to Beaujuge et al.[22] [b] Averages over at least 8 devices. [c] Device with CPE-TFSI cathodic interlayer.

Finally, photovoltaic devices were also fabricated from the PBDTTPD polymer (**P**flow,L) resulting from the up-scaled flow experiment (Fig. 3 and Table 1, entry 7). With an average PCE of 7.0% (best device 7.5%), the polymer solar cells fit nicely to the previous results. At this moment, such high OPV performance for a polymer prepared by continuous flow synthesis is unprecedented.

Conjugated polyelectrolytes (CPE's), conjugated polymers bearing ionic (side chain) moieties, have been successfully applied as efficiency-boosting interfacial materials in organic and hybrid solar cell devices.[28–30] Past efforts within our group on ionic polythiophene-based cathodic interlayers (to replace Ca) afforded clear PCE enhancements.[30,31] To optimize the photovoltaic performance of the PBDTTPD:$PC_{71}BM$ solar cells presented in this work, a specific CPE material (see Fig. S4)[32] was implemented in freshly prepared devices (using the **P**flow sample). As visualized in Table 1 and Fig. 3, a clear improvement in J_{sc}, from 11.3 to 12.5 mA/cm² (on average), was achieved, with minor increases in open-circuit voltage (V_{oc}) and FF. These improvements grant an average PCE increase from 7.1 to 8.2%, with a hero device of 9.1%, a record efficiency for PBDTTPD-based polymer solar cells (to the best of our knowledge). Investigation of the external quantum efficiency (EQE) spectra revealed a distinctly higher maximum (~82% at 500 nm) for the solar cell containing the CPE interlayer in comparison to the standard Ca/Al device (Fig. 4). The current densities extracted from the solar cells with and without interlayer employed for the EQE measurements (J_{EQE} = 13.2 and 10.6 mA/cm², respectively) correspond with the observed trend in J_{sc} (12.5 and 11.6 mA/cm², respectively), in accordance with standard measurement deviations.
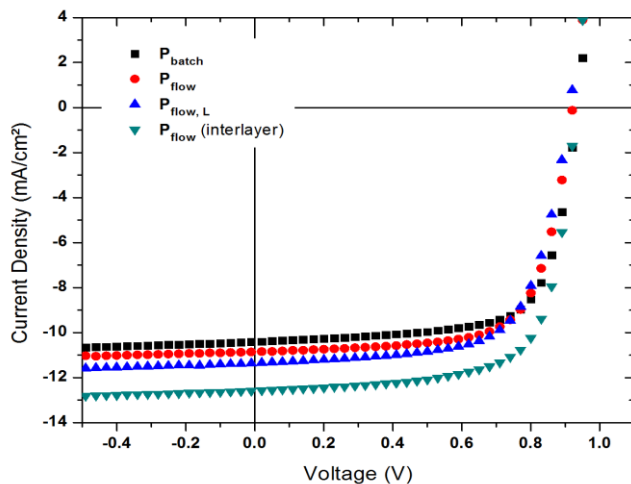
Figure 3. *J-V* curves of (average efficiency) BHJ OPV devices based on PBDTTPD synthesized by batch and flow (on different scale).

3.3 Conclusions

One of the major hurdles to overcome for OPV to achieve the next level of technology development is the lack in availability of high quality state of the art materials on a reasonable (multi-gram) scale. Continuous flow chemistry is known to be a viable method for intermediate-scale product synthesis, especially in the pre-commercialization stage, providing additional assets in terms of speed, safety and purity with limited investment costs. However, it is only recently being introduced for the synthesis of organic semiconducting materials. In this work, we have established an effective flow protocol for the high-performance copolymer PBDTTPD, recently proclaimed as one of the most promising materials for highly efficient and scalable organic solar cells. The flow procedure was performed on a (slightly adjusted) commercially available continuous flow system and up-scaling to 1.5 gram in a single run was readily achieved. The device-grade PBDTTPD flow samples afforded an average solar cell efficiency of 7.2% and this result was reproducible over several experiments. Furthermore, upon implementation of an ionic polythiophene-based cathodic interlayer, the efficiency could be enhanced to a maximum value of 9.1%, a record performance for this material to date. Future activities will focus on extending the flow procedure to an equipment allowing straightforward multi-gram production of PBDTTPD and related low bandgap copolymers.

3.4 Supporting information

3.4.1 Synthetic procedures

Materials and methods

[4,8-Bis(2-ethylhexyloxy)benzo[1,2-*b*:4,5-*b*']dithiophene-2,6-diyl]bis(trimethyl stannane) (Me$_3$Sn-BDT-SnMe$_3$) was synthesized according to a literature procedure.[22,33-34] 1,3-Dibromo-5-octyl-4*H*-thieno[3,4-*c*]pyrrole-4,6(5*H*)-dione (Br-TPD-Br) was either purchased from Sigma-Aldrich (≥ 99.5%) or prepared according to a literature procedure.[22,35] The imidazolium-substituted random copolythiophene (CPE-TFSI, 50/50; Fig. S4) used as a cathodic interlayer has previously been synthesized and applied in our group.[30-32] Commercial reagents were used as purchased without any prior purification.

Continuous flow experiments were conducted on a modified lab-scale flow chemistry reactor (Syrris Asia 330; see Fig. S3). The modular system comprises 4 pump channels, a pressurized input store (N$_2$/Ar atmosphere) and 4 injectors. For all reported experiments, an 11.6 mL PFA (perfluoroalkoxy) tubular reactor was connected to the system and for the up-scaling experiment the system was extended with a Knauer AZURA P2.1S HPLC pump.

NMR measurements were performed in CDCl$_3$ on 300/400 MHz instruments (Varian). Molar mass (distribution) data were obtained by size exclusion chromatography using a Spectra Series P100 pump equipped with two mixed-B columns (10 µm, 2 cm × 30 cm, Polymer Laboratories) and an Agilent 1100 diode array detector with chlorobenzene as an eluent at 60 °C and a flow rate of 1.0 mL min^{-1}. Additional measurements employing *ortho*-dichlorobenzene as an eluent at 140 °C were done on an Agilent PL-GPC-220 system equipped with a 10 µm mixed-B column. Both systems were calibrated using linear narrow polystyrene standards.

Batch synthesis

In a dry 50 mL round-bottom flask equipped with a magnetic stirring bar, 1,3-dibromo-5-octyl-4*H*-thieno[3,4-*c*]pyrrole-4,6(5*H*)-dione (Br-TPD-Br; 41.1 mg, 0.0974 mmol), [4,8-bis(2-ethylhexyloxy)-benzo[1,2-*b*:4,5-*b*']dithiophene-2,6-diyl]bis(trimethylstannane) (Me$_3$Sn-BDT-SnMe$_3$; 75.0 mg, 0.0969 mmol), Pd$_2$(dba)$_3$ (2.66 mg, 0.0029 mmol) and P(*o*-tol)$_3$ (3.55 mg, 0.0064 mmol) were loaded. Freshly degassed chlorobenzene (1.8 mL) was added and the reaction mixture was stirred for 24 h at 110 °C. After cooling down to room temperature, sodium diethyldithiocarbamate trihydrate (0.675 g, 2.99 mmol), dissolved in water (6 mL), was added and the mixture was additionally stirred for 1 h. The organic phase was then washed with water and the (crude) polymer was precipitated in methanol. The precipitate was filtered through a Soxhlet thimble, after which the polymer was purified using Soxhlet extractions with methanol (2

h) and dichloromethane (20 h). The polymer was then collected via Soxhlet extraction with chlorobenzene and subsequently precipitated once again in methanol. Filtration and drying under high vacuum finally yielded 48 mg (70%) of PBDTTPD (P_{batch}) as a dark purple solid.

Small scale flow synthesis (see fluidic set-up in Fig. 1)

The Syrris Asia flow chemistry system was connected to a home-made PFA tubular reactor with an internal volume of 11.6 mL and a channel diameter of 0.75 mm. The two injector (5 mL) solutions were prepared in freshly degassed chlorobenzene (5 freeze-pump-thaw cycles) under argon atmosphere. The BDT and TPD monomers were injected as a single solution with individual monomer concentrations of 0.055 M (injector 1). A 6 mol% catalyst solution (*i.e.* 3 mol% $Pd_2(dba)_3$ and 6 mol% $P(o\text{-tol})_3$) was injected from the second injector. The two reagent solutions were simultaneously pumped into the system, each with a flow rate of 100 µL/min, resulting in an overall residence time of ~1 h (58 min). A back pressure regulator (BPR) could not be attached to the exit of the reactor due to the adherence of the concentrated polymer to the tubing's inner wall, induced by the temperature drop at the outlet of the reactor. The BPR was hence only used during priming of the system. The polymerization was performed at a set temperature of 116 °C. The product was collected in a round-bottom flask containing a sodium diethyldithiocarbamate trihydrate solution (0.09 M in water) while stirring. The resulting biphasic mixture was stirred for another 15 min after complete collection. The mixture was then separated and the organic phase was added in a dropwise manner to an equal amount of methanol, resulting in precipitation of the polymer. The polymer suspension was then filtered over a Soxhlet thimble. The (crude) polymer was further purified by consecutive Soxhlet extractions with methanol (3 h) and dichloromethane (16 h), and then finally collected via Soxhlet extraction with chlorobenzene (8 h). The resulting polymer (in chlorobenzene) was again precipitated in methanol. After filtration and drying under high vacuum, the PBDTTPD material (P_{flow}) was obtained in a yield of 90% (200 mg). It was used in OPV tests without any further purification. Upon polymer fractionation, the (combined $P_{flow,F1-3}$) yield slightly dropped to 78% (168 mg) due to extra losses during the work-up and purification.

Large scale flow synthesis (see fluidic set-up in Fig. 2)

Similar to the small scale (fractionation) experiment, two (42 mL) solutions were prepared in freshly degassed chlorobenzene (5 freeze-pump-thaw cycles) under argon atmosphere, with a monomer concentration of 0.055 M and using 6 mol% of catalyst. In this case, the reagent solutions were pumped directly from the solvent bottles. In order to inject everything into the system, a solvent switch was implemented directly after the pumps. After complete injection, a switch was made to an additional pump with fresh chlorobenzene, pumping at a set

flow rate of 200 µL/min. The polymerization was performed at 116 °C (similar to the small scale flow experiments). The exit of the reactor was equipped with a T-piece delivering fresh chlorobenzene to flush the connection line in between of the reactor and the quenching vessel (5 mL/min pulse, done every 2 h as polymer material started to adhere to the walls of the tubing outside the reactor). The polymer was purified in a similar fashion as outlined above. Drying under high vacuum finally yielded 1.558 g (95%) of PBDTTPD (**P$_{flow,L}$**).

### 3.4.2 Photovoltaic device fabrication and characterization

Bulk heterojunction organic solar cells were fabricated using the conventional architecture glass/ITO/PEDOT:PSS/PBDTTPD:PC$_{71}$BM/Ca/Al. Prior to device processing, the ITO-coated substrates (100 nm, Kintec, sheet resistivity 20 Ω/sq) were subjected to a standard cleaning procedure using soap, demineralized water, acetone and isopropanol, followed by a UV/O$_3$ treatment for 15 min. PEDOT:PSS [poly(3,4-ethylenedioxythiophene):poly(styrenesulfonic acid), Heraeus Clevios] was deposited by spin-coating, aiming at a layer thickness of ~30 nm. Further processing was performed under nitrogen atmosphere in a glove box (<1 ppm O$_2$/H$_2$O), starting off with an annealing step at 130 °C for 15 min to remove any residual water taken up by the PEDOT:PSS layer. The photoactive layer solution was prepared by dissolving PBDTTPD and PC$_{71}$BM (Solenne) in the solvent mixture chlorobenzene:1-chloronaphthalene (95:5 vol%). A polymer:fullerene ratio of 1:1.5 (wt/wt) was used with a total concentration of 20 mg/mL and the solution was stirred overnight at 75 °C to ensure proper dissolution.[22] The active layer was deposited on top of the PEDOT:PSS layer by means of spin-coating at a processing temperature of 115 °C with an optimal layer thickness of 110−120 nm. To ensure proper removal of the additive from the photoactive layer, the samples were placed in a vacuum chamber with a pressure of 5 x 10^{-7} mbar for 2 h. In a final step, the top electrodes Ca and Al were deposited by vacuum deposition with layer thicknesses of 30 and 80 nm, respectively, to obtain complete solar cell devices with an active area of 3 mm². For the device employing the CPE-TFSI cathodic interlayer (Fig. S4), no Ca was employed in the device stack. Prior to spin-coating on top of the photoactive layer, the CPE material was dissolved in methanol with an optimized concentration of 0.6 mg/mL. The *I-V* characteristics of all photovoltaic devices were evaluated under AM1.5G solar illumination (100 mW/cm²) using a Newport class A solar simulator (model 91195A), calibrated with a silicon solar cell. EQE measurements were performed with a Newport Apex illuminator (100 W Xenon lamp, 6257) as light source, a Newport Cornerstone 130° monochromator and a Stanford SR830 lock-in amplifier for the current measurements. A silicon FDS100-CAL photodiode was employed as a reference cell.

3.4.3 ^{1}H NMR spectra of the applied BDT and TPD monomers

[4,8-Bis(2-ethylhexyloxy)benzo[1,2-b:4,5-b']dithiophene-2,6-diyl]bis(trimethylstannane)
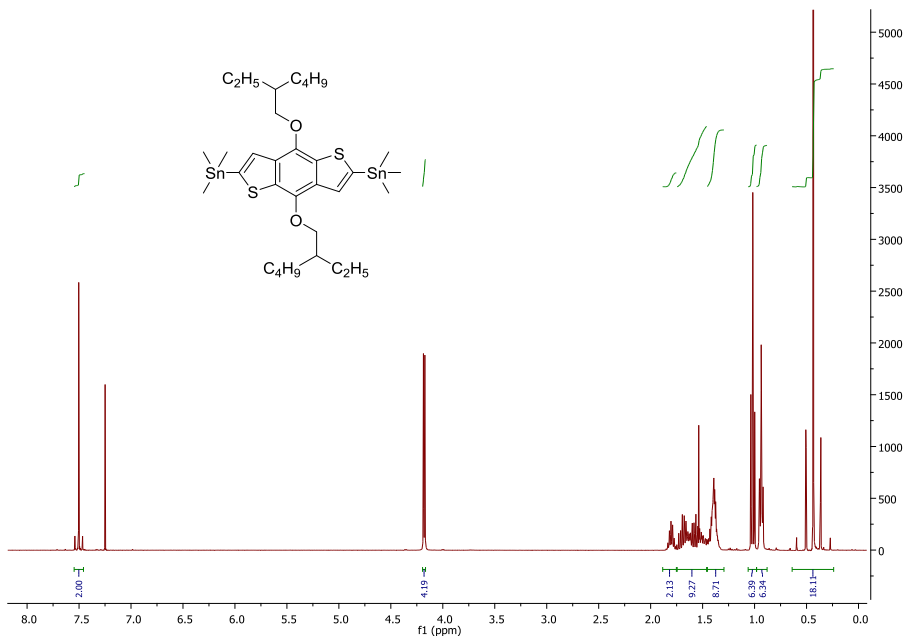
1,3-Dibromo-5-octyl-4H-thieno[3,4-c]pyrrole-4,6(5H)-dione
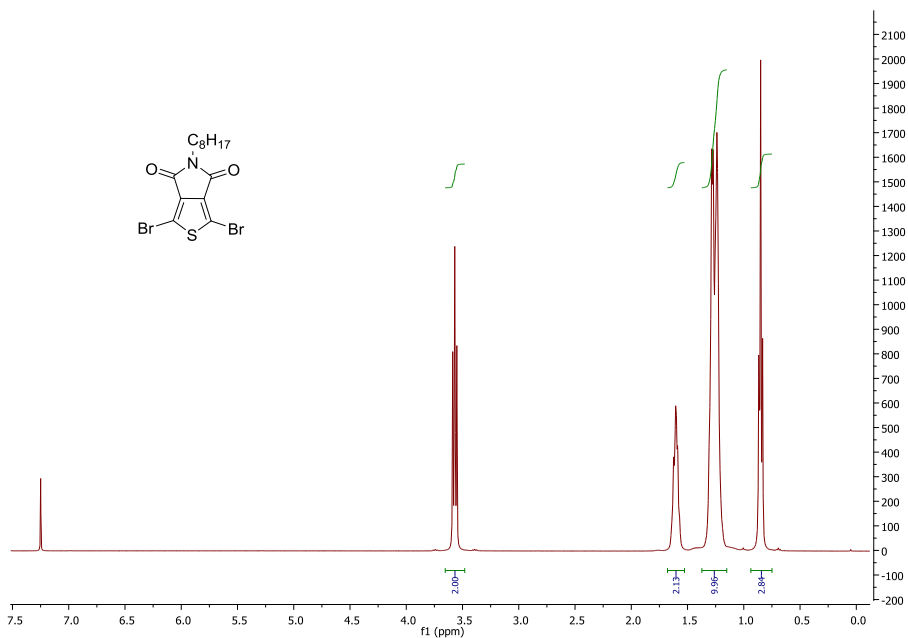
3.4.4 Size exclusion chromatograms
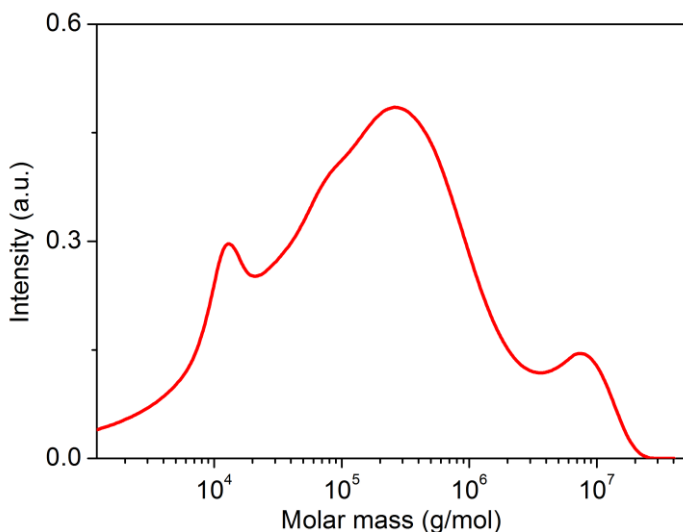
Figure S1. Molar mass distribution obtained from the analytical size exclusion chromatogram of PBDTTPD (**P_flow**) (after Soxhlet extractions; eluent chlorobenzene, 60 °C, optical detection).
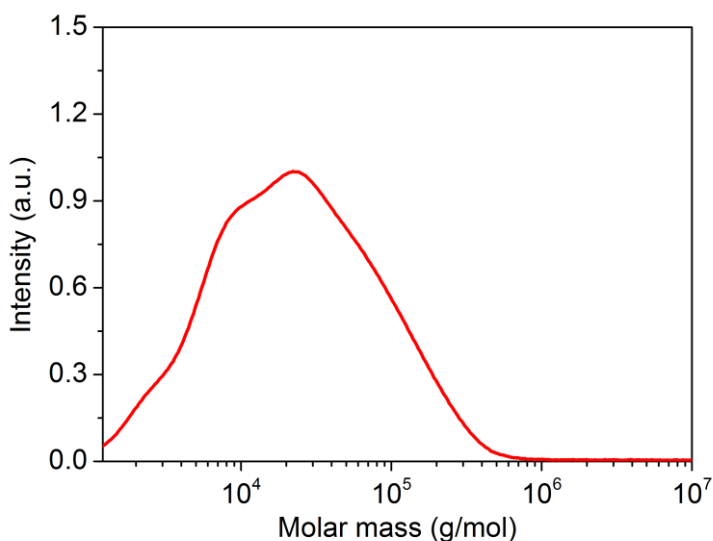
Figure S2. Molar mass distribution obtained from the analytical size exclusion chromatogram of PBDTTPD (**P_flow**) (after Soxhlet extractions; eluent *ortho*-dichlorobenzene, 140 °C, optical detection at 550 nm).

3.4.5   Picture of the fluidic set-up

Figure S3. Modified Syrris Asia continuous flow set-up: syringe pumps (Syrris Asia; **1**), Knauer AZURA P2.1S HPLC pump (**2**), solvent reservoir bottles (**3**), injectors (5 mL; **4**), solvent switcher (**5**), 11.6 mL tubular reactor (**6**), and T-piece mixer (**7**).

3.4.6   CPE interlayer material
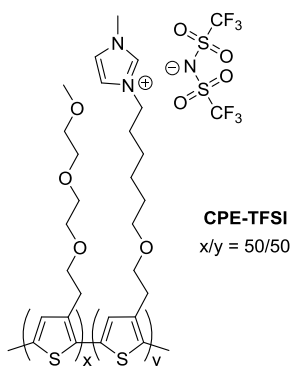
Figure S4. Structure of the conjugated polyelectrolyte applied as cathodic interlayer material (CPE-TFSI, with bis(trifluoromethylsulfonyl)imide counterion).[32]

3.5 References

(1)   L. Dou, J. You, Z. Hong, Z. Xu, G. Li, R. A. Street, Y. Yang, *Adv. Mater.* **2013**, 25, 6642.

(2)   J. Kong, S. Song, M. Yoo, G. Y. Lee, O. Kwon, J. K. Park, H. Back, G. Kim, S. H. Lee, H. Suh, K. Lee, *Nat. Commun.* **2014**, 5, 5688.

(3)   Z. He, C. Zhong, S. Su, M. Xu, H. Wu, Y. Cao, *Nat. Photonics* **2012**, 6, 593.

(4)   Y. Liu, J. Zhao, Z. Li, C. Mu, W. Ma, H. Hu, K. Jiang, H. Lin, H. Ade, H. Yan, *Nat. Commun.* **2014**, 5, 5293.

(5)   B. Kan, M. Li, Q. Zhang, F. Liu, X. Wan, Y. Wang, W. Ni, G. Long, X. Yang, H. Feng, Y. Zuo, M. Zhang, F. Huang, Y. Cao, T. P. Russell, Y. Chen, *J. Am. Chem. Soc.* **2015**, 137, 3886.

(6)   T. Vangerven, P. Verstappen, J. Drijkoningen, W. Dierckx, S. Himmelberger, A. Salleo, D. Vanderzande, W. Maes, J. V. Manca, *Chem. Mater.* **2015**, 27, 3726.

(7)   S. Lizin, S. Van Passel, E. De Schepper, W. Maes, L. Lutsen, J. Manca, D. Vanderzande, *Energy Environ. Sci.* **2013**, 6, 3136.

(8)   G. Jas, A. Kirschning, *Chem. Eur. J.* **2003**, 9, 5708.

(9)   P. Watts, S. J. Haswell, *Chem. Soc. Rev.* **2005**, 34, 235.

(10)   T. R. Dietrich, Microchemical Engineering in Practice, John Wiley & Sons, Inc., **2009**.

(11)   C. Wiles, P. Watts, *Green Chem.* **2012**, 14, 38.

(12)   S. G. Newman, K. F. Jensen, *Green Chem.* 2013, 15, 1456.

(13)   H. Seyler, J. Subbiah, D. J. Jones, A. B. Holmes, W. W. H. Wong, Beilstein *J. Org. Chem.* **2013**, 9, 1492.

(14)   J. H. Bannock, S. H. Krishnadasan, A. M. Nightingale, C. P. Yau, K. Khaw, D. Burkitt, J. J. M. Halls, M. Heeney, J. C. de Mello, *Adv. Funct. Mater.* **2013**, 23, 2123.

(15)   A. Kumar, J. Hasan, A. Majji, A. Avhale, S. Gopinathan, P. Sharma, D. Tarange, R. Bajpai, A. Kumar, *J. Flow Chem.* **2014**, 4, 206.

(16)   H. Seyler, D. J. Jones, A. B. Holmes, W. W. H. Wong, *Chem. Commun.* **2012**, 48, 1598.

(17)   F. Grenier, B. R. Aich, Y. Lai, M. Guérette, A. B. Holmes, Y. Tao, W. W. H. Wong, M. Leclerc, *Chem. Mater.* **2015**, 27, 2137.

(18) M. Helgesen, J. E. Carlé, G. A. dos Reis Benatto, R. R. Søndergaard, M. Jørgensen, E. Bundgaard, F. C. Krebs, *Adv. Energy Mater.* **2015**, 1401996.

(19) H. Seyler, W. W. H. Wong, D. J. Jones, A. B. Holmes, *J. Org. Chem.* **2011**, 76, 3551.

(20) E. Rossi, T. Carofiglio, A. Venturi, A. Ndobe, M. Muccini, M. Maggini, *Energy Environ. Sci.* **2011**, 4, 725.

(21) Y. Zou, A. Najari, P. Berrouard, S. Beaupré, B. R. Aïch, Y. Tao, M. Leclerc, *J. Am. Chem. Soc.* **2010**, 132, 5330.

(22) Cabanetos, A. El Labban, J. A. Bartelt, J. D. Douglas, W. R. Mateker, J. M. J. Fréchet, M. D. McGehee, P. M. Beaujuge, *J. Am. Chem. Soc.* **2013**, 135, 4656.

(23) J. A. Bartelt, J. D. Douglas, W. R. Mateker, A. El Labban, C. J. Tassone, M. F. Toney, J. M. J. Fréchet, P. M. Beaujuge, M. D. McGehee, *Adv. Energy Mater.* **2014**, 4, 1301733.

(24) A. Tournebize, J.-L. Gardette, C. Taviot-Guého, D. Bégué, M. A. Arnaud, C. Dagron-Lartigau, H. Medlej, R. C. Hiorns, S. Beaupré, M. Leclerc, A. Rivaton, *Polym. Degrad. Stab.* **2015**, 112, 175.

(25) R. Po, G. Bianchi, C. Carbonera, A. Pellegrino, *Macromolecules* **2015**, 48, 453.

(26) X. Lou, J. L. J. van Dongen, Y. Braeken, J. Brebels, G. W. P. van Pruissen, W. Li, M. M. Wienk, R. A. J. Janssen *Polym. Chem.* **2014**, 5, 558.

(27) Dyer-Smith, I. A. Howard, C. Cabanetos, A. El Labban, P. M. Beaujuge, F. Laquai, *Adv. Energy Mater.* **2015**, 1401778.

(28) Z. He, C. Zhong, X. Huang, W. Y. Wong, H. Wu, L. Chen, S. Su, Y. Cao, *Adv. Mater.* **2011**, 23, 4636.

(29) S. Liu, K. Zhang, J. Lu, J. Zhang, H. L. Yip, F. Huang, Y. Cao, *J. Am. Chem. Soc.* **2013**, 135, 15326.

(30) J. Kesters, T. Ghoos, H. Penxten, J. Drijkoningen, T. Vangerven, D. M. Lyons, B. Verreet, T. Aernouts, L. Lutsen, D. Vanderzande, J. Manca, W. Maes, *Adv. Energy Mater.* **2013**, 3, 1180.

(31) W. Vanormelingen, J. Kesters, P. Verstappen, J. Drijkoningen, J. Kudrjasova, S. Koudjina, V. Liégeois, B. Champagne, J. Manca, L. Lutsen, D. Vanderzande, W. Maes, *J. Mater. Chem. A* **2014**, 2, 7535.

(32) T. Ghoos, J. Brassinne, C.-A. Fustin, J.-F. Gohy, M. Defour, N. Van Den Brande, B. Van Mele, L. Lutsen, D. J. Vanderzande W. Maes, *Polymer* **2013**, 54, 6293.

(33)   J. Hou, M.-H. Park, S. Zhang, Y. Yao, L.-M. Chen, J.-H. Li, Y. Yang, *Macromolecules* **2008**, *41*, 6012.

(34)   Y. J. He, Y. Zhou, G. J. Zhao, J. Min, X. Guo, B. Zhang, M. J. Zhang, J. Zhang, Y. F. Li, F. L. Zhang, O. Inganas, *J. Polym. Sci. A: Polym. Chem.* **2010**, *48*, 1822.

(35)   D. Cornelis, H. Peeters, S. Zrig, B. Andrioletti, E. Rose, T. Verbiest, G. Koeckelberghs, *Chem. Mater.* **2008**, *20*, 2133.

Chapter 4

Molecular weight tuning of low bandgap polymers by continuous flow chemistry: increasing the applicability of PffBT4T for organic photovoltaics
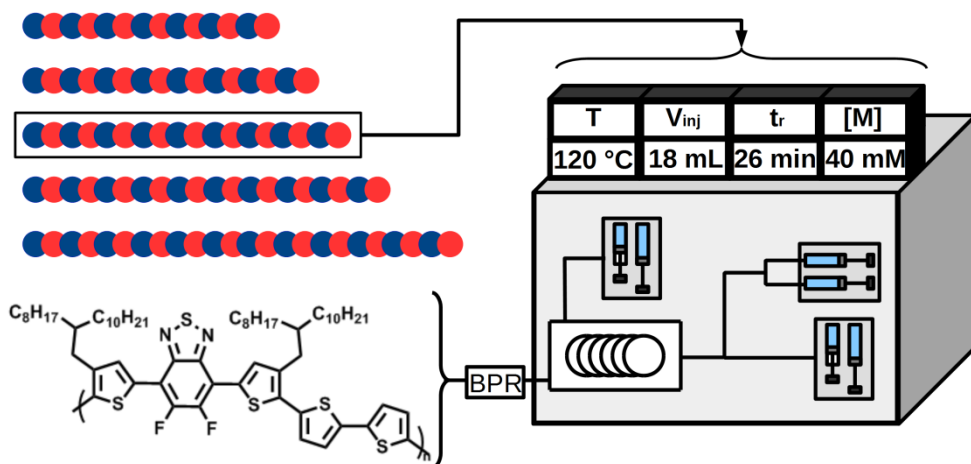
Abstract

Continuous flow chemistry has been shown to be a suitable method for the large-scale preparation of conjugated polymers with uniform structural and macromolecular characteristics, which is especially relevant when applying these materials in optoelectronic devices. The molecular weight and dispersity of conjugated polymers have a major effect on final device performance through a combination of processing and morphological considerations. In this work, the low bandgap polymer PffBT4T-2OD ('PCE-11'), which provides highly efficient bulk heterojunction solar cells, is synthesized by continuous flow chemistry using an easily mountable home-made apparatus. The influence of various reaction parameters on the material characteristics is investigated. Particular attention is devoted to tuning of the molecular weight, as this has a major impact on solubility and processability of the resultant polymer and, ultimately, solar cell performance. We find that temperature, monomer concentration, and injection volume of the polymerization mixture are significant parameters that can be used to optimize the control over molecular weight. The same protocol is then also applied to a structurally similar polymer with longer alkyl side chains, PffBT4T-2DT, affording important advantages in terms of processing due to its higher solubility. A power conversion efficiency of 9.4% for bulk heterojunction solar cells using $PC_{71}BM$ as the acceptor phase is achieved based on this flow-synthesized polymer.

Contribution to the publication

Construction continuous flow setup, all flow experiments, manuscript writing and revision.

4.1 Introduction

Over the past decade, bulk heterojunction (BHJ) organic photovoltaic (OPV) devices have received significant interest as potential renewable energy sources. Organic thin-films provide flexibility, tunable absorption profiles, and the ability to be printed. For these reasons OPV devices can be particularly attractive for portable and/or wearable consumer goods, building or automotive integration, and partial replacement of conventional power sources.[1,2] Several material combinations of electron donor polymers and acceptors affording power conversion efficiencies (PCEs) over 10% in solution processed (single-layer) BHJ devices have been reported, with further improvements still on the horizon, in particular for fullerene-free (so called non-fullerene) OPVs.[3–11] Along with higher efficiency and improved lifetime, upscaling of OPV technology in both materials preparation and processing is crucial if this technology is to become commercially relevant. Two major aspects are currently hampering the implementation of polymer-based solar cells in large area modules for industrial and domestic energy production, along with commercially viable niche products such as wearable electronics and portable energy sources. Firstly, there is a notable lack in the availability of large quantities (gram to kilogram scale) of high-quality photoactive polymers with uniform characteristics. Most low bandgap polymers are synthesized on a lab scale (maximum several hundreds of milligrams) and batch-to-batch variations must be avoided when moving to a production process. Secondly, most reports simply mention optimized solar cell efficiencies for spin-coated devices and the translation of these results to a large area printing facility (e.g. roll-to-roll, R2R[12–14]) is generally not performed, although this is required to push OPV to the market. Both the conventional synthesis and processing procedures thus lack the intrinsic character of being easily scalable and these aspects urgently need to be addressed by the research community.

Unfortunately, batch chemistry protocols for the synthesis of (push-pull type) conjugated polymers have a limited upscaling capacity.[15] Flow chemistry has several advantages over batch, which includes (i) superior mixing, (ii) precise control on reagent addition, and (iii) enhanced heat transfer, which minimizes the number of hotspots during reaction and also allows precise control over the temperature.[16–21] As the reaction kinetics and viscosity of the reaction mixture are highly temperature dependent, it is particularly interesting to synthesize these polymers via flow, as this will minimize batch-to-batch variations due to fluctuations in temperature. In order for OPV to become an industrially relevant technology, the active materials will ultimately need to be synthesized on a large scale, which goes well beyond the laboratory scale typically employed. Using flow chemistry methods, larger quantities of material can easily be made by longer operation times without altering the reaction conditions. Production rates can be further enhanced by increasing the reactor length or by parallelization of multiple set-ups.[22–28] With the latter approach, the operator scales out the entire

process rather than scaling it up. This has the advantage that the reaction conditions do not have to be optimized again and the safety risks are similar, which is for conventional upscaling frequently not the case.

Continuous flow chemistry has emerged as a versatile and readily accessible technology for the preparation of organic semiconductors. Over the past couple of years, several reports have been published on the flow synthesis of conjugated polymers via Kumada, Stille, and Suzuki cross-coupling approaches.[15,28–32] In addition to the use of these conventional coupling reactions, also direct arylation polymerization has been deployed in flow.[33] Continuous flow chemistry has thus created an accessible platform for the production of conjugated polymers on a gram scale. Moreover, the flow-synthesized polymers have shown a high reproducibility from batch-to-batch with respect to the final PCE in solar cell devices (with absolute differences <0.5%).[15,31]

There are multiple parameters that influence the efficiency of BHJ polymer solar cells. One of them, which finds its origin in the synthesis process, is the molecular weight of the deployed electron donor polymer.[34–38] It is rather difficult to define an optimal molecular weight as it influences multiple parameters simultaneously in both a positive and negative manner. High molecular weights have been shown to enhance the charge carrier mobility, photoactivity, and electrode surface interfacial ordering of the polymer.[39–44] On the other hand, the molecular weight also strongly influences the solubility of the polymer which is, together with its miscibility with the acceptor material, a key feature in achieving the desired 'intimately mixed' BHJ blend. Too high molecular weights can lead to materials that are not sufficiently soluble within the experimental window of device processing, and can cause large domain sizes to form during phase separation with the acceptor. With the latter type of morphology, a significant number of excitons will be generated in the bulk of the donor material, at distances larger than the exciton diffusion length from the acceptor phase. These excitons are more likely to decay before they reach the interface where charge separation can occur.

Although it has been shown that flow chemistry can effectively be used for the continuous production of OPV donor polymers[15,31], little investigation has been done on controlling the process itself. In this work, we elaborate on the influence of different parameters of the flow process, including monomer concentration, temperature, and reaction volume, on the final molecular weight of the produced polymer. For this purpose, the low bandgap donor polymer PffBT4T-2OD [poly[(5,6-difluoro-2,1,3-benzothiadiazol-4,7-diyl)-*alt*-(3,3'''-di(2-octyldodecyl)-2,2';5',2'';5'',2'''-quaterthiophen-5,5-diyl)], so called 'PCE11'; Scheme 4] was chosen, as it provides one of the highest PCEs in the field (>10% with multiple fullerene derivatives), while being prepared from relatively easy to synthesize monomers.[3,45] The high PCE is attributed to the strong temperature-dependent

aggregation property of the polymer, which heavily depends on the molecular weight.[3] A specific synthetic protocol that allows for the controlled preparation of specific molecular weights of PffBT4T-2OD has not been reported, but will be especially useful in active material and device development and optimization. Based on the evaluation of commercially available PffBT4T-2OD, specific number-average molecular weights (M_n) between 40 and 60 kDa were targeted. Batch-based protocols delivered molecular weights ranging from 36 to 85 kDa with batch-to-batch variations up to 9 kDa. Polymers synthesized by flow chemistry displayed an accessible molecular weight range from 26 up to 55 kDa. The controlled flow polymerization was investigated as a function of (i) temperature, (ii) residence time, (iii) injection volume, and (iv) concentration, specifically with regard to the molecular weight of the polymeric product. The highest control over the molecular weight was achieved by variation of the reaction concentration.

Lastly, an optimized synthetic flow protocol was applied for the synthesis of the analogous polymer PffBT4T-2DT (poly[(5,6-difluoro-2,1,3-benzothiadiazol-4,7-diyl)-*alt*-(3,3′′′-di(2-decyltetradecyl)-2,2′;5′,2″;5″,2′′′-quaterthiophen-5,5-diyl)]; Scheme 4) with longer alkyl side chains (decyltetradecyl as opposed to octyldodecyl). Combination of this polymer with the non-fullerene acceptor IDTBR has been shown to afford similar efficiencies as PffBT4T-2OD (±10%).[9] The flow-synthesized polymer has a similar molecular weight as its PffBT4T-2OD analogue and combination with $PC_{71}BM$ in organic solar devices gave PCEs up to 9.8%.

4.2 Results and discussion

4.2.1 Commercially available PffBT4T-2OD

PffBT4T-2OD was initially purchased from two independent suppliers. To evaluate the material quality of the two polymer samples, BHJ OPV devices were fabricated following the protocols provided by the suppliers. The devices were constructed using the inverted architecture glass/ITO/ZnO/PffBT4T-2OD:$PC_{71}BM$/MoO$_3$/Ag. The active layer blend (PffBT4T-2OD:$PC_{71}BM$) was prepared in a 1:1.2 ratio (wt/wt%) with a total concentration of 7.5 and 5.5 mg/mL for the first and second supplier, respectively, and the optimal solvent mixture chlorobenzene:*o*-dichlorobenzene 1:1 with 3% diiodooctane (DIO). Before spin-coating, both the active layer solution and the substrate were heated to 110 °C. During the deposition of the active layer blend, major differences between the two polymer batches were observed. The first commercial material afforded uniform films, whereas the active layer solution from the second polymer batch immediately formed a gel upon contact with the substrate. Due to this gel formation, the active layer solution loses its capability to spread out evenly over the substrate during spin coating and remains

accumulated where it has been deposited (see Figure S4a). Both samples were analysed by gel permeation chromatography (GPC) at 140 °C with 1,2,4-trichlorobenzene as the eluent, exhibiting number-average molecular weights of 41.8 kDa (Đ 1.7) and 57.2 kDa (Đ 2.3) for the first and second material, respectively. It should be noted that the elevated temperature is necessary for solubilizing the polymer completely and to achieve a reliable estimate of the molecular weight. The difference in molecular weight of ~15 kDa seemingly lead to a significant difference in solubility of the polymers, with the sample from the first commercial supplier almost completely soluble in hot chloroform (>95 wt% collected by soxhlet extraction), whereas the second sample displayed almost no solubility in hot chloroform. Complete dissolution of sample 2 was only achieved by using hot chlorobenzene (quantitative collection by soxhlet extraction).

Processing of the second commercial sample required a technical modification of our standard spin-coating protocols. In the initial protocol, the heated glass substrate was put on a room temperature metallic chuck surface of the spin-coater, likely resulting in the polymer solution cooling rapidly, leading to gelation of the active layer solution and incomplete coverage of the substrate (Figure S4-a). With a modification of the chuck (the substrate was put in an elevated position to minimize contact with the metal surface, Figure S3), the processing could be performed at a higher substrate temperature. This adapted protocol allowed for proper film formation of the higher molecular weight PffBT4T-2OD from the second supplier, similar as films produced by the initial processing set-up for lower molecular weight PffBT4T-2OD (Figure S4-b).

The PffBT4T-2OD sample from the first commercial supplier, with the lower molecular weight, reached an average PCE of 9.8%, with a maximum of 10.1% (Table 5, entry 1). The higher molecular weight PffBT4T-2OD from the second supplier afforded a significantly lower average PCE of 8.4%, although it displayed a similar maximum PCE of 9.9% (Table 5, entry 2). We attribute the lower average value to the solubility difference between the two materials, leading to increased difficulty in obtaining reproducible results with the higher molecular weight sample in our hands. For these reasons, we were motivated to carry out a careful synthetic flow study to examine molecular weight control in these PffBT4T-2OD materials.

4.2.2   Batch polymerization

A careful evaluation of the batch process prior to developing a flow synthesis protocol is essential, as it provides important information concerning the solubility of the reaction components (monomers, polymer, catalyst, and intermediates), viscosity, kinetics, etc. Therefore, PffBT4T-2OD was first synthesized by a standard batch Stille polycondensation (Scheme 1).
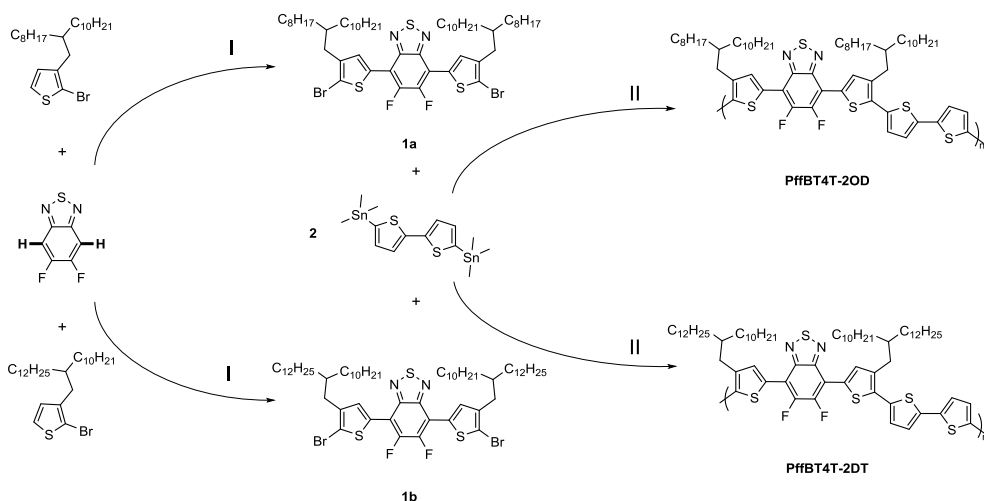
Scheme 4. Synthesis of the bisthiophene-benzothiadiazole monomers by dehydrogenative cross-coupling, followed by the Stille polycondensation reaction yielding the PffBT4T-2OD and PffBT4T-2DT polymers (I) Pd(OAc)2, AgOPiv, DMSO, 80 °C, 20 h; II) Pd2(dba)3, P(o-tol)3, chlorobenzene).

The required stannylated monomer, 5,5'-bis(trimethylstannyl)-2,2'-bithiophene (**2**), was prepared by a literature procedure.[46] 4,7-Bis(5-bromo-4-(2-octyldodecyl)thiophen-2-yl)-5,6-difluorobenzo[*c*][1,2,5]thiadiazole (**1a**) was synthesized by dehydrogenative cross-coupling (Scheme 4).[47–49] Dehydrogenative cross-coupling and other types of direct arylation protocols have recently received an increased attention as they eliminate the need for toxic intermediates.[50–54] The direct arylation protocol allows the preparation of monomer **1a** in 60% yield and employs two reaction steps less than the commonly used Stille cross-coupling approach.[3] This significantly simplifies the 'synthetic complexity' for the preparation of the monomers, classifying PffBT4T-2OD and derivatives, combined with their high efficiency, as potentially industrially viable candidates for solar cell applications.[55]

To gain some basic insight into the kinetics of the batch polymerization process, five polymerizations were conducted and analysed as a function of time (Table 1). Experimentally, the monomer concentration was chosen to be 376 mM and the polymer samples were purified by soxhlet extractions with methanol, hexanes, dichloromethane, and chloroform, and then finally collected with chlorobenzene. The initial rate of the Stille cross-coupling is relatively high, as an average molecular weight of 36 kDa is already reached within one hour (entry 1). In comparison to the polymerizations run over a longer time (entry 2-5), one can see that 80% or more of the time is used for making the final couplings leading to higher molecular weights. This behaviour is expected as the increase of the chain length leads to a decrease in active group concentration and can also increase the viscosity, both of which can lead to a decreased reaction rate.[56–58] This latter behaviour is intrinsic to polycondensation reactions.

The end phase of the polymerization lies between 6 and 12 hours (entry 2-4). Beyond that point (entry 3-5), the final M_n reaches a plateau at about 80 kDa within experimental error. In our hands, batch chemistry was effectively used on a lab scale to synthesize PffBT4T-2OD with high molecular weights ranging from 75 to 85 kDa, but did not provide the fine degree of control we require to obtain polymer of optimum molecular weight for processing and device fabrication.

Table 1. Number average molecular weights of the PffBT4T-2OD polymers synthesized in batch as a function of polymerization time.[a]

Entry	Reaction time (h)	M_n (kDa)	Đ
1[b]	1	36.0	1.8
2	6	64.3	1.8
3	12	82.2	1.8
4	24	75.0	1.8
5	72	84.2	2.1

[a] All reactions were performed at 145 °C with a monomer concentration of 376 mM and a catalyst loading of 0.5 mol%.
[b] Due to the lower M_n, the polymer was collected quantitatively with chloroform.

4.2.3 Flow polymerization

Flow polymerization set-up
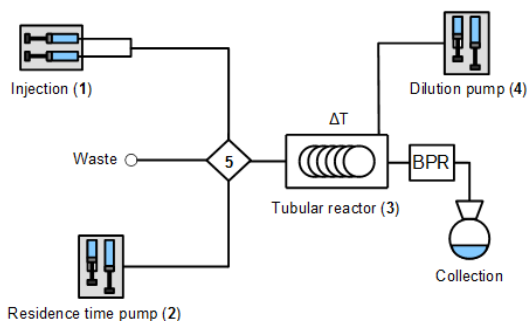
Figure 9. Graphical representation of the continuous flow set-up.

Given the limitations that were uncovered in the batch polymerization, we then investigated the influence of different reaction parameters, both physical and chemical, on the molecular weight of the PffBT4T-2OD polymer as prepared using flow polymerization methods. As the processability of higher molecular weight samples is limited, molecular weights below 60 kDa were targeted, simultaneously limiting the risk of over-pressurizing the system due to increased viscosity. All flow experiments were conducted on a custom-designed flow reactor apparatus (Figure 1, S1, S2), taking the strong temperature-dependent solubility of PffBT4T-2OD into account (as the polymer can only be completely

dissolved in chlorobenzene at temperatures above 80−90 °C). Three reaction temperatures of 120, 130 and 140 °C were employed. As these temperatures are close to the boiling point of chlorobenzene (131 °C), the reaction solvent, the system was pressurized to 40 psi with a back pressure regulator (BPR) to avoid the formation of gas bubbles inside the system, which would lead to an irregular flow and thereby a non-uniform residence time. The flow reactor was designed to account for viscosity changes, application of a wide range of flow rates, and accurate temperature control. The reactor volume was chosen to be sufficiently large (20 mL) to allow for an acceptable flow rate at different residence times, for which cooling of the reaction mixture is sufficiently slow, such that no accumulation of polymer material or gelation occurs upon collection. The reaction mixture was diluted 1:1 immediately before exiting the reactor. Diethylammonium diethyldithiocarbamate was added to the dilution stream to facilitate catalyst removal upon purification.[31] The polymers were collected by precipitation in methanol. Prior to GPC analysis, the polymers were purified by consecutive soxhlet extractions with methanol, hexanes, and dichloromethane. The polymer samples were then finally collected with chlorobenzene and precipitated again in methanol.

Influence of experimental parameters

Temperature

To monitor the effect of temperature on the molecular weight of PffBT4T-2OD, three reaction temperatures - 120, 130, and 140 °C - were investigated. For consistency, the polymers were produced from the same stock solution for each temperature experiment. The overall residence time was chosen to be 30 minutes and the injected volume for each polymer was approximately 1.75 mL, yielding 30−40 mg of polymer.

As for most reactions, at first glance, one would expect the reaction rate of the Stille polycondensation to increase with increased temperature and this increase in rate would lead to an increase in the molecular weight of the polymer, prior to events leading to a saturation of the molecular weight. However, for these experiments the opposite effect was observed (Table 2, entries 1a-c). An increase of the temperature by 10 °C reduced the molecular weight by approximately 10 kDa. Since the batch experiments were conducted at a temperature of 145 °C, degradation of the monomers or catalyst was considered to be unlikely. To verify that degradation neither takes place in the separate monomer and catalyst solutions before injection, as there is a significant time span between the injections, the experiment was also performed in the reversed order (entries 2a-2c). As the 130 °C experiment is always done as the second injection, a third experiment (entry 3) was used to independently determine the molecular weight at this temperature. From the results that were obtained, it is clear that the molecular weights are comparable, irregardless of the order of

injection or the time between the preparation of the solution and the actual injection.

Table 2. Number average molecular weights of the PffBT4T-2OD polymers synthesized in flow at different temperatures.[a]

Entry	T (°C)	M_n (kDa)	Đ
1a	120	48.6	2.1
1b	130	39.9	1.9
1c	140	30.9	1.8
2a	140	31.9	2.0
2b	130	39.3	2.0
2c	120	45.0	2.1
3	130	40.4	1.9

[a] An overall flow rate of 666 µL/min and a monomer concentration of 59.2 mM were used.

Before and after injection, the feed of the reactor exists out of pure solvent. This creates a slug of the reaction mixture that travels through the flow reactor. The slug is initially confined with pure solvent at the start (head) and end (tail). A visual observation during these experiments is that the collected volume is significantly larger, 2−5 times, than the initial injection. As the reaction mixture is in contact with pure solvent at the head and tail, the concentration difference causes the solutes to diffuse into the pure solvent over time. This phenomenon is dependent on the diffusion coefficient, which is proportional to the temperature and inversely proportional to the viscosity of the reaction mixture. As the viscosity itself is inversely proportional to the temperature, the diffusion effect will further increase with increasing temperature. Diffusion is therefore suspected to reduce the effective concentration of the reactant solution close to the head and tail of the injection, leading to a decrease in reaction rate, which results in shorter polymer chains. This effect can explain the increase of the volume of the reaction mixture and the decrease of the average molecular weight with increasing temperature. The effective influence of diffusion can be investigated in more detail by performing studies on the injected volume and concentration of the reaction mixture.

Residence time and injection volume

The residence time experiments were divided in 3 different series based on the scale of the injection volume, i.e. 1.75, 4.5, and 9 mL for the first, second, and third series, respectively (Table 3). This volume difference was implemented to evaluate the effect of forward and backward diffusion on the polymer molecular weight. For the first series (entries 1a-b), extending the residence time to 60 minutes did not show a significant increase of the molecular weight, indicating that 30 minutes is sufficient to reach the experimental end stage of the flow polymerization. For the second series, the residence time was shortened to 20, 10, and 5 minutes (entries 2a-c), whereas in the third series, 15 and 20 minutes

were compared (entries 3a-b). Overall, no major changes in the molecular weight were observed unless the residence time was reduced to 5 minutes (entry 2c). These results suggest that the initial polymerization rate of the Stille cross-coupling in flow is high and shortly after the reaction mixture enters the reactor, conjugated polymer chains of moderate length are already formed. This effect can also be visually observed as the reaction mixture changes from orange/reddish to deep purple within centimetres upon entering the reactor (Figure S1, S2). This initial fast rate was also observed in the batch experiments, but on a different time scale, as within 5 minutes an average molecular weight of 43.8 kDa is reached in flow (entry 2c), compared to 35 kDa after 1 hour in batch (*vide supra*).

Table 3. Number average molecular weights of the PffBT4T-2OD polymers synthesized in flow at different projected residence times and injection volumes.[a]

Entry	t_r (min)	Injected volume (mL)	M_n (kDa)	Đ
1a	30	1.75	48.6	2.1
1b	60	1.75	47.7	2.1
2a	20	4.5	47.8	2.1
2b	10	4.5	47.8	2.1
2c	5	4.5	43.8	2.1
3a	20	9	51.7	2.0
3b	15	9	50.9	2.1
4	26	18	54.9	2.0

[a] A residence time of 5, 10, 15, 20, 26, 30 and 60 min correlates with a set overall flow rate of 4000, 2000, 1332, 1000, 754, 666 and 333 µL/min, respectively. A constant monomer concentration of 59.2 mM and a temperature of 120 °C were used.

The flow experiments at different reactor temperatures are fully consistent with the notion that the polymerization is significantly influenced by the phenomenon of forward and backward diffusion. The contact area with pure solvent, which is the actual location where diffusion takes place, only exists at the head and tail of the injection slug and is determined by the cross-sectional area of the tubing. Increasing the injection volume increases the length scale of the reaction mixture slug as the cross-section remains constant. Therefore, the absolute amount of diffusion that takes place is irrespective of the injection volume. On the contrary, the relative percentage of diffusion with respect to the reaction mixture decreases when the injection volume becomes bigger, and the influence of the diffused part on the number-average molecular weight of the polymer should diminish. This effect is clearly visible from the data in Table 3, as the molecular weight increases when the injection volume is doubled (entry 2a v.s. 3a). The strongest increase can be observed by comparison of the smallest (entry 1a) and largest (entry 4) injection size, even though the residence time is slightly shorter.

While screening for conditions, the injection size has to be chosen sufficiently large to cause the diffusion effect to be almost negligible. Otherwise, the conversion of the reaction, in this case correlated with the molecular weight, with respect to the upscaling will differ too much. For PffBT4T-2OD, slight alterations in the molecular weight cause a large fluctuation in the solubility of the material and thereby drastically change its processability, which in turn leads to notable changes in the PCEs of the photovoltaic devices. When scalability is defined as the transformation from single injection to continuous operation, a flow protocol is only scalable when the relative percentage of forward and backward diffusion is negligibly small. Without resource limitations or with a direct aim for synthesizing larger quantities, initial screening can, however, directly be done under continuous operation instead of using injections and therefor there will be no diffusion effect as there is no head or tail front at which it can happen.

Concentration

From the previous experiments it can be concluded that it is difficult to control the molecular weight of the final polymer only with residence time. The polymerization rate is highly dependent on the reactive group concentration. Therefore, a concentration screening was performed, using 100, 66, and 33% of the standard concentration used so far, allowing a material production rate of 1.2, 0.8, and 0.4 g per hour, respectively. In order to minimize the influence of diffusion, the injected volume was chosen to be sufficiently large (18 mL). Table 4 shows that effective reduction of the molecular weight can indeed be achieved by lowering the concentration. The molecular weights of the first two experiments (entries 1 and 2) are close to those of the second and first commercial polymer samples, respectively. The concentration is hence a key parameter in efficient processes utilizing flow technology to prepare PffBT4T-2OD polymers with narrow control over the molecular weight. The availability of different molecular weights provides additional opportunities to tune the active layer morphology and the donor-acceptor interactions inside the BHJ layer of OPV devices. This can be particularly interesting when combining PffBT4T-2OD with novel promising non-fullerene acceptors.[7–11] Their solubility can differentiate strongly from the conventionally used fullerene acceptors, which can cause problems in obtaining the desired morphology.

Table 4. Number average molecular weights of the PffBT4T-2OD polymers synthesized in flow at different injection concentrations.[a]

Entry	Monomer concentration (mM)	M_n (kDa)	Đ
1	59.2	54.9	2.0
2	39.5	43.9	2.0
3	19.7	26.6	1.8

[a] All polymerizations were conducted at 120 °C and the residence time was chosen to be 26 min (754 µL/min overall flow rate).

Synthesis PffBT4T-2DT

As a higher molecular weight can be beneficial for certain optoelectronic properties, including charge mobility, but causes severe processing issues for PffBT4T-2OD, we carried out the flow synthesis of a polymer with an analogous backbone, i.e. PffBT4T-2DT (Scheme 4).[59,60] For similar molecular weights, the PffBT4T-2DT polymer should have a higher solubility, and therefore processability, than PffBT4T-2OD because of the increased side chain length. The flow conditions which resulted in a number-average molecular weight of 54.9 kDa for PffBT4T-2OD were used for comparative reasons (t_r = 26 min, T = 120 °C, [M] = 59.2 mM, V_{inj} = 18 mL; Table 3, entry 4). A similar molecular weight (M_n = 56.1 kDa) was achieved, indicating that the degree of polymerization is similar for both polymers. In general, molecular weights of PffBT4T-2DT synthesized under the same flow conditions as PffBT4T-2OD can be slightly higher due to the ±10% difference in molecular weight of the polymer repeat unit.

4.2.4 Photovoltaic properties

Similar to the commercial samples, the material quality of the synthesized flow polymers was evaluated by their application in BHJ OPV devices (*I-V* figures in ESI). Devices were fabricated with the same protocol, with a polymer concentration of 7.5 mg/mL. Two samples from the concentration experiment, employing large injection volumes, were used as these conditions can readily be employed for continuous production and their molecular weight approaches the values of the commercial samples (Table 5, entry 3 and 4). Additionally, one small-scale injection volume sample with a molecular weight of 41.8 kDa was used, as it approaches the molecular weight of the commercial sample from the first supplier (41.8 kDa) more closely, although the difference is within the experimental GPC error (Table 5, entry 5). The PffBT4T-2OD high molecular weight commercial sample (Table 5, entry 2) and its flow-synthesized equivalent (Table 5, entry 3) display a similar photovoltaic performance, although the commercial material has a higher maximum PCE value. We attribute the large difference between the average and maximum PCE to the higher molecular weight of the polymer, resulting in a lower device reproducibility due to the increased difficulty in processing these materials. The PffBT4T-2OD lower molecular weight commercial sample (Table 5, entry 1) and both of its large- and small-scale flow-synthesized equivalents (Table 5, entry 4 and 5) also display a similar photovoltaic performance, with maximum values reaching the threshold of 10%. From these results it can be concluded that continuous flow is capable of synthesizing high quality PffBT4T-2OD material, which performs equally well in BHJ solar cells as the commercially available PffBT4T-2OD, with the additional advantage that the production of larger quantities of material is straightforward.

Finally, the analogous PffBT4T-2DT material was tested for its photovoltaic performance. As outlined before, this material has a higher solubility than the traditional PffBT4T-2OD and is therefore easier to handle in device fabrication. To our knowledge, the highest reported efficiency for this material in combination with $PC_{71}BM$ is 7.6%.[59] The significantly higher PCE of the flow-synthesized material in this study (9.4%; Table 5, entry 6) is likely due to the higher molecular weight (56.1 vs 46.4 kDa). In the OPV field, alternative acceptors to replace the rather expensive fullerenes are currently being investigated intensively. The PffBT4T-2DT analogue has already been shown to reach an efficiency of 9.95% in combination with the alternative acceptor IDTBR, confirming the high potential of this material.[9]

Table 5. Photovoltaic performances of the BHJ polymer solar cells employing PffBT4T-2OD and PffBT4T-2DT produced by continuous flow chemistry (in combination with $PC_{71}BM$ in a 1:1.2 (wt/wt%) ratio; spin-coating from 1:1 (vol/vol %) chlorobenzene-dichlorobenzene + 3% diiodooctane).

Entry	Polymer	M_n (kDa)	J_{sc} (mA/cm²)	V_{oc} (V)	FF (%)	PCE (%)[a]
1	PffBT4T-2OD (Supplier 1)	41.8	18.6	0.74	68	9.8 (10.1)
2	PffBT4T-2OD (Supplier 2)	57.2	18.3	0.73	64	8.4 (9.9)
3	PffBT4T-2OD	54.9	18.7	0.72	66	8.8 (9.0)
4	PffBT4T-2OD	43.9	18.8	0.72	68	9.3 (9.8)
5	PffBT4T-2OD	41.8	20.8	0.72	62	9.4 (10.1)
6	PffBT4T-2DT	56.1	19.4	0.74	64	9.4 (9.8)

[a] Averages over at least 8 devices; values in parentheses are maximum efficiencies.

4.3 Conclusions

In this work, two prototype OPV donor polymers, PffBT4T-2OD and PffBT4T-2DT, were successfully synthesized via continuous flow chemistry, which allows reproducible production of device-quality materials. Through careful selection of the flow conditions, specific molecular weights were targeted and attained. The influence of reaction temperature, residence time, injection volume, and concentration on the final molecular weight of the PffBT4T-2OD polymer was investigated. When using injections to screen the flow conditions, diffusion was found to play a major role and its influence on small-scale reactions cannot be neglected. High molecular weight PffBT4T-2OD (54.9 kDa) can be produced via flow at a rate of 1.2 g/hour, affording polymer solar cells with an efficiency up to 9.0%, while somewhat lower molecular weight PffBT4T-2OD can be produced at a rate of 0.8 g/hour, affording devices with efficiencies up to 9.8%. Although the

production rate of the lower molecular weight polymer is slightly lower, it was found to be significantly easier to be processed into BHJ solar cell devices. It therefore may have advantages for use in R2R printing processes. Along with PffBT4T-2OD, the PffBT4T-2DT analogue was also successfully synthesized by flow, affording OPV devices with efficiencies up to 9.8%. The synthesized PffBT4T-2DT polymer exhibits an improved ease of processing, even relative to the lower molecular weight PffBT4T-2OD batch, and may not only be suitable for R2R processing, but also opens up a window of opportunities for combinations with emerging alternative acceptor materials.

4.4 Experimental

4.4.1 Materials and methods

All reagents and chemicals were obtained from commercial sources and used without further purification. Silver pivalate,[61] 2-bromo-3-(2-decyltetradecyl)thiophene,[62] 2-bromo-3-(2-octyldodecyl)thiophene,[3] and 5,6-difluoro-2,1,3-benzothiadiazole[48] were synthesized according to literature procedures. Commercial samples of PffBT4T-2OD were purchased from 1-Material (supplier 1) and Solarmer (supplier 2).

^{1}H NMR spectra were acquired using a Bruker AMX-500 spectrometer and the signals were referenced to a residual solvent peak (δ 7.26 ppm for CHCl$_3$) or the internal standard TMS (δ 0.0 ppm). ^{19}F NMR spectra (470 MHz) were recorded using trifluorotoluene as an external standard (δ -63.73 ppm). Chromatographic separations were performed by standard flash column chromatography methods using silica gel purchased from Sorbent Technologies (60 Å, 32−63 μm). Molecular weights and dispersities were determined by GPC using an EcoSEC High Temperature GPC system HLC-8321GPC/HT with RI detector manufactured by Tosoh Bioscience. Experiments were carried out with 1,2,4-trichlorobenzene as the eluent at a flow rate of 1 mL/min at 140 °C on two 7.8 mm × 30 cm, 13 μm TSK-Gel GMH$_{HR}$-H(S) HT2 columns in series (Tosoh Bioscience). The instrument was calibrated using polystyrene standards (4,930−1,214,000 g/mol) and the data were analysed using 8321GPC-WS Analysis software. To prepare the polymer samples for the GPC measurements, the polymer was wrapped in stainless steel mesh (96 μm pore size, Tosoh Bioscience) and heated in 1,2,4-trichlorobenzene at 120 °C for 3 h to afford a solution of 1.0 mg/mL. The resulting solution was transferred to a sample vial for injection.

All flow experiments were conducted on a home-made continuous flow apparatus (Figure 1, S1, S2). The system is comprised of a KDS-200 Legacy syringe pump (1) used for the injection of the reaction mixture, an ISCO 260D high pressure syringe pump system (2) for pushing the reaction mixture through the reactor, a perfluoroalkoxy (PFA) tubular reactor of 20 mL (3) immersed in a

heated oil bath, an Eldex Optos model 1 high pressure liquid metering pump (4) for in-line dilution, and a 4-way valve (5) to establish the injection. The entire flow system was pressurized outside the heating compartment with a back pressure regulator (BPR) of 40 psi from Upchurch Scientific. After the initial set-up of the system, all pumps, connection lines, valves, and the flow reactor itself were flushed with acetone, anhydrous toluene, and finally with degassed chlorobenzene to assure an inert atmosphere inside the flow reactor. The entire flow system was stored under chlorobenzene in between experiments and was flushed with freshly degassed chlorobenzene before every injection series. All reported reaction temperatures were allowed to equilibrate for a least 30 min before the actual experiment started.

4.4.2   Monomer synthesis

4,7-Bis[5-bromo-4-(2-decyltetradecyl)thiophen-2-yl]-5,6-difluorobenzo [*c*][1,2,5]thiadiazole (1a)[59]

5,6-Difluoro-2,1,3-benzothiadiazole[48] (172 mg, 1 mmol), 2-bromo-3-(2-octyldodecyl)thiophene[3] (1.76 g, 4 mmol), Pd(OAc)$_2$ (22.4 mg, 0.1 mmol), and silver pivalate (1.68 g, 8 mmol) were added sequentially to a collared tube (CEM Corp., Prod # 89079-404) with a magnetic stirring bar. The tube was crimp-sealed with a septum-cap inside a glove box. DMSO (5 mL) was added and the reaction mixture was heated in a 80 °C aluminum block. After 20 h, the reaction mixture was cooled to room temperature, diluted with CH_2Cl_2 (100 mL), and filtered through Celite® (10 mL). The filtrate was concentrated under reduced pressure. The resulting residue was purified by silica gel chromatography (200 mL of silica gel, hexanes as eluent), followed by precipitation in dichloromethane/methanol to yield the product as an orange solid (715 mg, 68%). ^{1}H NMR (400 MHz, CDCl$_3$) *δ* 7.97 (s, 2H), 2.59 (d, *J* = 7.2 Hz, 4H), 1.80–1.60 (m, 2H), 1.35–1.20 (m, 64H), 0.90–0.60 (m, 12H). ^{19}F NMR (470 MHz, CDCl$_3$) *δ* -129.41.

4,7-Bis[5-bromo-4-(2-octyldodecyl)thiophen-2-yl]-5,6-difluorobenzo [*c*][1,2,5]thiadiazole (1b)[3]

5,6-Difluoro-2,1,3-benzothiadiazole[48] (172 mg, 1 mmol), 2-bromo-3-(2-decyltetradecyl)thiophene[62] (2.00 g, 4 mmol), Pd(OAc)$_2$ (22.4 mg, 0.1 mmol), and silver pivalate (1.68 g, 8 mmol) were added sequentially to a collared tube (CEM Corp., Prod # 89079-404) with a magnetic stirring bar. The tube was crimp-sealed with a septum-cap inside a glove box. DMSO (5 mL) was added and the reaction mixture was heated in a 80 °C aluminum block. After 20 h, the reaction mixture was cooled to room temperature, diluted with dichloromethane (100 mL), and filtered through Celite® (10 mL). The filtrate was concentrated under reduced pressure. The resulting residue was purified by silica gel chromatography (200 mL of silica gel, hexanes as eluent), followed by precipitation in dichloromethane/methanol to yield the product as an orange solid (700 mg, 60%). ^{1}H NMR (500 MHz, CDCl$_3$) *δ* 7.97 (s, 2H), 2.62 (d, *J* = 7.2

Hz, 4H), 1.80–1.60 (m, 2H), 1.33–1.20 (m, 80H), 1.00–0.80 (m, 12H). ^{19}F NMR (470 MHz, CDCl$_3$) δ -128.12.

4.4.3   Typical procedure for the batch polymerization

A microwave reaction tube equipped with a magnetic stirring bar was charged with 4,7-bis[5-bromo-4-(2-octyldodecyl)thiophen-2-yl]-5,6-difluorobenzo[c][1, 2,5]thiadiazole (50.0 mg, 0.047 mmol) and 5,5'-bis(trimethylstannyl)-2,2'-bithiophene (23.3 mg, 0.047 mmol). The reaction tube was transferred into a glove box before the addition of Pd$_2$(dba)$_3$·CHCl$_3$ (0.25 mg, 0.5 mol%), P(o-tol)$_3$ (0.5 mg, 3.5 mol%) and freshly degassed chlorobenzene (0.25 mL). Afterwards, the tube was sealed in the glove box and transferred out to be immersed into an oil bath preheated to 145 ^{o}C. The reaction mixture turned from dark red to viscous deep purple within 10 min. The polymerization reaction was carried out for the designated reaction time (see Table 1) before being cooled to 100 ^{o}C or less, and opened up to air.* Excess amount of the Pd scavenger diethylammonium diethyldithiocarbamate was added in approximately 5 mL of toluene. The mixture was then stirred at 80−100 ^{o}C for 1 h before it was precipitated in methanol (100 mL). The precipitates were filtered into an extraction thimble and the polymer was purified by successive soxhlet extractions with methanol, acetone, hexanes, dichloromethane, and chloroform. Finally, the product was collected with chlorobenzene. The solution was concentrated under reduced pressure and the polymer was precipitated again in methanol (100 mL). The solids were collected by vacuum filtration and dried under vacuum to yield the polymer as a dark green solid.

* For entry 5 of Table 1, A second portion of the catalyst Pd$_2$(dba)$_3$/P(o-tol)$_3$ (0.25 mol%) in degassed chlorobenzene was added to the reaction mixture via syringe after the mixture was heated under stirring for 15 min.

4.4.4   General procedure for the flow polymerization

A vial equipped with a magnetic stirring bar was charged with a 1:1 ratio of 4,7-bis[5-bromo-4-(2-octyldodecyl)thiophen-2-yl]-5,6-difluorobenzo[c][1,2,5]thiadiazole and 5,5'-bis(trimethylstannyl)-2,2'-bithiophene, while a second vial was charged with 3 mol% Pd$_2$(dba)$_3$ and 12 mol% P(o-tol)$_3$.[31] Both vials were flushed with nitrogen and transferred into a glovebox. Equal amounts of freshly degassed chlorobenzene were added and the solutions were stirred for 10−15 min. Two SGE gastight syringes (maximum volume of 10 mL) were charged with the solutions and transferred outside the glovebox. The syringes were placed onto the KDS-200 Legacy syringe pump and rapidly connected to the system by a luer lock mechanism. Immediately after connection, the line connecting the syringes with the 4-way valve was flushed with a small amount of the reaction mixture to retain an inert atmosphere (as much as possible) within the flow system. The two injection streams were mixed in a T-piece mixer before entering the reactor. The reaction stream was diluted with chlorobenzene 1:1 right before exiting the reactor. An excess amount of the

Pd scavenger diethylammonium diethyldithiocarbamate was added to the dilution stream. The polymer was collected by precipitation in methanol. Further purification was done by successive soxhlet extractions with methanol, hexanes, and dichloromethane and the product was finally collected with chlorobenzene. Re-precipitation of the product in methanol and vacuum filtration finally yielded the polymer as a dark green solid.

4.4.5 Device fabrication

An inverted bulk heterojunction solar cell architecture comprising of glass/ITO/ZnO/PffBT4T:$PC_{71}BM$/MoO_3/Ag was used. Before device processing, the ITO-coated substrates (Tinwell Technology Ltd, Sheet resistance 15 Ω/sq) were cleaned by sonicating with soap solution, DI water, acetone and isopropanol, followed by a UV/O_3 treatment for 10 min. The ZnO electron transport layer was deposited on the cleaned ITO substrates using spin-coating in ambient atmosphere to get a layer thickness of ~30 nm. After spin-coating, the ZnO layer was annealed in air at 150 °C for 10 min followed by slow cooling to room temperature. The ZnO solution used for spin-coating was prepared using a standard procedure, i.e. employing a 1:1 molar ratio of zinc acetate and ethanolamine in 2-methoxyethanol as solvent. The photoactive layer solution was prepared by dissolving PffBT4T-2OD or PffBT4T-2DT and $PC_{71}BM$ in the solvent mixture chlorobenzene:1,2-dichlorobenzene (1:1 vol ratio) with 3% DIO as additive. The ratio of polymer:fullerene used was 1:1.2 (wt/wt) with a polymer concentration of 7.5 mg/mL for all samples, except for the commercial sample from the second supplier (provided protocol). The solution was stirred at 110 °C for 2 h to ensure proper dissolution. The active layer was coated on top of the ZnO layer in an Ar glove box at 600 r.p.m. to obtain thicknesses of ~300 nm. Prior to spin-coating, both the polymer solution and the ITO substrate were preheated on a hot plate at 110 °C. Active layers were spin-coated from the warm polymer solutions on the preheated substrates in an Ar glovebox. To remove the additive from the photoactive layer, the samples were placed in a vacuum chamber with a pressure of 1 x 10^{-5} mbar for 45 min. The top electrodes, MoO_3 and Ag, were deposited by vacuum deposition with layer thicknesses of 20 and 160 nm, respectively, to obtain complete solar cell devices with an active area of 0.08 cm², defined by a metal mask with an aperture aligned with the device area. The *I-V* characteristics of all photovoltaic devices were evaluated under AM 1.5G solar illumination (100 mW/cm²) using a Keithley 4200 semiconductor parameter analyzer system with a Newport Thermal Oriel 94021 solar simulator calibrated with a reference silicon solar cell.

4.5 Supporting information

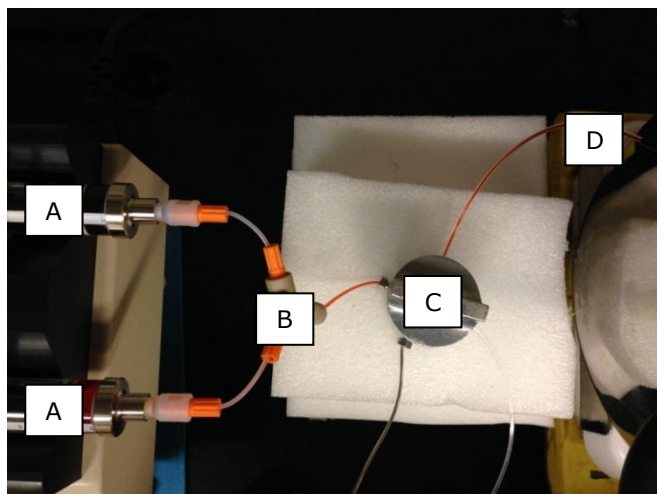### 4.5.1   Continuous flow set-up and operation

Figure S10. Reagents are injected into the continuous flow reactor (D) by two SGE gastight syringes (A), a T-piece mixer (B) and a 4-way valve (C).
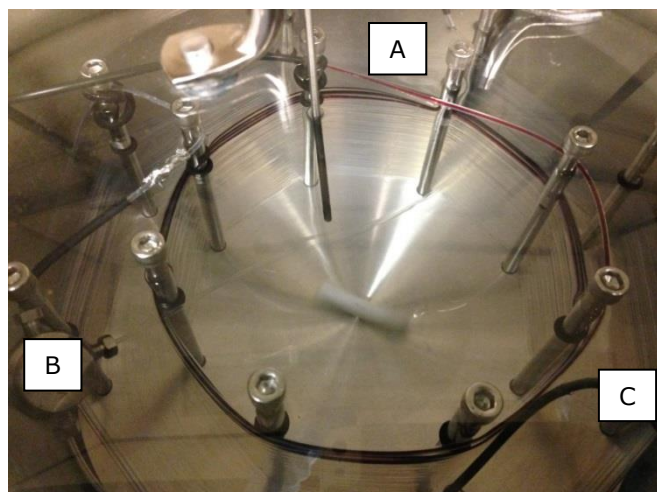

Figure S11. The tubular flow reactor is immersed in an oil bath. The incoming reaction mixture (A) rapidly turns deep purple. Before exiting the reactor (C), the reaction mixture is diluted (B) by a stream of fresh solvent, in which also the palladium scavenging agent is dissolved.
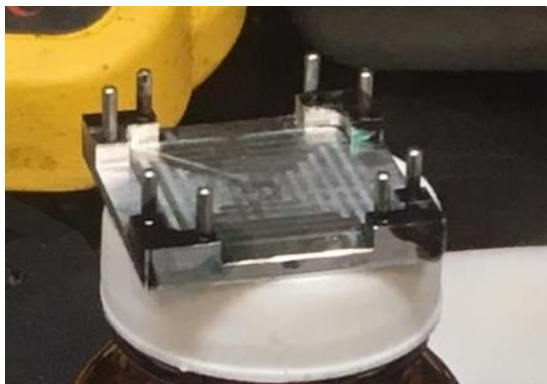
4.5.2 Modified processing chuck

Figure S12. The modified processing chuck, which allows elevation of the glass substrate from the cold metal surface. The substrate rests on the four corners and is kept in place with 8 pins.

4.5.3 Dependence of the photoactive layer film formation on molecular weight and the processing set-up
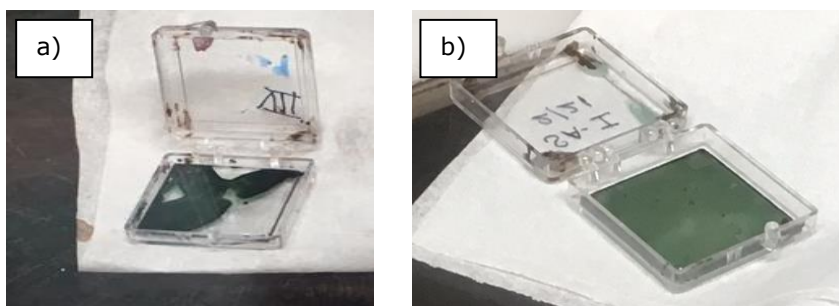
Figure S13. a) Example of incomplete coverage of the substrate and gelation in case of higher molecular weight PffBT4T-2OD with the initial processing set-up; b) Example of a properly spin-coated active layer, either with lower molecular weight PffBT4T-2OD using the initial set-up or with higher molecular weight PffBT4-2OD using the modified chuck.

4.5.4 *J-V* curves

Figure S5: *J-V* curves of (maximum efficiency) BHJ OPV devices based on PffBT4T-2OD from commercial sources and synthesized by flow.

Figure S6: *J-V* curve of an average efficiency BHJ OPV device based on PffBT4T-2DT synthesized by flow.

4.5.5 Flow parameters and GPC data
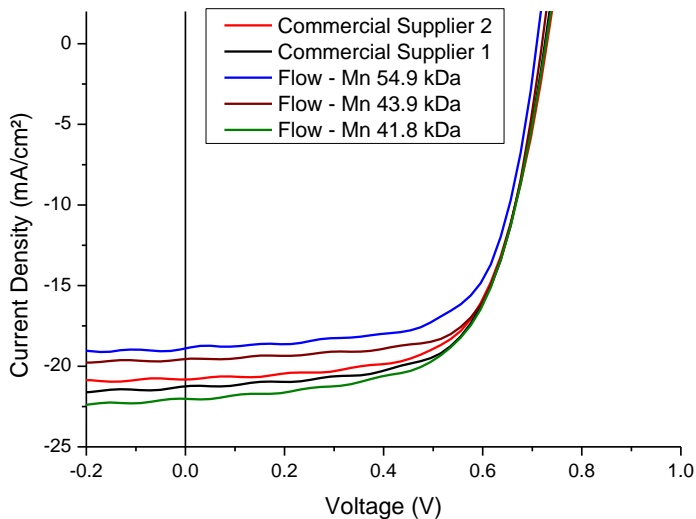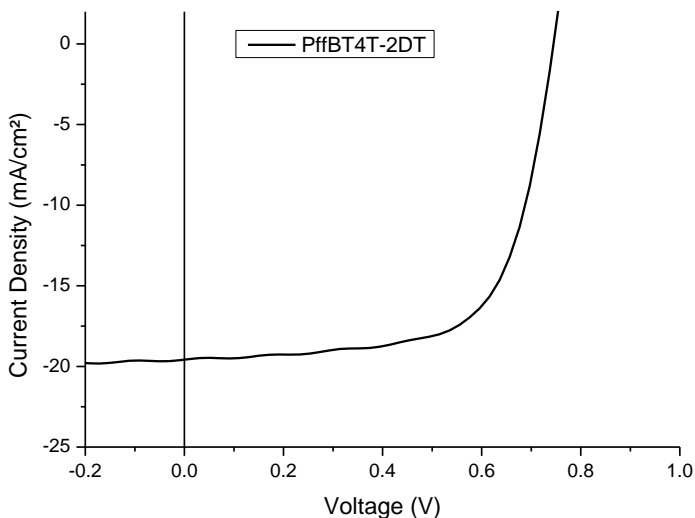
Table S1: Overview of the flow parameters and GPC data of all polymers synthesized within this project.

Injection	t_r (min)	T (°C)	Flow rate (µL/min)	[M] mM	V_{inj} (mL)	M_n (kg/mol)	M_w (kg/mol)	Đ
1 - PffBT4T-2OD[a,b]								
1	30	117	666		1.75	43.5	84.6	1.95
2	45	117	444	29.6	1.75	41.8	78.4	1.87
3	60	120	333		3.50	37.7	69.3	1.84
2 - PffBT4T-2OD[b]								
1		120			1.00	38.1	71.2	1.87
2	30	130	666	29.4	1.00	32.0	58.1	1.82
3		140			1.00	28.7	49.5	1.72
3 - PffBT4T-2OD[b]								
1		120			1.00	43.0	86.1	2.00
2	45	130	444	29.4	1.00	36.8	69.5	1.89
3		140			1.00	26.8	47.7	1.78
4 - PffBT4T-2OD								
1		120			1.75	48.6	101.2	2.08
2	30	130	666	29.6	1.75	39.9	76.4	1.91
3		140			1.44	30.9	55.1	1.78
5 - PffBT4T-2OD								
1		120			1.25	47.8	99.4	2.08
2	60	130	333	29.5	1.25	41.8	82.6	1.97
3		140			2.45	33.8	60.3	1.78
6 - PffBT4T-2OD								
1	26	120	754	29.6	17.74	54.9	108.1	1.97
7 - PffBT4T-2OD								
1		140			1.75	32.0	64.0	2.00
2	30	130	333	29.5	1.75	39.4	78.4	1.99
3		120			1.75	45.0	94.2	2.09

[a] Performed without Back Pressure Regulator (lead to gas formation and irregular flow).
[b] The monomers and catalyst were injected as one solution into the system.

Injection	t_r (min)	T (°C)	Flow rate (µL/min)	[M] mM	V_{inj} (mL)	M_n (kg/mol)	M_w (kg/mol)	Đ
8 - PffBT4T-2OD								
1	30	130	333	29.2	1.75	40.4	76.5	1.89
9 - PffBT4T-2OD								
1	15	120	1332	29.6	8.99	50.9	103.1	2.03
10 - PffBT4T-2OD								
1	20	120	1000	29.6	9.00	51.8	105.9	2.05
11 - PffBT4T-2OD								
1	10	120	2000	29.6	4.50	47.8	98.5	2.06
2	5	120	4000	29.6	4.50	43.8	88.6	2.02
3	20	120	1000	29.6	4.50	47.8	101.4	2.12
4	20	140	1000	29.6	4.50	32.7	62.6	1.92
12 - PffBT4T-2OD								
1	26	120	754	19.74	17.74	43.9	89.9	2.05
13 - PffBT4T-2OD								
1	26	120	754	9.87	17.74	26.6	46.7	1.76
PffBT4T-2DT								
1	26	120	754	29.6	18.00	56.1	113.9	2.03
Commercial Sample Solarmer								
	N/A	N/A	N/A	N/A	N/A	57.2	130.0	2.27
Commercial sample One-Material								
	N/A	N/A	N/A	N/A	N/A	41.8	69.7	1.67

4.6 References

(1)   L. Dou, J. You, Z. Hong, Z. Xu, G. Li, R. A. Street and Y. Yang, *Adv. Mater.* **2013**, 25, 6642.

(2)   K. A. Mazzio and C. K. Luscombe, *Chem. Soc. Rev.* **2015**, 44, 78.

(3)   Y. Liu, J. Zhao, Z. Li, C. Mu, W. Ma, H. Hu, K. Jiang, H. Lin, H. Ade and H. Yan, *Nat. Commun.* **2014**, 5, 5293.

(4)   G. Li, R. Zhu and Y. Yang, *Nat. Photonics* **2012**, 6, 153.

(5)   L. K. Jagadamma, M. Al-Senani, A. El-Labban, I. Gereige, G. O. Ngongang Ndjawa, J. C. D. Faria, T. Kim, K. Zhao, F. Cruciani, D. H. Anjum, M. A. McLachlan, P. M. Beaujuge and A. Amassian, *Adv. Energy Mater.* **2015**, 5, 1500204.

(6)   Z. He, B. Xiao, F. Liu, H. Wu, Y. Yang, S. Xiao, C. Wang, T. P. Russell and Y. Cao, *Nat. Photonics* **2015**, 9, 174.

(7)   Y. Lin, F. Zhao, Y. Wu, K. Chen, Y. Xia, G. Li, S. K. K. Prasad, J. Zhu, L. Huo, H. Bin, Z. G. Zhang, X. Guo, M. Zhang, Y. Sun, F. Gao, Z. Wei, W. Ma, C. Wang, J. Hodgkiss, Z. Bo, O. Inganäs, Y. Li and X. Zhan, *Adv. Mater.* **2016**, 29, 1604155.

(8)   W. Zhao, D. Qian, S. Zhang, S. Li, O. Inganäs, F. Gao and J. Hou, *Adv. Mater.* **2016**, 28, 4734.

(9)   D. Baran, T. Kirchartz, S. Wheeler, S. Dimitrov, M. Abdelsamie, J. Gorman, R. Ashraf, S. Holliday, A. Wadsworth, N. Gasparini, P. Kaienburg, H. Yan, A. Amassian, C. J. Brabec, J. Durrant and I. McCulloch, *Energy Environ. Sci.* **2016**, 9, 3783.

(10)   D. Meng, D. Sun, C. Zhong, T. Liu, B. Fan, L. Huo, Y. Li, W. Jiang, H. Choi, T. Kim, J. Y. Kim, Y. Sun, Z. Wang and A. J. Heeger, *J. Am. Chem. Soc.* **2016**, 138, 375.

(11)   S. Holliday, R. S. Ashraf, A. Wadsworth, D. Baran, S. A. Yousaf, C. B. Nielsen, C.-H. Tan, S. D. Dimitrov, Z. Shang, N. Gasparini, M. Alamoudi, F. Laquai, C. J. Brabec, A. Salleo, J. R. Durrant and I. McCulloch, *Nat. Commun.* **2016**, 7, 11585.

(12)   F. C. Krebs, T. Tromholt and M. Jørgensen, *Nanoscale* **2010**, 2, 873.

(13)   M. Jørgensen, K. Norrman, S. A. Gevorgyan, T. Tromholt, B. Andreasen and F. C. Krebs, *Adv. Mater.* **2012**, 24, 580.

(14)   K. Zhao, H. Hu, E. Spada, L. K. Jagadamma, B. Yan, M. Abdelsamie, Y. Yang, L. Yu, R. Munir, R. Li, G. O. N. Ndjawa and A. Amassian, *J. Mater. Chem. A* **2016**, 4, 16036.

(15)   M. Helgesen, J. E. Carlé, G. A. dos Reis Benatto, R. R. Søndergaard, M. Jørgensen, E. Bundgaard and F. C. Krebs, *Adv. Energy Mater.* **2015**, 5, 1401996.

(16)   C. Wiles and P. Watts, *Green Chem.* **2012**, 14, 38.

(17)   C. Wiles and P. Watts, *Eur. J. Org. Chem.* **2008**, 1655.

(18) J. Wegner, S. Ceylan and A. Kirschning, *Adv. Synth. Catal.* **2012**, 354, 17.

(19) G. Jas and A. Kirschning, *Chem. Eur. J.* **2003**, 9, 5708.

(20) P. Watts and S. J. Haswell, *Chem. Soc. Rev.* **2005**, 34, 235.

(21) S. G. Newman and K. F. Jensen, *Green Chem.* **2013**, 15, 1456.

(22) P. Styring and A. I. R. Parracho, *Beilstein J. Org. Chem.* **2009**, 5.

(23) N. Jongen, M. Donnet, P. Bowen, J. Lemaître, H. Hofmann, R. Schenk, C. Hofmann, M. Aoun-Habbache, S. Guillemet-Fritsch, J. Sarrias, A. Rousset, M. Viviani, M. T. Buscaglia, V. Buscaglia, P. Nanni, A. Testino and J. R. Herguijuela, *Chem. Eng. Technol.* **2003**, 26, 303.

(24) F. Ullah, T. Samarakoon, A. Rolfe, R. D. Kurtz, P. R. Hanson and M. G. Organ, *Chem. Eur. J.* **2010**, 16, 10959.

(25) P. V. Snytnikov, D. I. Potemkin, E. V. Rebrov, V. A. Sobyanin, V. Hessel and J. C. Schouten, *Chem. Eng. J.* **2010**, 160, 923.

(26) J. D. Moseley and E. K. Woodman, *Org. Process Res. Dev.* **2008**, 12, 967.

(27) P. Löb, H. Löwe and V. Hessel, *J. Fluor. Chem.* **2004**, 125, 1677.

(28) J. H. Bannock, S. H. Krishnadasan, A. M. Nightingale, C. P. Yau, K. Khaw, D. Burkitt, J. J. M. Halls, M. Heeney and J. C. De Mello, *Adv. Funct. Mater.* **2013**, 23, 2123.

(29) H. Seyler, J. Subbiah, D. J. Jones, A. B. Holmes and W. W. H. Wong, *Beilstein J. Org. Chem.* **2013**, 9, 1492.

(30) A. Kumar, J. Hasan, A. Majji, A. Avhale, S. Gopinathan, P. Sharma, D. Tarange, R. Bajpai and A. Kumar, *J. Flow Chem.* **2014**, 4, 206.

(31) G. Pirotte, J. Kesters, P. Verstappen, S. Govaerts, J. Manca, L. Lutsen, D. Vanderzande and W. Maes, *ChemSusChem* **2015**, 8, 3228.

(32) J. H. Bannock, W. Xu, T. Baïssas, M. Heeney and J. C. de Mello, *Eur. Polym. J.* **2016**, 80, 240.

(33) F. Grenier, B. R. Aich, Y. Lai, M. Guérette, A. B. Holmes, Y. Tao, W. W. H. Wong and M. Leclerc, *Chem. Mater.* **2015**, 27, 2137.

(34) C. Liu, K. Wang, X. Hu, Y. Yang, C.-H. Hsu, W. Zhang, S. Xiao, X. Gong and Y. Cao, *ACS Appl. Mater. Interfaces* **2013**, 5, 12163.

(35) P. Schilinsky, U. Asawapirom, U. Scherf, M. Biele and C. J. Brabec, *Chem. Mater.* **2005**, 17, 2175.

(36) E. Bundgaard and F. C. Krebs, *Sol. Energy Mater. Sol. Cells* **2007**, 91, 954.

(37) T. Vangerven, P. Verstappen, J. Drijkoningen, W. Dierckx, S. Himmelberger, A. Salleo, D. Vanderzande, W. Maes and J. V. Manca, *Chem. Mater.* **2015**, 27, 3726.

(38) D. Spoltore, T. Vangerven, P. Verstappen, F. Piersimoni, S. Bertho, K.

Vandewal, N. Van Den Brande, M. Defour, B. Van Mele, A. De Sio, J. Parisi, L. Lutsen, D. Vanderzande, W. Maes and J. V. Manca, *Org. Electron.* **2015**, 21, 160.

(39)   A. Zen, J. Pflaum, S. Hirschmann, W. Zhuang, F. Jaiser, U. Asawapirom, J. P. Rabe, U. Scherf and D. Neher, *Adv. Funct. Mater.* **2004**, 14, 757.

(40)   J. J. Intemann, K. Yao, H. L. Yip, Y. X. Xu, Y. X. Li, P. W. Liang, F. Z. Ding, X. Li and A. K. Y. Jen, *Chem. Mater.* **2013**, 25, 3188.

(41)   R. J. Kline, M. D. McGehee, E. N. Kadnikova, J. Liu and J. M. J. Fréchet, *Adv. Mater.* **2003**, 15, 1519.

(42)   M. Tong, S. Cho, J. T. Rogers, K. Schmidt, B. B. Y. Hsu, D. Moses, R. C. Coffin, E. J. Kramer, G. C. Bazan and A. J. Heeger, *Adv. Funct. Mater.* **2010**, 20, 3959.

(43)   X. Zhao, H. Tang, D. Yang, H. Li, W. Xu, L. Yin and X. Yang, *Chinese J. Chem.* **2012**, 30, 2052.

(44)   J.-F. Chang, J. Clark, N. Zhao, H. Sirringhaus, D. W. Breiby, J. W. Andreasen, M. M. Nielsen, M. Giles, M. Heeney and I. McCulloch, *Phys. Rev. B* **2006**, 74, 115318.

(45)   H. W. Ro, J. M. Downing, S. Engmann, A. A. Herzing, D. M. DeLongchamp, L. J. Richter, S. Mukherjee, H. Ade, M. Abdelsamie, L. K. Jagadamma, A. Amassian, Y. Liu and H. Yan, *Energy Environ. Sci.* **2016**, 9, 2835.

(46)   J. S. Ha, K. H. Kim and D. H. Choi, *J. Am. Chem. Soc.* **2011**, 133, 10364.

(47)   J. Zhang, T. C. Parker, W. Chen, L. Williams, V. N. Khrustalev, E. V. Jucov, S. Barlow, T. V. Timofeeva and S. R. Marder, *J. Org. Chem.* **2016**, 81, 360.

(48)   J. Zhang, W. Chen, A. J. Rojas, E. V. Jucov, T. V. Timofeeva, T. C. Parker, S. Barlow and S. R. Marder, *J. Am. Chem. Soc.* **2013**, 135, 16376.

(49)   H. Hu, K. Jiang, G. Yang, J. Liu, Z. Li, H. Lin, Y. Liu, J. Zhao, J. Zhang, F. Huang, Y. Qu, W. Ma and H. Yan, *J. Am. Chem. Soc.* **2015**, 137, 14149.

(50)   D. Alberico, M. E. Scott and M. Lautens, *Chem. Rev.* **2007**, 107, 174.

(51)   A. Nitti, R. Po, G. Bianchi and D. Pasini, *Molecules* **2016**, 22, 21.

(52)   A. S. Dudnik, T. J. Aldrich, N. D. Eastham, R. P. H. Chang, A. Facchetti and T. J. Marks, *J. Am. Chem. Soc.* **2016**, 138, 15699.

(53)   W. Wu, H. Xin, C. Ge and X. Gao, *Tetrahedron Lett.* **2017**, 58, 175.

(54)   C. S. Yeung and V. M. Dong, *Chem. Rev.* **2011**, 111, 1215.

(55)   R. Po, G. Bianchi, C. Carbonera and A. Pellegrino, *Macromolecules* **2015**, 48, 453.

(56)   P. Espinet and A. M. Echavarren, *Angew. Chem. Int. Ed.* **2004**, 43, 4704.

(57)   V. Farina and G. P. Roth, *Adv. Met.-Org. Chem.* **1996**, 5, 1.

(58)   V. Farina, *Pure Appl. Chem.* **1996**, 68, 73.

(59)   Z. Chen, P. Cai, J. Chen, X. Liu, L. Zhang, L. Lan, J. Peng, Y. Ma and Y. Cao, *Adv. Mater.* **2014**, 26, 2586.

(60)   M. Li, C. An, T. Marszalek, M. Baumgarten, H. Yan, K. Müllen and W. Pisula, *Adv. Mater.* **2016**, 28, 9430.

(61)   K. Endo and R. H. Grubbs, *J. Am. Chem. Soc.* **2011**, 133, 8525.

(62)   J. Zhao, Y. Li, H. Lin, Y. Liu, K. Jiang, C. Mu, T. Ma, J. Y. L. Lai, H. Hu, D. Yu and H. Yan, *Energy Environ. Sci.* **2015**, 8, 520.

Chapter 5

The impact of acceptor-acceptor homocoupling on the optoelectronic properties and photovoltaic performance of PDTSQx$_{ff}$ low bandgap polymers
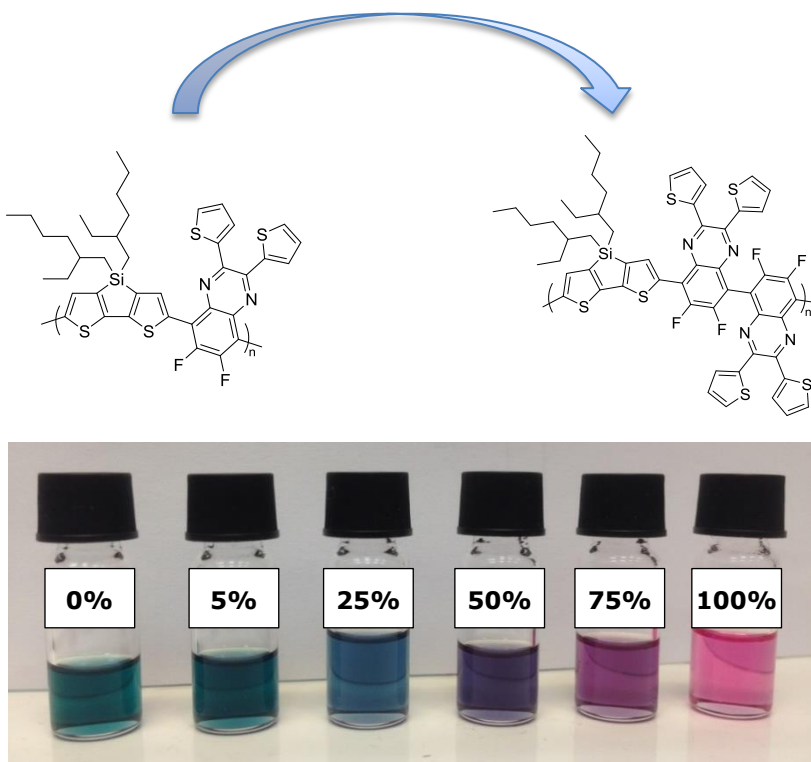
Geert Pirotte, Jurgen Kesters, Pieter Verstappen, Dirk Vanderzande, Laurence Lutsen, Wouter Maes, *Manuscript in preparation*, 2017

Abstract

In recent years it has been shown that the structure of push-pull conjugated polymers designed for organic photovoltaic applications does not always contain a perfect alternation of donor (electron-rich) and acceptor (electron-poor) building blocks. Instead, miss-couplings can occur, which have a noticeable effect on the optoelectronic properties of these materials and the resulting devices. Within this work, the influence of homocoupling on the optoelectronic properties and photovoltaic performance of PDTSQx$_{ff}$ polymers is investigated, with a specific focus on the quinoxaline acceptor units. A homocoupled segment of the quinoxaline monomer is intentionally prepared and added in a specific ratio to the polymerization. The resulting homocoupled structural units cause a gradual blue-shift in the absorption spectra, while the LUMO energy levels remain almost constant and the HOMO energy levels decrease only significantly upon the presence of 75 to 100% of homocouplings. The virtually homocoupling-free PDTSQx$_{ff}$ affords a power conversion efficiency of 4.84% in bulk heterojunction polymer solar cells, which only decreases strongly upon incorporating a homocoupling content of over 50%. The purely homocoupled polymer gives an efficiency of only 1.35%. The homocouplings mainly effect the short-circuit current and the fill factor, while the open-circuit voltage remains rather constant. Although it is known from literature that homocouplings in the donor unit also effectively decrease the photovoltaic performance, they have a different 'signature', as for donor homocouplings the open-circuit voltage strongly decreases, while for acceptor homocouplings mainly the short-circuit current is affected.

Contribution to the chapter

Monomer/polymer synthesis and characterization (NMR, UV-VIS, GPC and interpretation MALDI-TOF spectra), manuscript writing.

5.1 Introduction

Over the two past decades, bulk heterojunction (BHJ) organic photovoltaic (OPV) devices evolved into attractive candidates for renewable energy production.[1,2] This organic thin-film PV technology shows intrinsic properties like flexibility, tunable absorption profiles and printing ability, allowing low-cost large scale device fabrication. Multiple combinations of efficiently intermixed electron donor polymers and acceptors (fullerenes as well as non-fullerene alternatives) have been developed, affording power conversion efficiencies (PCEs) over 12% in solution processed single layer devices.[3–11] The state of the art electron donor polymers are push-pull copolymers, existing out of alternating electron-rich (push or donor) and electron-poor (pull or acceptor), mainly heterocyclic, building blocks. These polymers are generally synthesized by palladium-catalysed cross-coupling reactions of bifunctionalized monomers, such as Stille and Suzuki cross-couplings. Although frequently neglected, these reactions do not always provide the desired perfect alternation of push and pull building blocks. Even upon applying 'nearly perfect' conditions, e.g. an oxygen free reaction atmosphere and a proper palladium-ligand stoichiometry, homocoupling between either two organotin/boron units or two arylhalide units readily occurs.[12–15] The importance and possible abundance of these miss-coupled structural units for the organic solar cells has only recently been realized and only a few reports on this have recently appeared.[16–22]

By synthesizing PDPPTPT under different conditions, Janssen *et al.* in 2014 showed that the presence of homocoupling defects of the polymer donor unit causes a red-shift in the absorption spectrum.[21] It was further emphasized that homocoupling defects can lead to low-lying energy trap sites and they effectively increase the HOMO and decrease the LUMO of the polymer. The main effects on the solar cell level were a decrease in the photocurrent and a significantly lower PCE. Another polymer for which homocoupling defects have been shown to be important, is the popular material PTB7. In 2015, Vangerven and co-workers investigated several commercial batches of PTB7 by Gel Permeation Chromatography (GPC) and Matrix Assisted Laser Desorption Ionisation – Time of Flight mass spectrometry (MALDI-TOF).[20] The lower molecular weight batches clearly showed a bimodal molecular weight distribution. Analysis by MALDI-TOF revealed that homocoupling occured for both the brominated and stannylated monomers used in the Stille polycondensation. Similarly as observed by Janssen *et al*., homocoupling caused a clear red-shift in the absorption spectra. The large differences in the PCE's of the resulting solar cells (from 4.5 to 7.5%)was mainly caused by a strong fluctuation in the short-circuit current density (J_{sc}) and the fill factor (FF). Besides altering the HOMO and LUMO levels of the polymers, homocoupling can also cause changes in the aggregation behaviour upon film formation, which is of crucial importance for achieving high efficiencies. In the same year, Yu *et al*. reported similar effects of homocoupling on the performance of PTB7 polymer solar cells.[19] Additionally, it was identified that

homocoupling leads to increased bimolecular recombination in the solar cells. In 2016, Sommer *et al.*, reported on the occurrence of homocouplings in the PCDTBT polymer synthesized by Suzuki polycondensation. Up to 8% homocoupling of the carbazole unit was observed, leading to a strong decrease in J_{sc}, resulting in lower device performances.[16]

Although the reports are limited, the presence of homocoupling in the donor polymer clearly has a strong influence on the photovoltaic performance. Characterization of the effect of homocoupling remains, however, a difficult task as it does not influence one parameter solemnly and the extent to which homocoupling occurs can differ from batch to batch. It also remains difficult to precisely analyse and quantify the specific amount of homocoupling that is present in the donor polymer. ^{1}H NMR analysis, as regularly applied for conjugated polymers prepared by direct arylation polymerization, is often complicated due to significant signal broadening. Therefore, there is certainly a need to further analyse the effects of homocoupling, preferentially for cases which allow proper characterization of the polymer backbone structure. Cyclopentadithiophene – quinoxaline copolymers are perfectly suited for such studies as they show minimal signal broadening in ^{1}H NMR and can easily be analysed by MALDI-TOF. Upon fluorination of the quinoxaline unit, average efficiencies up to 5% have been reached.[23,24] In this study, a structurally very similar polymer, PDTSQx$_{ff}$, was used, which is synthesized by Stille polycondensation between the stannylated dithienosilole and the brominated difluoroquinoxaline. PDTSQx$_{ff}$ has a high solubility in various solvents (chloroform, chlorobenzene, tetrahydrofuran, etc.) allowing an easy characterization and it affords a moderate solar cell efficiency of 5.5%, which allows proper detection of fluctuations of the photovoltaic performance. PDTSQx$_{ff}$ can easily be analysed by MALDI-TOF up to molecular weights of 20 kDa to enable proper determination of the homocoupling content.[17,18,20]

Previous studies have mainly focussed on the influence of homocoupling of the donor unit, although it has been shown that homocoupling in the acceptor unit also readily occurs,[25] and in a rare case even improved the photovoltaic performance.[26] For this reason, the acceptor unit was specifically targeted in the present study. A homocoupled biquinoxaline acceptor unit was synthesized and added to the polymerization mixture for PDTSQx$_{ff}$. Effective built-in of this building block is confirmed by MALDI-TOF. The impact of acceptor-acceptor homocoupling on the photovoltaic performance is analysed and correlated to the gradually changing physical and optoelectronic properties of the polymers.

5.2 Results and discussion

To mimic homocoupling, the quinoxaline monomer was deliberately homocoupled prior to the polymerization (Scheme 1). Br-(Qx$_{ff}$)$_2$-Br can be synthesized directly from the standard Br-Qx$_{ff}$-Br monomer by reaction with hexabutylditin under Stille cross-coupling conditions. Although only 0.4 equivalents of the hexabutylditin compound were added to favour dimer formation, the reaction mixture consisted out of a distribution of oligomers, ranging from monomers to pentamers. The different oligomers were separated by recycling preparative size-exclusion chromatography (prep-SEC) in order to yield the pure dibrominated diquinoxaline. Despite the low yield, this method was more effective than other direct coupling methods such as Ni(COD)$_2$, which also yielded a large portion of debrominated products, hindering purification. To assure proper polymerization, the Me$_3$Sn-DTS-SnMe$_3$ monomer was directly used after purification (removal of the monostannylated compound) with prep-SEC.

Specific quantities of the quinoxaline dimer, ranging from 0, 5, 25, 50, 75 to 100% with respect to the standard quinoxaline monomer, were then added to the polymerization reaction. After the reactions, palladium was removed by addition of the diethyldithiocarbamate trihydrate scavenging agent and precipitation in methanol. The resulting polymers were further purified by prep-SEC, which also allowed tuning of the final number average molecular weight (M_n) of the polymers. As large differences in molecular weight of the polymer could also cause differences in the optoelectronic properties and morphology of the bulk heterojunction solid state blend, the molecular weight of all samples was tuned between 25 and 30 kDa (Table 1).
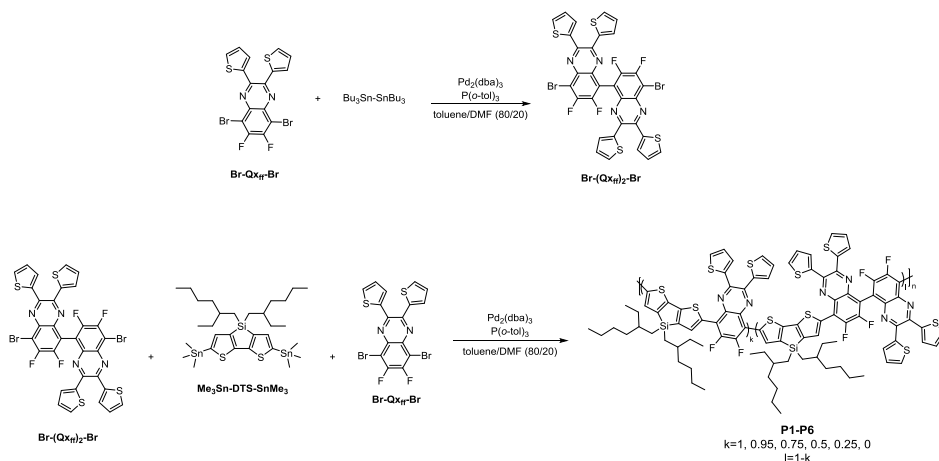
Scheme 1. Top: Synthesis of the homocoupled quinoxaline monomer. Bottom: Stille polycondensation yielding the PDTSQxff polymer series (**P1**-**P6**) with different quantities of homocoupling.

All polymers were analysed by ^{1}H NMR spectroscopy (Figure S16-S21). The amount of homocoupling along the polymer chain, which can be calculated by integration of the proton signals of the quinoxaline dimer compared to the standard quinoxaline unit, matches with the stoichiometric ratio of the monomers used for the polymer synthesis.

MALDI-TOF was then used to confirm the effective built-in of homocouplings along the polymer chain and for determination of the end groups of the polymers (Figure S1-S10). For **P1**, molecular weights up to 20 kDa could be observed and no clear signals of homocoupling segments were found (Figure 1). The end groups were mainly methyl groups or a combination of one hydrogen and one methyl, independent of the amount of homocoupling. End group determination is most easily done in the lower molecular weight region as the resolution goes down with increasing molecular weight. The methyl end groups are most likely the result of a methyl-shift originating from the trimethyl stannyl functionalities.[27] Methyl end groups are rather found on the quinoxaline polymer chain ends and hydrogen groups on the dithienosilole polymer chain ends.
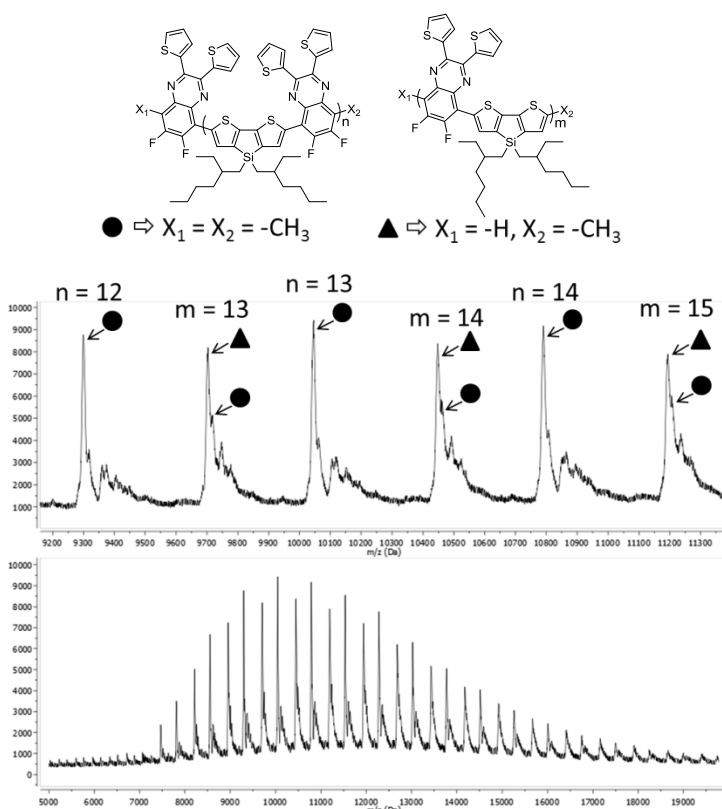

Figure 1. MALDI-TOF mass spectrum of the virtually defect-free PDTSQx$_{ff}$ polymer **P1** prepared by Stille polycondensation.
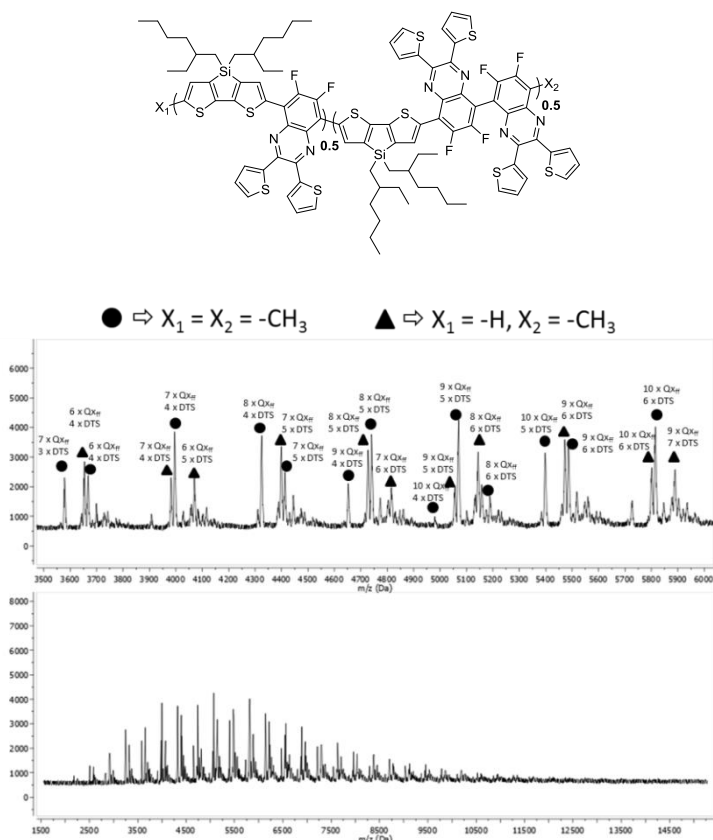
Figure 2. MALDI-TOF mass spectrum of lower molecular weight PDTSQx$_{ff}$ polymer P4 with 50% homocoupling.

Careful analysis of the MALDI-TOF mass spectrum of lower molecular weight **P4** (Figure 2) shows a distribution of polymer chain lengths with different quinoxaline to dithienosilole ratios, which on average match the projected percentage of homocoupling, confirming successful polymerization and effective built-in of the quinoxaline dimer. A similar overall analysis can be made for the MALDI-TOF mass spectra of the other PDTSQx$_{ff}$ polymer with different homocoupling content (Figure S1-S10).

The polymers were also characterized by UV-VIS absorption spectroscopy in solution and thin film (Figure 3). A small percentage of homocoupling (5%) does not significantly change the absorption profile of the polymer, while the presence of larger amounts clearly causes a blue-shift of the absorption maximum (Table 1). The blue-shift is most pronounced when comparing 0-25, 25-50 and 50-75% of homocoupling, whereas increasing the homocoupling content from 75 to 100% only changes the width of the absorption band. Very similar observations were made for the solid-state spectra and the difference in absorption was also visually seen by the difference in colour of the polymer solutions (Figure S11).
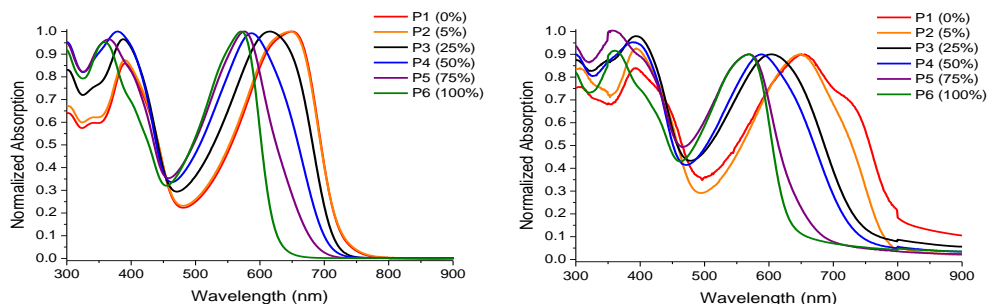
Figure 3. Normalized UV-VIS absorption spectra of polymers **P1–P6** in chloroform solution (left) and in thin film (right).

Determination of the oxidation/reduction potentials and the derived frontier orbital energy levels was done by performing cyclic voltammetry on thin films of the different polymer samples. The obtained values (Table 1) show that the LUMO energy level of the pristine PDTSQx$_{ff}$ polymer is barely affected by the presence of homocoupling. The HOMO energy levels also remain constant up to 50% homocoupling and significant differences were only detected for the 75% and pure homocoupled polymer. With a constant LUMO energy level and a decreasing HOMO energy level, the bandgap of the polymer increases with increased homocoupling content, in good agreement with the solid-state UV-VIS data. Comparison of the HOMO and LUMO energy levels of Br-Qx$_{ff}$-Br (-6.26 eV and -3.50 eV) and Br-(Qx$_{ff}$)$_2$-Br (-6.26 eV and -3.46 eV) indicates that the acceptor strength remains constant upon dimerization of the quinoxaline.

Table 1. Overview of the characterization data for PDTSQx$_{ff}$ polymers **P1-P6** with different homocoupling content.

	P1	**P2**	**P3**	**P4**	**P5**	**P6**
(Qx$_{ff}$)$_2$ (%)	0	5	25	50	75	100
M_n (kDa)	30.1	25.2	27.6	24.5	25.6	30.2
PDI	1.29	1.12	1.31	1.49	1.25	1.28
λ_{max} (nm)[a]	649	647	617	587	570	568
ΔE_{opt} (eV)	1.65	1.68	1.66	1.68	1.89	1.95
ΔE_{EC} (eV)	2.09	2.09	2.08	2.11	2.20	2.28
E_{ox} (eV)	0.58	0.60	0.57	0.61	0.72	0.81
E_{red} (eV)	-1.51	-1.49	-1.51	-1.51	-1.48	-1.47
E(HOMO) (eV)	-5.49	-5.51	-5.48	-5.51	-5.62	-5.71
E(LUMO) (eV)	-3.40	-3.42	-3.40	-3.40	-3.42	-3.43

[a] Determined from UV-VIS absorption spectra of the polymer solutions in chloroform.

All polymers were then tested for their photovoltaic performance. The virtually defect-free PDTSQx$_{ff}$ polymer **P1** shows the highest performance with a V_{oc} of 0.88 V, a J_{sc} of 10.16 mA/cm² and a FF of 0.54, resulting in an average power conversion efficiency (PCE) of 4.84% (Table 2). The presence of up to 25%

homocoupling only slightly influences the performance of the solar cells. Further increase of the homocoupling content decreases the J_{sc} significantly, and simultaneously the FF, which results in an overall lower average PCE for higher homocoupling content. The HOMO energy level decreases significantly for a homocoupling content of 75 and 100%, but this is not fully reflected in the V_{oc} of the **P5** and **P6** polymer solar cells, pointing to additional voltage losses in the (far from optimal) devices. The surface topography of the solar cells was investigated with Atomic Force Microscopy (AFM, Figure S28), but no significant differences were found.

Table 2. Photovoltaic performances of BHJ polymer solar cells prepared from PDTSQx$_{ff}$ polymers **P1-P6** with different homocoupling content.

Active layer composition	(Qx$_{ff}$)$_2$ (%)	V_{oc} (V)	J_{sc} (mA/cm²)	FF	PCE$_{Aver}$ (%)[a]	PCE$_{max}$ (%)
P1/PC$_{71}$BM	0	0.88	10.16	0.54	4.84	5.05
P2/PC$_{71}$BM	5	0.86	9.70	0.56	4.66	4.83
P3/PC$_{71}$BM	25	0.88	9.50	0.54	4.52	4.71
P4/PC$_{71}$BM	50	0.91	8.69	0.45	3.56	3.58
P5/PC$_{71}$BM	75	0.86	5.80	0.33	1.67	1.85
P6/PC$_{71}$BM	100	0.90	4.92	0.31	1.35	1.46

[a] Averages over at least 8 devices

5.3 Conclusions

An increase in the number of homocouplings in the acceptor unit of a PDTSQx$_{ff}$ polymer induces a blue-shift in the UV-VIS absorption spectra and a decrease in the band-width. High homocoupling contents dramatically decrease the BHJ solar cell performance, mainly by a decreased short-circuit current and a poor fill factor. Although a significant increase in V_{oc} was expected, based on the HOMO and LUMO energy levels of the different polymers, the V_{oc} only slightly rises and a further increase is hampered by additional voltage losses inside the solar cells.

5.4 Experimental

Materials and methods

All reagents and chemicals were obtained from commercial sources and used without further purification. Solvents were dried by a solvent purification system (MBraun, MB-SPS-800) equipped with alumina columns. 4,4-Bis(2-ethylhexyl)-2,6-bis(trimethylstannyl)-4*H*-silolo[3,2-*b*:4,5-*b*']dithiophene and 5,8-dibromo-6,7-difluoro-2,3-di(thiophen-2-yl)quinoxaline were synthesized according to literature procedures. Preparative (recycling) size exclusion chromatography was performed on a JAI LC-9110 NEXT system equipped with JAIGEL 1*H* and 2*H* columns (eluent CHCl$_3$, flow rate 3.5 mL/min). ^{1}H NMR spectra were recorded in

CDCl$_3$ or CD$_2$Cl$_2$ and chemical shifts (δ, in ppm) were determined relative to the residual CHCl$_3$ (7.26 ppm) or CD$_2$Cl$_2$ (5.32 ppm) absorption. The ^{13}C NMR spectrum of Br-(Qx$_{ff}$)$_2$-Br was recorded in d$_8$-THF and chemical shifts were determined relative to the residual d$_8$-THF (67.21 and 25.31 ppm) absorptions. High resolution electrospray ionization mass spectrometry (ESI-MS) was performed using an LTQ Orbitrap Velos Pro mass spectrometer equipped with an atmospheric pressure ionization source operating in the nebulizer assisted electrospray mode. The instrument was calibrated in the *m/z* range 220−2000 using a standard solution containing caffeine, MRFA and Ultramark 1621. MALDI-TOF mass spectra were recorded on a Bruker Daltonics Ultraflex II Tof/Tof. 1 μL of the matrix solution (16 mg/mL DTCB (*trans*-2-[3-(4-*tert*-butylphenyl)-2-methyl-2-propenylidene]malononitrile) in CHCl$_3$) was spotted onto an MTP Anchorchip 600/384 MALDI plate. The spot was allowed to dry and 1 μL of the analyte solution (0.5 mg/mL in CHCl$_3$) was spotted on top of the matrix. UV-Vis measurements were performed on a VARIAN Cary 500 UV-Vis-NIR spectrophotometer at a scan rate of 600 nm/min. The films for the UV-Vis measurements were prepared by drop casting a solution of the polymer in chloroform on a quartz substrate. The solid-state UV-Vis spectra were used to estimate the optical HOMO-LUMO gaps (from the wavelength at the intersection of the tangent line drawn at the low energy side of the absorption spectrum with the x-axis: E_g (eV) = 1240/(wavelength in nm)). Electrochemical measurements (cyclic voltammetry) were performed with an Eco Chemie Autolab PGSTAT 30 potentiostat/galvanostat using a three-electrode microcell with a platinum working electrode, a platinum counter electrode and a Ag/AgNO$_3$ reference electrode (silver wire dipped in a solution of 0.01 M AgNO$_3$ and 0.1 M NBu$_4$PF$_6$ in anhydrous acetonitrile). The reference electrode was calibrated against ferrocene/ferrocenium as an external standard. Samples were prepared by dip coating the platinum working electrode in the respective monomer/polymer solutions (also used for the solid-state UV-Vis measurements). The CV measurements were done on the resulting films with 0.1 M NBu$_4$PF$_6$ in anhydrous acetonitrile as electrolyte solution. To prevent air from entering the system, the experiments were carried out under a curtain of argon. Cyclic voltammograms were recorded at a scan rate of 100 mV s^{-1}. For the conversion of V to eV, the onset potentials of the first oxidation/reduction peaks were used and referenced to ferrocene/ferrocenium, which has an ionization potential of −4.98 eV *vs.* vacuum. This correction factor is based on a value of 0.31 eV for Fc/Fc$^+$ *vs.* SCE[28] and a value of 4.68 eV for SCE *vs.* vacuum[29] : $E_{HOMO/LUMO}$ (eV) = $-4.98 - E_{\text{onset ox/red}}^{\text{Ag/AgNO3}}$ (V) + $E_{\text{onset Fc/Fc+}}^{\text{Ag/AgNO3}}$ (V). The reported values are the means of the first four redox cycles.

Synthetic procedures

8,8'-Dibromo-6,6',7,7'-tetrafluoro-2,2',3,3'-tetra(thiophen-2-yl)-5,5'-biquinoxaline (Br–(Qx$_{ff}$)$_2$–Br)

1,1,1,2,2,2-Hexabutyldistannane (1.72 g, 2.97 mmol), 5,8-dibromo-6,7-difluoro-2,3-di(thiophen-2-yl)quinoxaline (3.00 g, 6.15 mmol), Pd$_2$(dba)$_3$ (0.140 g, 0.15 mmol) and P(o-tol)$_3$ (0.187 g, 0.61 mmol) were dissolved in freshly degassed dry DMF (12 mL) and dry toluene (48 mL), under nitrogen atmosphere. The solution was purged with nitrogen for 30 min and heated to 100 °C for 20 h. The solution was then allowed to cool to room temperature and water was added. After extraction with chloroform, the organic layer was washed with brine, dried over MgSO$_4$, filtered and the solvent was removed under reduced pressure. The crude material was further purified by recycling prep-SEC and the pure compound was collected as a yellow solid (300 mg, 6%). ^{1}H NMR (400 MHz, CDCl$_3$) δ 7.56 (dd, J = 5.0, 1.1 Hz, 2H), 7.44 (dd, J = 3.8, 1.1 Hz, 2H), 7.25 (dd, J = 5.1, 1.1 Hz, 2H), 7.19 (dd, J = 3.8, 1.1 Hz, 2H), 7.04 (dd, J = 5.0, 3.7 Hz, 2H), 6.86 (dd, J = 5.0, 3.8 Hz, 2H). ^{13}C NMR (101 MHz, THF-d_8) δ 152.8 (dd, J = 37.6, 16.2 Hz), 150.3 (dd, J = 44.3, 16.5 Hz), 147.9, 147.6, 142.0, 137.0, 136.4, 132.4 – 127.6 (m), 116.7 (d, J = 11.2 Hz), 111.8 (d, J = 17.6 Hz).

Polymerization procedure

The appropriate amounts of 5,8-dibromo-6,7-difluoro-2,3-di(thiophen-2-yl)quinoxaline, 8,8'-dibromo-6,6',7,7'-tetrafluoro-2,2',3,3'-tetra(thiophen-2-yl)-5,5'-biquinoxaline and 4,4-bis(2-ethylhexyl)-2,6-bis(trimethylstannyl)-4H-silolo[3,2-b:4,5-b']dithiophene, together with Pd$_2$(dba)$_3$ (3 mol%) and P(o-tol)$_3$ (12 mol%), were charged in a dry Schlenk tube equipped with a magnetic stirring bar. A freshly degassed mixture of dry DMF:toluene (2:8) was added, resulting in an overall monomer concentration of 110 mM. The reaction mixture was then stirred for 16 h at 110 °C. After cooling down to 70 °C, sodium diethyldithiocarbamate trihydrate (0.675 g, 2.99 mmol), dissolved in water (6 mL), was added and the mixture was stirred heavily for an additional 30 min. The organic phase was added to methanol, causing polymer precipitation, and the crude polymer material was collected by filtration and dried under reduced pressure. The polymer was further purified by recycling prep-SEC. Yield: **P1** = 73%, **P2** = 84%, **P3** = 66%, **P4** = 80%, **P5** = 84%, **P6** = 80%.

Photovoltaic device fabrication and characterization

Bulk heterojunction polymer solar cells were fabricated using the standard architecture glass/ITO/PEDOT:PSS/polymer:$PC_{71}BM$/Ca/Al. Prior to device construction, the prepatterned indium tin oxide (ITO, Kintec, 100 nm, 20 Ohm/sq) containing glass substrates were thoroughly cleaned using soap, demineralized water, acetone, isopropanol and a UV/O_3 treatment. Consequently, a thin layer of PEDOT:PSS [poly(3,4-ethylenedioxythiophene): poly(styrenesulfonic acid), Heraeus Clevios] was deposited by spin-coating with a thickness of ~30 nm, followed by an annealing step at 130 °C for 15 mins to remove residual water. Further processing was carried out under nitrogen atmosphere in a glovebox (O_2/H_2O < 0.1 ppm). The polymer:$PC_{71}BM$ active layer blend solution was spin-coated on top of PEDOT:PSS with concentration, solvent and polymer:fullerene ratio as described in Table S1-S4. Finally, the devices were finished off with Ca/Al (~30/80 nm). In this way an active area of ~8.5 mm² was obtained. The *J-V* curves under illumination were obtained using a Newport class A solar simulator (model 91195A) calibrated with a silicon solar cell to give an AM 1.5G spectrum. A shadow mask was employed to ensure a more accurate active area of 3 mm² and to prevent indirect lighting to influence the measurements. AFM experiments were performed with a JPK NanoWizard 3 AFM (JPK Instruments AG, Berlin, Germany) using AC mode in air. Silicon ACTA-50 tips from AppNano with cantilever length ~125 mm, spring constant ~40 N/m and resonance frequency ~300 kHz were used. The scan angle, set point height, gain values and scan rate were adjusted according to the calibration of the AFM tip.

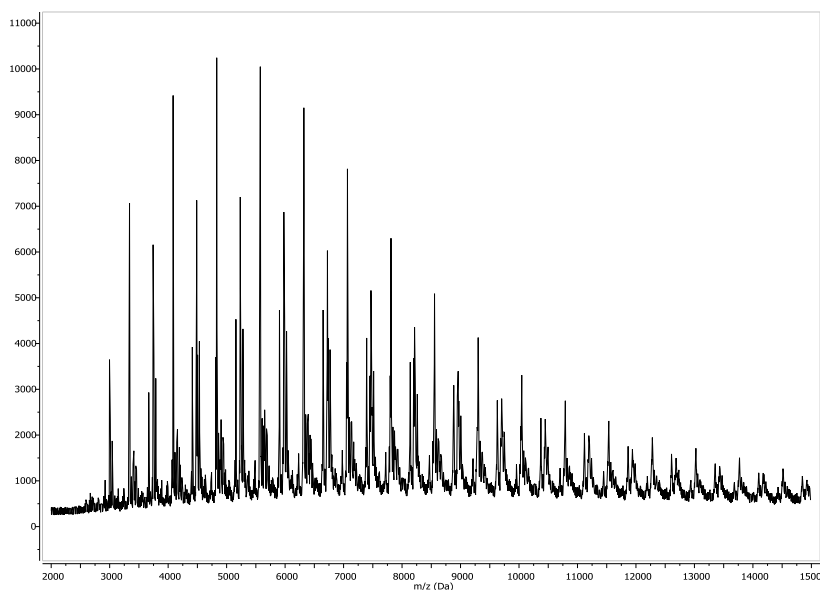# 5.5 Supporting information

5.5.1 MALDI-TOF mass spectra

Figure S1. MALDI-TOF mass spectrum of the low molecular weight fraction of PDTSQx$_{ff}$ with 5% homocoupling (**P2**).
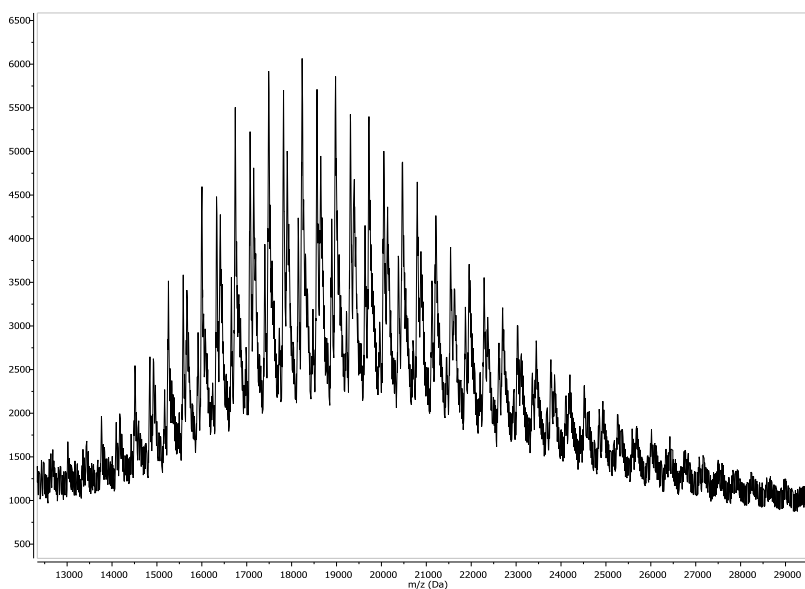

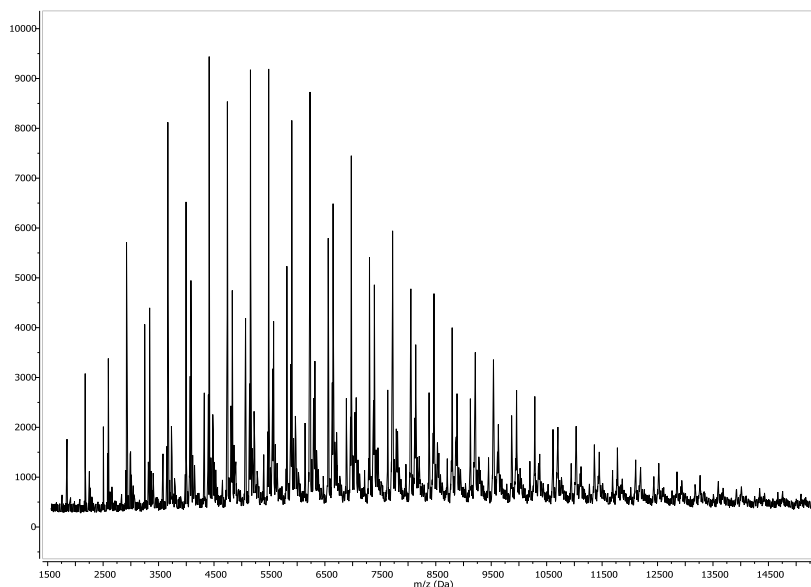**Figure S2.** MALDI-TOF mass spectrum of the high molecular weight fraction of PDTSQx$_{ff}$ with 5% homocoupling (**P2**).

Figure S3. MALDI-TOF mass spectrum of the low molecular weight fraction of PDTSQx$_{ff}$ with 25% homocoupling (**P3**).
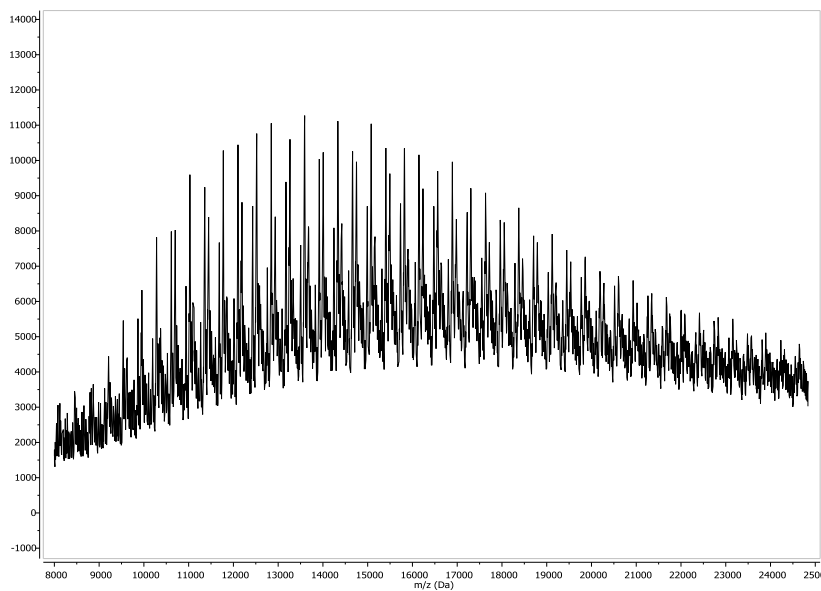

Figure S4. MALDI-TOF mass spectrum of the high molecular weight fraction of PDTSQx$_{ff}$ with 25% homocoupling (**P3**).
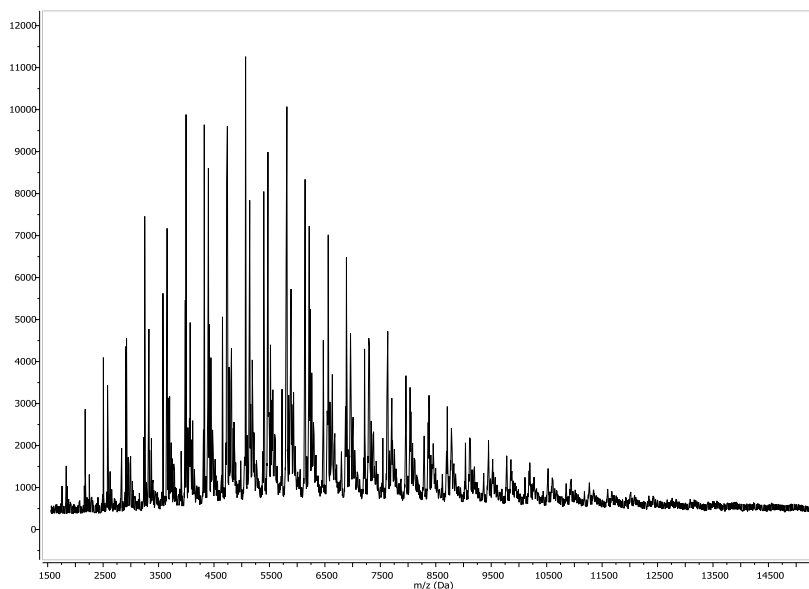
Figure S5. MALDI-TOF mass spectrum of the lower molecular weight fraction of PDTSQx_{ff} with 50% homocoupling (**P4**).
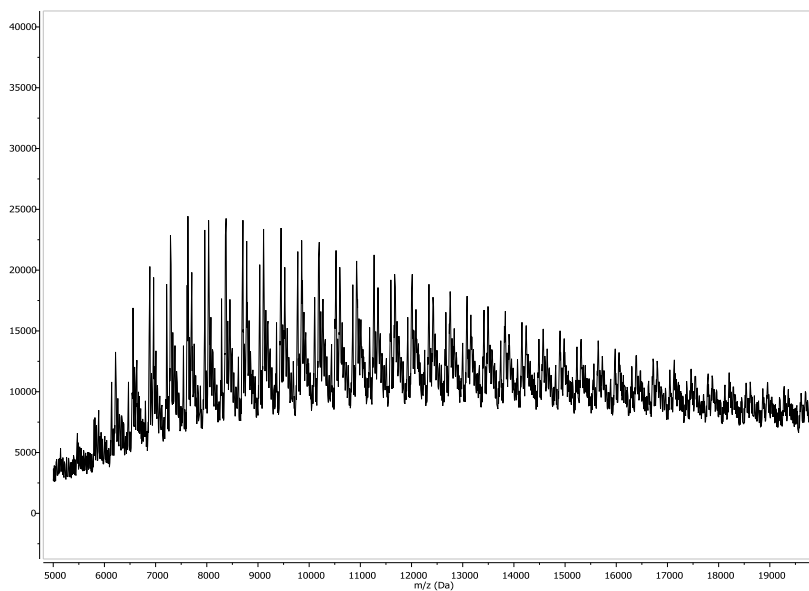

Figure S6. MALDI-TOF mass spectrum of the higher molecular weight fraction of PDTSQx_{ff} with 50% homocoupling (**P4**).
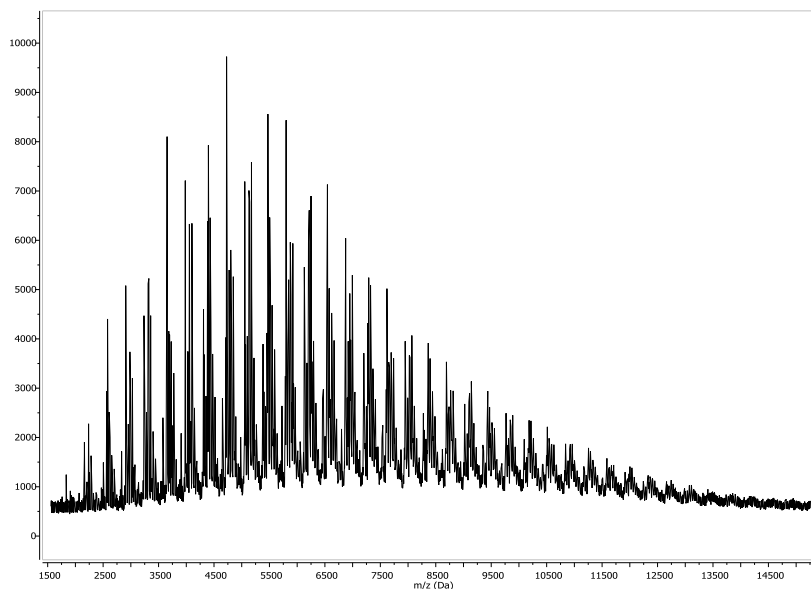
Figure S7. MALDI-TOF mass spectrum of the lower molecular weight fraction of PDTSQx$_{ff}$ with 75% homocoupling (**P5**).
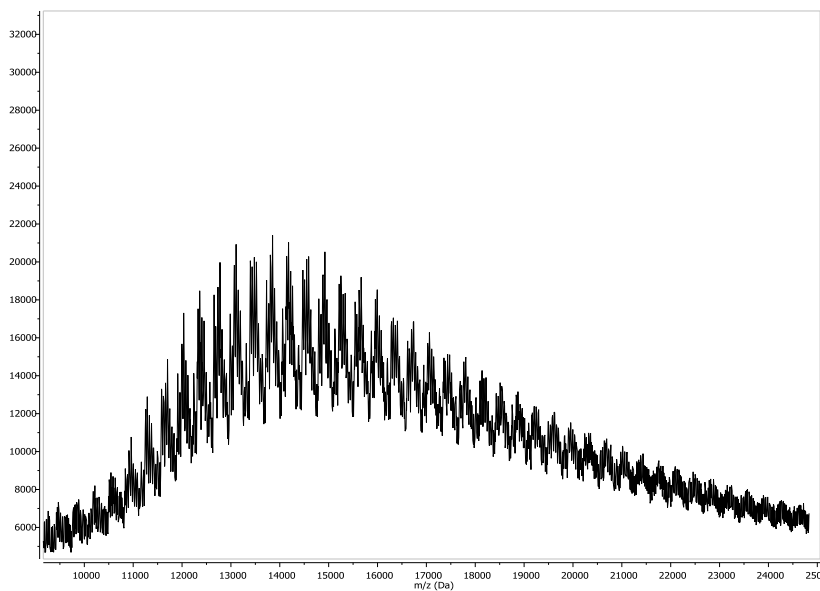

Figure S8. MALDI-TOF mass spectrum of the higher molecular weight fraction of PDTSQx$_{ff}$ with 75% homocoupling (**P5**).
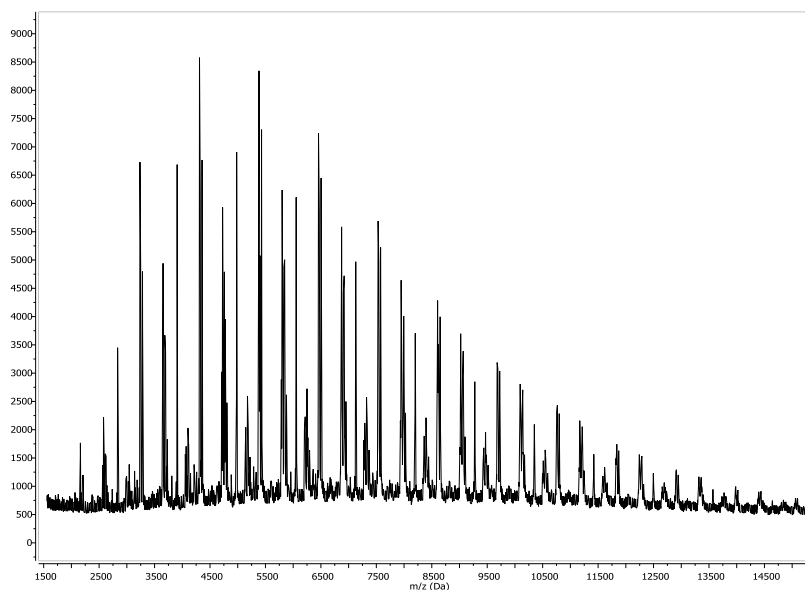
Figure S9. MALDI-TOF mass spectrum of the lower molecular weight fraction of PDTS(Qx$_{ff}$)$_2$ (**P6**).
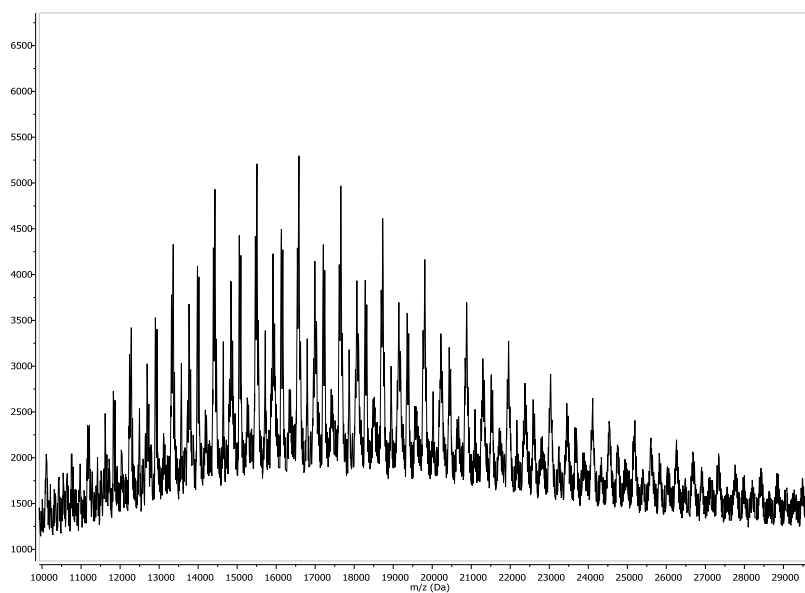
Figure S10. MALDI-TOF mass spectrum of the higher molecular weight fraction of PDTS(Qx$_{ff}$)$_2$ (**P6**).

5.5.2 Polymer solutions
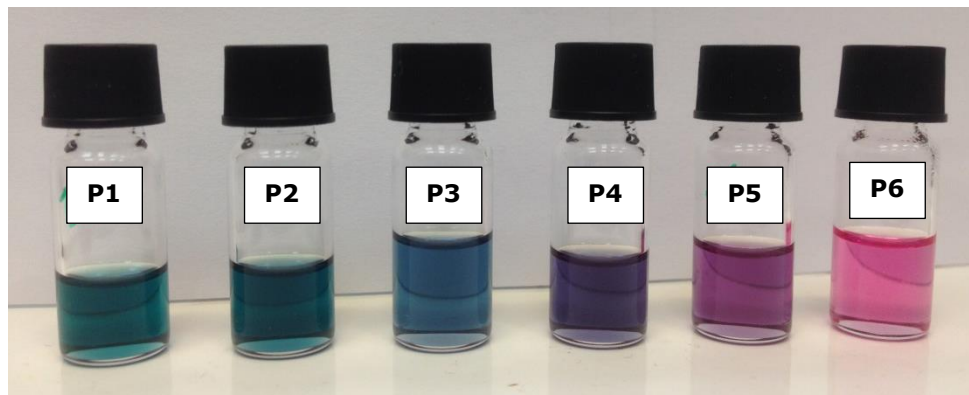
Figure S11. The colour of the polymer in solution (chloroform) changes gradually with the amount of homocouplings.

5.5.3 NMR spectra

Figure S12. ^{1}H NMR spectrum of 5,8-dibromo-6,7-difluoro-2,3-di(thiophen-2-yl)quinoxaline (Br-Qx_ff-Br).

Figure S13. ^{1}H NMR spectrum of 4,4-bis(2-ethylhexyl)-2,6-bis(trimethylstannyl)-4*H*-silolo[3,2-*b*:4,5-*b'*]dithiophene.

Figure S14. ^{1}H NMR spectrum of 8,8'-dibromo-6,6',7,7'-tetrafluoro-2,2',3,3'-tetra(thiophen-2-yl)-5,5'-biquinoxaline (Br-(Qx$_{ff}$)$_2$-Br).

Figure S15. ^{13}C NMR spectrum of 8,8'-dibromo-6,6',7,7'-tetrafluoro-2,2',3,3'-tetra(thiophen-2-yl)-5,5'-biquinoxaline (Br-(Qx$_{ff}$)$_2$-Br).

Figure S16. ^{1}H NMR spectrum of virtually defect free PDTSQx$_{ff}$ (**P1**).

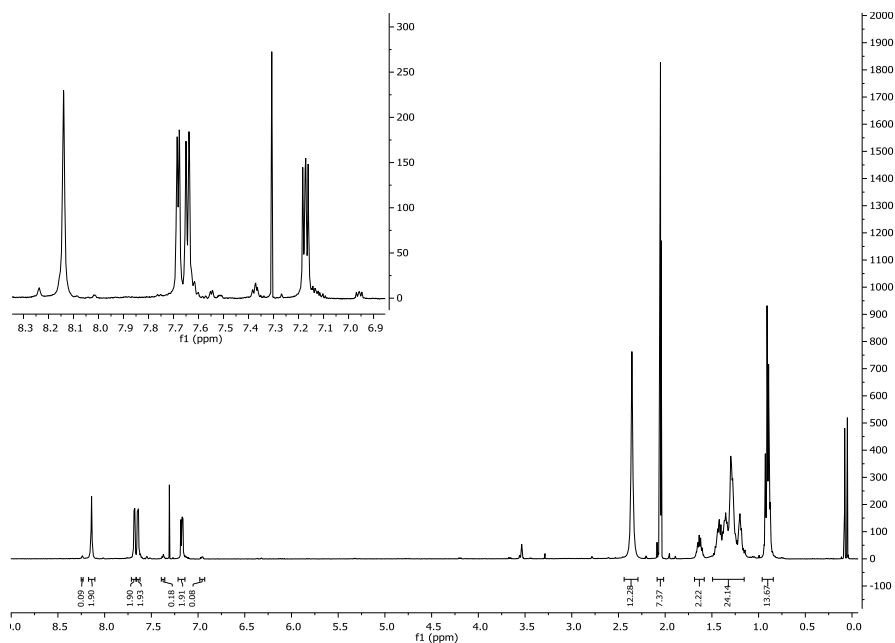**Figure S17.** ^{1}H NMR spectrum of PDTSQx$_{ff}$ with 5% homocoupling (**P2**).
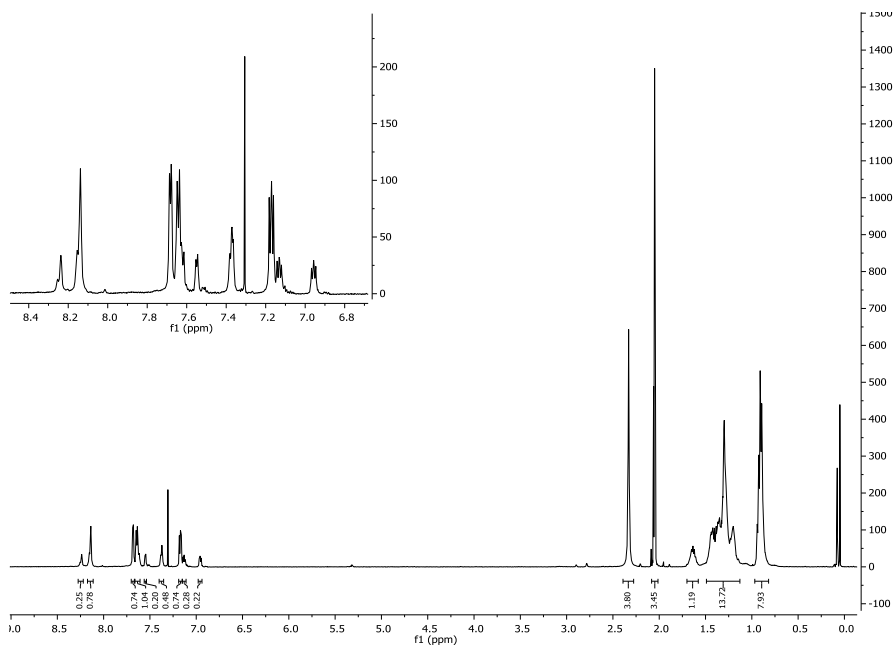
Figure S18. ^{1}H NMR spectrum of PDTSQx$_{ff}$ with 25% homocoupling (**P3**).
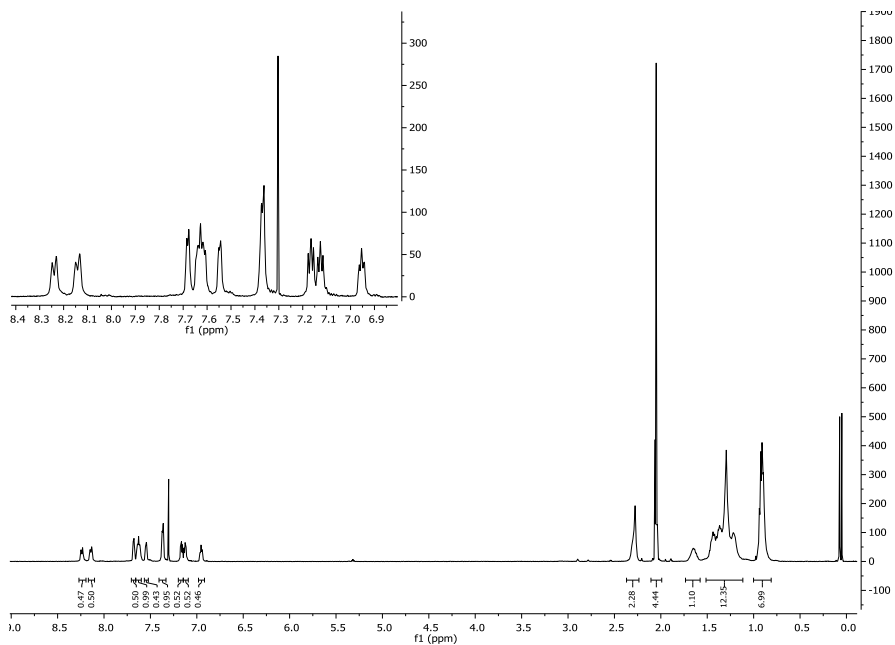
Figure S19. ^{1}H NMR spectrum of PDTSQx$_{ff}$ with 50% homocoupling (**P4**).
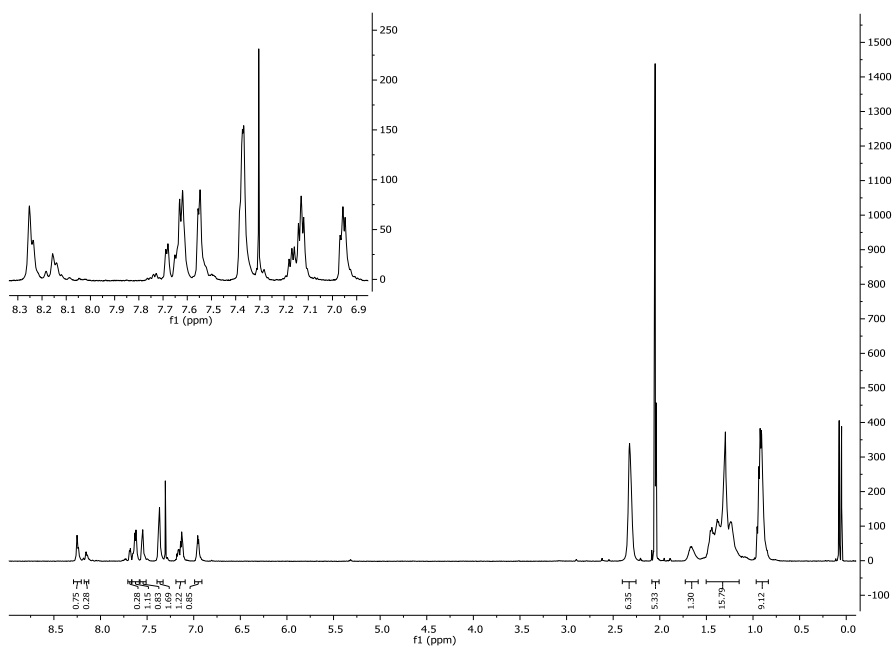
Figure S20. ^{1}H NMR spectrum of PDTSQx$_{ff}$ with 75% homocoupling (**P5**).
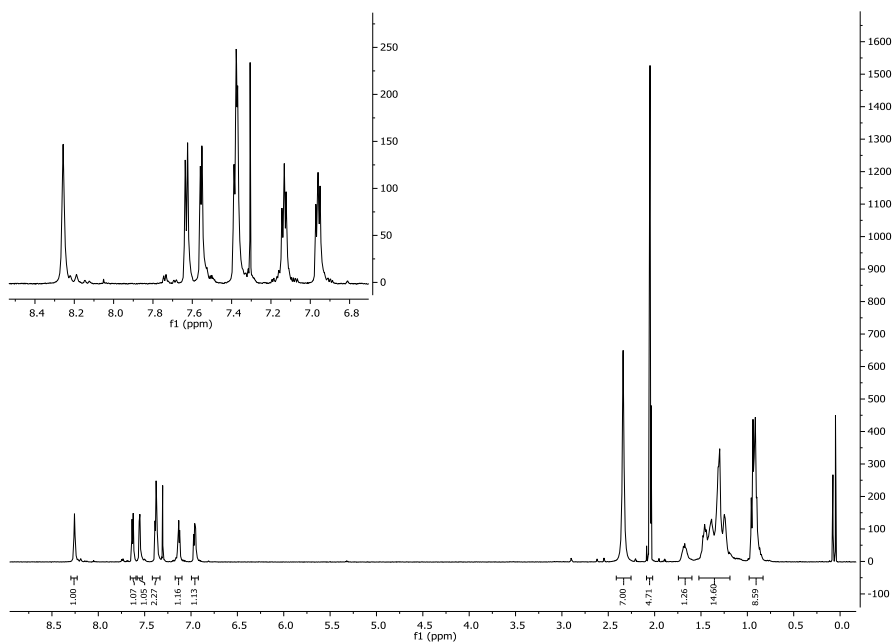
Figure S21. ^{1}H NMR spectrum of PDTS(Qx$_{ff}$)$_2$ (**P6**).

5.5.4 Cyclic voltammograms
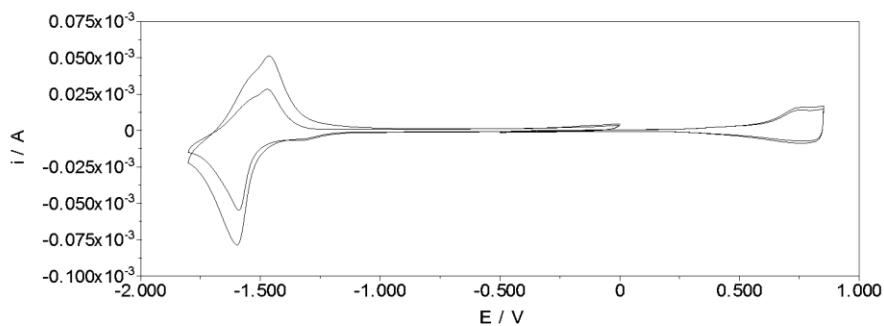
Figure S22: Cyclic voltammogram of PDTSQx$_{ff}$ (**P1**).

Figure S23: Cyclic voltammogram of PDTSQx$_{ff}$ with 5% homocoupling (**P2**).

Figure S24: Cyclic voltammogram of PDTSQx$_{ff}$ with 25% homocoupling (**P3**).
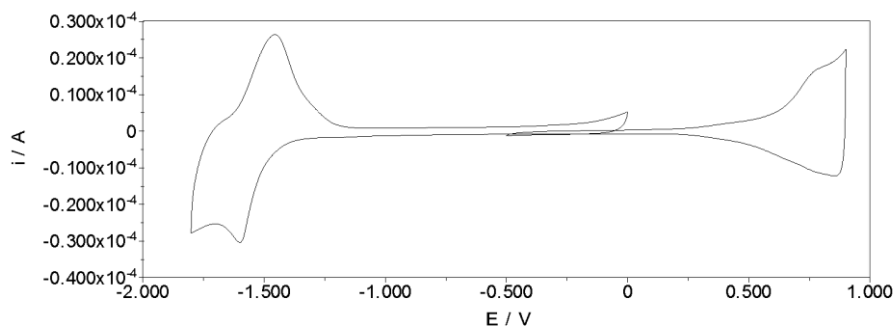
Figure S25: Cyclic voltammogram of PDTSQx$_{ff}$ with 50% homocoupling (**P4**).

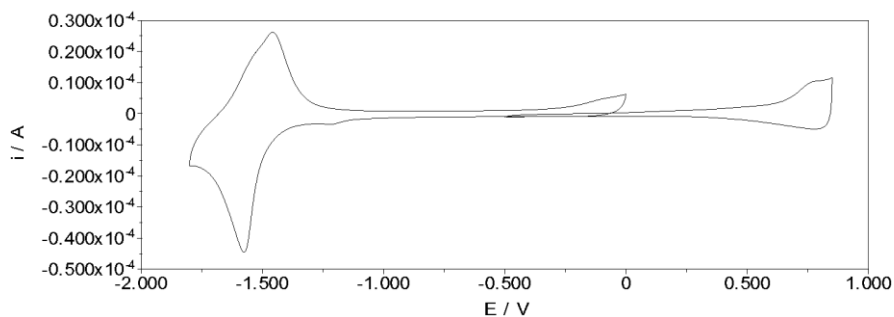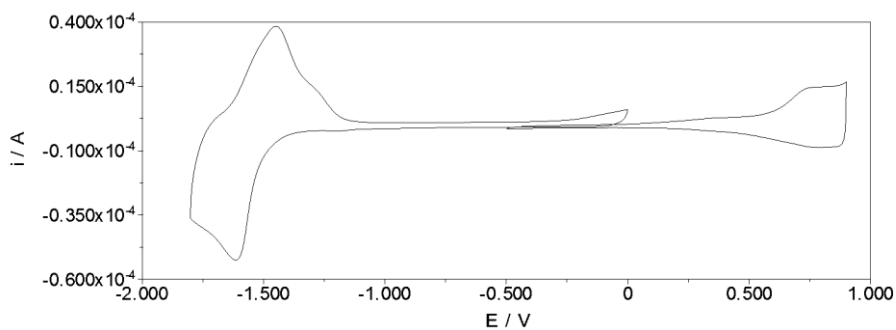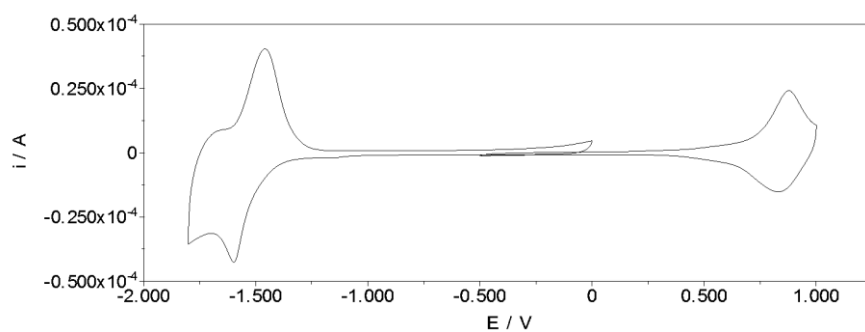**Figure S26:** Cyclic voltammogram of PDTSQx$_{ff}$ with 75% homocoupling (**P5**).
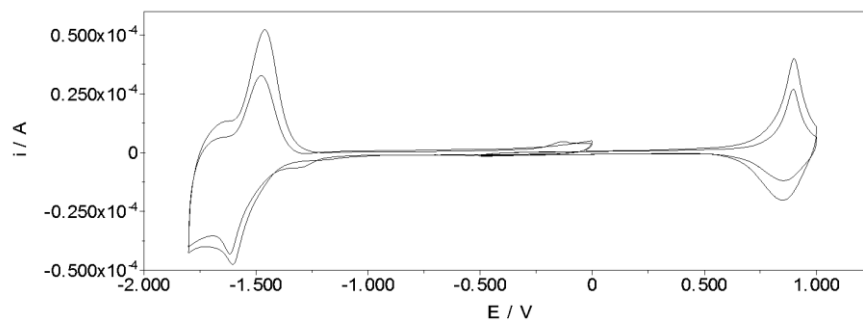
Figure S27: Cyclic voltammogram of PDTS(Qx$_{ff}$)$_2$ (**P6**).

5.5.5 Solar cell optimization data

Table S1. Photovoltaic performances of BHJ polymer solar cells prepared from PDTSQx$_{ff}$ polymers **P1-P6**, with different spin-coating speeds (polymer concentration of 6.4 mg/mL, chlorobenzene as a solvent, and polymer:PC$_{71}$BM ratio of 1:4).

Polymer	Spin-coating speed (rpm)	V_{oc} (V)	J_{sc} (mA/cm²)	FF	PCE $_{Aver}$ (%)	PCE$_{max}$ (%)
	1300	0.85	10.66	0.60	5.45	5.69
P1	1500	0.85	10.53	0.61	5.43	5.62
	1800	0.85	10.51	0.59	5.29	5.73
	1000	0.85	9.61	0.54	4.46	4.68
P2	1500	0.85	9.71	0.56	4.62	4.92
	2000	0.86	9.70	0.56	4.66	4.83
	1000	0.88	8.84	0.49	3.77	3.91
P3	1500	0.88	9.63	0.53	4.51	4.69
	2000	0.88	9.50	0.54	4.52	4.71
	1000	0.89	7.42	0.36	2.42	2.63
P4	1500	0.89	8.00	0.40	2.84	2.86
	2000	0.91	8.69	0.45	3.56	3.58
	1000	0.85	3.73	0.32	1.00	1.11
P5	1500	0.85	5.07	0.32	1.36	1.40
	2000	0.86	5.80	0.33	1.67	1.85
	1000	0.88	2.74	0.30	0.71	0.79
P6	1500	0.87	3.89	0.30	1.00	1.09
	2000	0.90	4.92	0.31	1.35	1.46

Table S2. Photovoltaic performances of BHJ polymer solar cells prepared from PDTSQx$_{ff}$ polymer **P1** with different spin-coating speeds and percentages of the solvent additive chloronaphthalene, (polymer concentration of 6.4 mg/mL, chlorobenzene as a solvent, and polymer:PC$_{71}$BM ratio of 1:4).

Additive amount (%)	Spin-coating speed (rpm)	V_{oc} (V)	J_{sc} (mA/cm²)	FF	PCE$_{aver}$ (%)	PCE$_{max}$ (%)
	1300	0.85	10.66	0.60	5.45	5.69
0%	1500	0.85	10.53	0.61	5.43	5.62
	1800	0.85	10.51	0.59	5.29	5.73
	1300	0.85	10.07	0.57	4.85	4.97
3%	1500	0.85	9.94	0.56	4.72	4.76
	1800	0.85	9.23	0.59	4.66	4.73
	1300	0.85	9.69	0.53	4.33	4.35
5%	1500	0.85	8.58	0.57	4.19	4.91
	1800	0.85	9.54	0.58	4.73	4.94

Table S3. Photovoltaic performances of BHJ polymer solar cells prepared from PDTSQx$_{ff}$ polymer **P1** by spin-coating from different solvents (polymer:PC$_{71}$BM ratio of 1:3).

Solvent[a]	[**P1**][b] (mg/mL)	V_{oc} (V)	J_{sc} (mA/cm²)	FF	PCE$_{aver}$ (%)	PCE$_{max}$ (%)
CB	8	0.88	10.16	0.54	4.84	5.05
ODCB	8	0.88	9.16	0.53	4.30	4.30
CHCl$_3$	5	0.84	9.87	0.53	4.39	4.55

[a] CB = Chlorobenzene, ODCB = *o*-dichlorobenzene
[b] A different batch of PDTSQx$_{ff}$ **P1** than used throughout this work, was used for this screening. This additional batch was prepared according to the same procedure and has similar molecular weight (M$_n$ = 30.2 kDa and PDI = 1.29).

Table S4. Photovoltaic performances of BHJ polymer solar cells prepared from PDTSQx$_{ff}$ polymer **P1** with different polymer:PC$_{71}$BM ratios (with constant overall concentration in chlorobenzene).

[**P1**] (mg/mL)	**P1**:PC$_{71}$BM	V_{oc} (V)	J_{sc} (mA/cm²)	FF	PCE$_{aver}$ (%)	PCE$_{max}$ (%)
9.1	1:2.5	0.88	10.39	0.53	4.82	4.97
8.0	1:3	0.88	10.27	0.55	4.98	5.17
7.1	1:3.5	0.87	10.21	0.57	5.08	5.40
6.4	1:4	0.87	10.24	0.58	5.14	5.35

*A different batch of PDTSQx$_{ff}$ **P1** than used throughout this work, was used for this screening. This additional batch was prepared according to the same procedure and has similar molecular weight (M$_n$ = 30.2 kDa and PDI = 1.29).
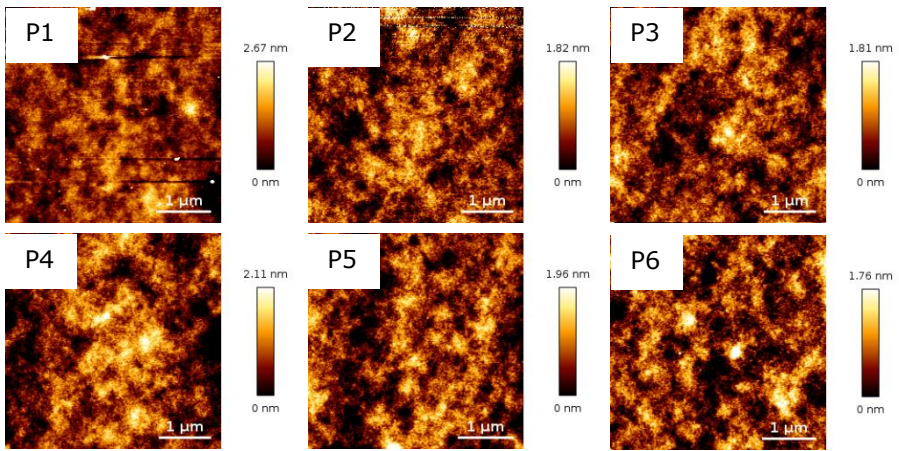
5.5.6 Atomic Force Microscopy images

Figure S28. AFM images of the active layers of the PDTSQx$_{ff}$ **P1–P6** solar cells.

5.6 References

(1)   L. Dou, J. You, Z. Hong, Z. Xu, G. Li, R. A. Street and Y. Yang, *Adv. Mater.*, **2013**, 25, 6642.

(2)   K. A. Mazzio and C. K. Luscombe, *Chem. Soc. Rev.*, **2015**, 44, 78.

(3)   Y. Liu, J. Zhao, Z. Li, C. Mu, W. Ma, H. Hu, K. Jiang, H. Lin, H. Ade and H. Yan, *Nat. Commun.*, **2014**, 5, 5293.

(4)   G. Li, R. Zhu and Y. Yang, *Nat. Photonics*, **2012**, 6, 153.

(5)   L. K. Jagadamma, M. Al-Senani, A. El-Labban, I. Gereige, G. O. Ngongang Ndjawa, J. C. D. Faria, T. Kim, K. Zhao, F. Cruciani, D. H. Anjum, M. A. McLachlan, P. M. Beaujuge and A. Amassian, *Adv. Energy Mater.*, **2015**, 5, 1500204.

(6)   Z. He, B. Xiao, F. Liu, H. Wu, Y. Yang, S. Xiao, C. Wang, T. P. Russell and Y. Cao, *Nat. Photonics*, **2015**, 9, 174.

(7)   Y. Lin, F. Zhao, Y. Wu, K. Chen, Y. Xia, G. Li, S. K. K. Prasad, J. Zhu, L. Huo, H. Bin, Z. G. Zhang, X. Guo, M. Zhang, Y. Sun, F. Gao, Z. Wei, W. Ma, C. Wang, J. Hodgkiss, Z. Bo, O. Inganäs, Y. Li and X. Zhan, *Adv. Mater.*, **2016**, 29, 1604155.

(8)   W. Zhao, D. Qian, S. Zhang, S. Li, O. Inganäs, F. Gao and J. Hou, *Adv. Mater.*, **2016**, 28, 4734.

(9)   D. Baran, T. Kirchartz, S. Wheeler, S. Dimitrov, M. Abdelsamie, J. Gorman, R. Ashraf, S. Holliday, A. Wadsworth, N. Gasparini, P. Kaienburg, H. Yan, A. Amassian, C. J. Brabec, J. Durrant and I. McCulloch, *Energy Environ. Sci.*, **2016**, 9, 3783.

(10)   D. Meng, D. Sun, C. Zhong, T. Liu, B. Fan, L. Huo, Y. Li, W. Jiang, H. Choi, T. Kim, J. Y. Kim, Y. Sun, Z. Wang and A. J. Heeger, *J. Am. Chem. Soc.*, **2016**, 138, 375.

(11)   S. Holliday, R. S. Ashraf, A. Wadsworth, D. Baran, S. A. Yousaf, C. B. Nielsen, C.-H. Tan, S. D. Dimitrov, Z. Shang, N. Gasparini, M. Alamoudi, F. Laquai, C. J. Brabec, A. Salleo, J. R. Durrant and I. McCulloch, *Nat. Commun.*, **2016**, 7, 11585.

(12)   C. Amatore, E. Carré, A. Jutand, H. Tanaka, Q. Ren and S. Torii, *Chem. Eur. J.*, **1996**, 2, 957.

(13)   A. L. Casado, J. A. Casares and P. Espinet, *Organometallics*, **1997**, 16, 5730.

(14)   P. Espinet and A. M. Echavarren, *Angew. Chem. Int. Ed.*, **2004**, 43, 4704.

(15)   B. Carsten, F. He, H. J. Son, T. Xu and L. Yu, *Chem. Rev.*, **2011**, 111, 1493.

(16)   F. Lombeck, H. Komber, D. Fazzi, D. Nava, J. Kuhlmann, D. Stegerer, K. Strassel, J. Brandt, A. D. de Zerio Mendaza, C. Müller, W. Thiel, M. Caironi, R. Friend and M. Sommer, *Adv. Energy Mater.*, **2016**, 6, 1601232.

(17)   P. Verstappen, I. Cardinaletti, T. Vangerven, W. Vanormelingen, F. Verstraeten, L. Lutsen, D. Vanderzande, J. Manca and W. Maes, *RSC Adv.*, **2016**, 6, 32298.

(18)   T. Vangerven, P. Verstappen, N. Patil, J. D'Haen, I. Cardinaletti, J. Benduhn, N. Van den Brande, M. Defour, V. Lemaur, D. Beljonne, R. Lazzaroni, B. Champagne, K. Vandewal, J. W. Andreasen, P. Adriaensens, D. W. Breiby, B. Van Mele, D. Vanderzande, W. Maes and J. Manca, *Chem. Mater.*, **2016**, 28, 9088.

(19)   L. Lu, T. Zheng, T. Xu, D. Zhao and L. Yu, *Chem. Mater.*, **2015**, 27, 537.

(20)   T. Vangerven, P. Verstappen, J. Drijkoningen, W. Dierckx, S. Himmelberger, A. Salleo, D. Vanderzande, W. Maes and J. V. Manca, *Chem. Mater.*, **2015**, 27, 3726.

(21)   K. H. Hendriks, W. Li, G. H. L. Heintges, G. W. P. Van Pruissen, M. M. Wienk and R. A. J. Janssen, *J. Am. Chem. Soc.*, **2014**, 136, 11128.

(22)   F. Lombeck, R. Matsidik, H. Komber and M. Sommer, *Macromol. Rapid Commun.*, **2015**, 36, 231.

(23)   P. Verstappen, J. Kesters, W. Vanormelingen, G. H. L. Heintges, J. Drijkoningen, T. Vangerven, L. Marin, S. Koudjina, B. Champagne, J. Manca, L. Lutsen, D. Vanderzande and W. Maes, *J. Mater. Chem. A*, **2015**, 3, 2960.

(24)   P. Verstappen, J. Kesters, L. D'Olieslaeger, J. Drijkoningen, I. Cardinaletti, T. Vangerven, B. J. Bruijnaers, R. E. M. Willems, J. D'Haen, J. V. Manca, L. Lutsen, D. J. M. Vanderzande and W. Maes, *Macromolecules*, **2015**, 48, 3873.

(25)   A. E. Rudenko and B. C. Thompson, *J. Polym. Sci. Part A Polym. Chem.*, **2015**, 53, 135.

(26)   H. Li, X. Qiao, W. Chen, Q. Wu, S. Zhang, H. Wu, Z. Liu and R. Yang, *Chem. Commun.*, **2017**, 53, 3543–3546.

(27)   F. Brouwer, J. Alma, H. Valkenier, T. P. Voortman, J. Hillebrand, R. C. Chiechi and J. C. Hummelen, *J. Mater. Chem.*, **2011**, 21, 1582.

(28)   S. Wen, C. Wang, P. Ma, Y. Zhao, C. Li and S. Ruan, *J. Mater. Chem. A*, **2015**, 3, 13794.

(29)   J. Bard and L. R. Faulkner, in *Electrochemical methods: fundamentals and applications, 2nd Ed.*, Wiley, 2001.

(30)   S. Trasatti, *Pure Appl. Chem.*, **1986**, 58, 955.

Chapter 6

Summary and outlook

6.1 Summary

In the past decade, a tremendous amount of research has been performed in the field of organic photovoltaics, resulting in power conversion efficiencies (PCE's) of over 10% for single junction polymer-based solar cells. Unfortunately, the photovoltaic performance can differ from batch to batch and it remains rather difficult to synthesize conjugated polymer materials on a large scale and with a high reproducibility in material properties, a necessity for organic photovoltaics to become an economically viable technology. In this PhD thesis, continuous flow chemistry was used as an easily scalable synthesis method with an intrinsically high output reproducibility. Also the influence of homocoupling, a synthesis based defect in the polymer backbone, on the optoelectronic properties and the photovoltaic performance was investigated, as this can also influence the reproducibility of the synthesis method.

At first instance, we have focussed on the flow synthesis of the frequently used N,N'-dialkyl-6,6'-dibromoisoindigo building block. Both symmetrically and asymmetrically alkylated derivatives were synthesized. The synthetic pathway, which starts from the commercially available 6-bromoisatine, has three distinct reaction steps: a nitrogen alkylation, a reduction and a condensation step. Depending on the physical composition of the reaction mixture (homogeneous/heterogeneous) or scale, either a glass-chip, a tubular or packed-bed reactor was used. Through careful batch synthesis, reagent and solvent optimization, all reaction steps were successfully transferred to flow. In three cases the flow chemistry process outperformed the batch process, while in two other cases similar yields were achieved and in one case the batch process slightly outperformed the flow process. All flow protocols have the intrinsic property of being easily scalable, allowing for large scale production of N,N'-dialkyl-6,6'-dibromoisoindigo derivatives.

A wide variety of push-pull conjugated polymers affording a reasonable high photovoltaic performance nowadays exist. Each donor or acceptor building block of the conjugated polymer has a different synthesis protocol and different reaction types have to be employed. One common aspect that these polymers share, is that the actual polymerization is frequently done by a Stille

polycondensation reaction. Unfortunately, this reaction is difficult to scale in batch and frequently batch-to-batch variations arise, resulting in variations in the solar cell performance. Therefore, our next step was to translate the Stille polycondensation reaction to flow. The high-performance benzodithiophene–thienopyrroledione copolymer PBDTTPD was used for this purpose. The continuous flow production process showed a high reproducibility and delivered a constant output of high quality material with uniform characteristics. The flow process was also successfully upscaled, yielding 1.55 g of material. The photovoltaic performance of the PBDTTPD material was further increased from 7.2 to 9.1% by incorporation of an ionic polythiophene-based cathodic interlayer.

The molecular weight and dispersity of conjugated polymers have a major effect on the final device performance through a combination of processing and morphological considerations. Proceeding from the previous work, we investigated the potential of continuous flow chemistry to tune the final molecular weight of the synthesized polymers. The low bandgap polymer PffBT4T-2OD or 'PCE-11', was used for this purpose as it provides highly efficient bulk heterojunction solar cells and its temperature dependent aggregation behaviour is dependent on the molecular weight of the polymer. The influence of various reaction parameters on the molecular weight of the polymer is investigated in terms of temperature, monomer concentration and injection volume of the polymerization mixture. The polymers were tested in organic solar cells in combination with $PC_{71}BM$ as the acceptor phase. It was observed that diffusion has a large influence on small scale injections and, in order for the process to be readily scalable to continuous operation, the injection volume has to be chosen large enough to screen for conditions. Variation of the monomer concentration allowed the highest control over the molecular weight. The same protocol was then also applied to a structurally similar polymer with longer alkyl side chains, PffBT4T-2DT, affording important advantages in terms of processing due to its higher solubility.

Push-pull copolymers ideally show a perfect alternation of electron-rich (donor, D) and electron-poor (acceptor, A) building blocks. Unfortunately, a common side reaction of the Stille cross-coupling is the formation of homocoupled products, resulting in polymer main chain structures with a double donor or acceptor block and not a perfect alternation of the two. It is rather difficult to control the extent of homocoupling and this frequently leads to batch-to-batch variations and lower PCE's than expected. The specific influence of homocoupling in the donor unit of the polymer has been previously investigated, but no records exist on homocoupling of the acceptor unit. Therefore, we used a dithienosilole-quinoxaline copolymer to investigate the actual influence of acceptor homocoupling on the polymer's optoelectronic properties and photovoltaic performance. A homocoupled quinoxaline monomer was prepared and added in specific ratios to the polymerization mixture. The different

polymers were analysed by UV-VIS, MALDI-TOF and cyclic voltammetry and then tested for their photovoltaic performance. Homocoupling induces a blue-shift in the absorption spectrum and, in higher quantities, causes a strong decrease in photovoltaic performance.

6.2 Conclusions and outlook

The thesis started off with the investigation of the applicability of continuous flow chemistry for the synthesis of a standard monomer building block. It has been clearly shown that the entire synthesis process for the isoindigo building block can be performed efficiently in flow. However, this does not imply that a pure continuous flow based synthetic pathway is always superior to the traditional batch process. The most efficient synthetic pathway will most likely consist out of a combination of the two techniques. Conversion of a batch process to a continuous flow protocol can also be time consuming. The benefits of flow chemistry for the synthesis of monomers in academic OPV research might be limited, as scalability is not a key concern. However, this work demonstrates that continuous flow chemistry is a versatile synthesis technique which can be employed for many chemical reactions in both academic research and industrial processes. Toward industry, it shows that OPV building blocks can readily be synthesized in a continuous fashion and on a sufficiently large scale that will allow large scale application of organic photovoltaics in the future.

While the impact of monomer synthesis in flow will rather be found in industry, the continuous flow based protocols for synthesizing conjugated polymers, used as active layer materials, will definitely affect both industry and academia. As stressed out several times within this work, there are often significant batch-to-batch variations when conjugated polymers are synthesized via traditional batch protocols. A wide application of continuous flow based synthesis protocols would not only increase the reproducibility within one single lab, but will also make it much easier to compare results with other labs. Increasing the reproducibility of the material properties is not only important for academia, but also for industry. Uniformity will facilitate the process of selecting high potential materials for commercial applications and it will allow industry to make certain promises toward their customers with respect to the device performance and stability.

The difficulties to produce conjugated polymers in a reproducible fashion are partially related to the scalability of the batch process. So far, the conjugated polymers used as active layer materials, were only synthesized on a 100 to 300 milligram scale. Production of larger material quantities mainly occurred through repetition of the same synthetic protocol as increasing the scale of the reaction rapidly induced batch-to-batch variations. With the continuous flow based protocol, upscaling is easily achieved by increasing the operation time. The accessibility to larger quantities is not only important for industry, as it

determines large scale application, but also for academia. With increasing material availabilities, more physical tests can be performed and other device fabrication techniques than conventional spincoating, like roll-to-roll printing, can readily be tested.

Although it has clearly been shown in literature that the polymer molecular weight can have a tremendous impact on the device performance, screening of different molecular weights for one type of material is not often done, as it is a time and material consuming process when performed in batch. However, implementation of continuous flow for conjugated polymer synthesis, as demonstrated in chapter 4, can easily allow this. It can become an important tool to tune the properties of the donor polymers with respect to the employed acceptors, which is especially important for the development of non-fullerene acceptors. Certain material combinations which were of high potential but failed practically due to solubility-morphology issues, might become successful with a screening of the molecular weight.

The final part of the thesis focussed on the structural defect of homocoupling along the polymer chain. It was demonstrated that acceptor-acceptor homocoupling can drastically decrease the device performance, similar as has been shown for donor-donor homocoupling before. Although the defects have been identified, it remains rather difficult to detect them. The strong stacking abilities and often low solubility of the employed conjugated polymers hamper the characterization via ^{1}H NMR, which might be the reason why little attention has been devoted to these defects. Within the thesis, MALDI-TOF has been shown to be a strong tool for tracking down these defects, especially in the lower molecular weight fractions of the polymers. Further research is required, but as MALDI-TOF only needs minor material amounts (< 1 mg) and does not require high concentrations, it is expected to be applicable to a large variety of materials and could therefore be used as a standard characterization technique for tracking down homocoupling defects. This cannot only be applied for new materials but one can also revalidate old material combinations which have been discarded because of disappointing performances. It is very well possible that some of these materials performed poorly due to the presence of homocoupling.

Although organic photovoltaics have been envisaged for the end application for the synthesized conjugated polymers in this thesis, the concluding remarks on the efficient flow synthesis methods and careful characterization of the produced polymers are also of importance for other applications based on these materials (organic photodetectors, field-effect transistors, bio-imaging,…).

6.3 Nederlandse samenvatting

Tijdens het laatste decennium is er intensief onderzoek gedaan naar organische zonnecellen en heeft men zonnecelefficiënties kunnen bereiken van meer dan 10% in *single junction* polymeer-gebaseerde zonnecellen. Desondanks kan de zonnecel efficiëntie verschillen afhankelijk van de polymeerbatch en is het nog steeds moeilijk om geconjugeerde polymeren te synthetiseren op grote schaal en met een voldoende hoge reproduceerbaarheid. In deze thesis hebben we continue flowchemie gebruikt om deze materialen op een gemakkelijk schaalbare manier en met een hoge reproduceerbaarheid te synthetiseren. Bijkomend is er onderzoek gedaan naar het fenomeen van homokoppeling, een synthese-gebaseerd defect in de polymeerhoofdketen dat de reproduceerbaarheid vermindert, aangezien dit een sterke invloed kan hebben op de opto-elektronische eigenschappen en zonnecelprestaties van de polymeren.

In eerste instantie hebben we ons toegelegd op de flow-synthese van de frequent gebruikte N,N'-dialkyl-6,6'-dibroomoisoindigo bouwsteen. Zowel symmetrische als asymmetrische derivaten werden gesynthetiseerd. Het synthetisch reactiepad, vertrekkende van het commercieel beschikbare 6-broom isatine, kan opgedeeld worden in drie verschillende chemische transformaties: een alkyleringsstap, een reductie en een condensatie. Afhankelijk van de fysische samenstelling van het reactiemengsel of de schaal van de reactie werd een glazen chip-reactor, een buis of gepakte bed-reactor gebruikt. Voorafgaand door een uitgebreide batch-, reagens- en solventoptimalisatie, werden alle reactiestappen succesvol omgezet naar een flow-proces. In drie gevallen presteerde het flow-proces beter dan het batch-proces, voor twee andere reacties hadden ze ongeveer dezelfde efficiëntie en voor één proces presteerde de batch-reactie beter. Onafhankelijk van de exacte reactieopbrengsten, hebben alle flowprocessen de intrinsiek eigenschap gemakkelijk schaalbaar te zijn en hebben we gedemonstreerd dat continue flowchemie kan gebruikt worden om verschillende N,N'-dialkyl-6,6'-dibroomisoindigo-derivaten op grote schaal te produceren.

Er bestaat de dag van vandaag een grote variëteit aan *push-pull* geconjugeerde polymeren die goed presteren in organische zonnecellen. Elke donor- en acceptor bouwsteen van het polymeer heeft een verschillend synthese protocol waarvoor verschillende chemische reacties worden gebruikt. De vorming van het effectieve polymeer wordt frequent gedaan door middel van een Stille polycondensatiereactie. Helaas is deze reactie moeilijk schaalbaar en treden er regelmatig *batch-to-batch* variaties op, wat ook resulteert in een variatie van de zonnecel parameters. Daarom zijn we in de volgende stap gaan kijken of we de Stille polycondensatiereactie kunnen uitvoeren in flow. Hiervoor hebben we het benzodithiofeen–thiënopyrroolion copolymeer PBDTTPD gebruikt. Het continue flow-proces vertoonde een hoge *batch-to-batch* reproduceerbaarheid en

resulteerde in een continue output van materiaal met uniforme eigenschappen. Het flow-proces werd ook met succes opgeschaald, wat ongeveer 1.55 gram aan materiaal opleverde. De fotovoltaïsche prestatie van het PBDTTPD materiaal werd verder versterkt van 7.2 tot 9.1% door het implementeren van een ionische polythiofeen-gebaseerde kationische interlaag in de zonnecel.

Het molecuulgewicht en de dispersiteit van geconjugeerde polymeren kunnen een groot effect hebben op de zonnecelprestaties, aangezien het een invloed heeft op de verwerking van de materialen en de uiteindelijke morfologie van de fotoactieve laag. Voortgaand op het vorig werk hebben we het potentieel van continue flowchemie onderzocht om het molecuulgewicht van de gesynthetiseerde polymeren te controleren. Het *low bandgap* polymeer PffBT4T-2OD ('PCE11') werd hiervoor gebruikt omwille van zijn hoge prestatie in organische zonnecellen (>10%) en omdat het een temperatuurafhankelijk aggregatiegedrag vertoont dat correleert met het molecuulgewicht. De invloed van verschillende reactieparameters zoals temperatuur, monomeerconcentratie en injectievolume, op het molecuulgewicht werd onderzocht. De polymeren werden dan getest in zonnecellen in combinatie met PC$_{71}$BM als acceptor. De resultaten tonen aan dat diffusie een grote invloed heeft op het molecuulgewicht bij experimenten met kleine injectievolumes. Opdat het flowprotocol kan gebruikt worden op grote schaal zonder dat de eigenschappen van het polymeer veranderen, moet men een voldoende groot reactievolume gebruiken voor de screening zodat continue operatie zoveel mogelijk benaderd wordt. De parameter die de grootste controle over het molecuulgewicht, geeft is de monomeerconcentratie. Uiteindelijk werd hetzelfde flowprotocol ook gebruikt voor de productie van een gelijkaardig polymeer met langere alkylzijketens, PffBT4T-2DT, omdat dit polymeer gemakkelijker verwerkbaar is in organische zonnecellen.

Push-pull copolymeren hebben idealiter een perfect alternerende structuur van elektronen-rijke (donor) en elektronen-arme (acceptor) bouwstenen. In werkelijkheid treed er echter regelmatig een nevenreactie op in Stille kruis-koppeling polymerisaties, namelijk homokoppeling, waarbij de polymeerhoofdketen twee donor- of twee acceptorblokken achter elkaar kan bevatten en dus niet de perfecte alternatie van de twee. Het is vrij moeilijk om deze nevenreactie volledig te vermijden en daarom ligt ze ook regelmatig aan de basis van de *batch-to-batch* variaties van de polymeren en leveren de zonnecellen lagere prestaties dan verwacht. De specifieke invloed van homokoppeling van de donoreenheid is al eerder onderzocht, maar tot op heden is onderzoek naar de invloed van homokoppeling in de acceptoreenheid uitgebleven. Daarom werd het dithienosiloöl-quinoxaline copolymeer in dit werk gebruikt om de invloed van homokoppeling in de acceptoreenheid op de opto-elektronische eigenschappen van het polymeer en de zonnecelprestatie te onderzoeken. Hiervoor werd een homogekoppeld quinoxalinedimeer gesynthetiseerd en toegevoegd in welbepaalde verhoudingen aan het

polymerisatiemengsel. De verschillende polymeren werden geanalyseerd door middel van UV-VIS, MALDI-TOF en cyclische voltammetrie en daarna getest op hun zonnecel karakteristieken. Homokoppeling veroorzaakt een *blue-shift* in het absorptiespectrum en vermindert de zonnecel prestatie.

List of publications

V. Maes, **G. Pirotte**, J. Brebels, P. Verstappen, L. Lutsen, D. Vanderzande, W. Maes, *Synthesis of N, N'-dialkyl-6, 6'-dibromoisoindigo derivatives by continuous flow*, J. Flow Chem., **2015**, *5* (4), 201

G. Pirotte, J. Kesters, P. Verstappen, S. Govaerts, J. Manca, L. Lutsen, D. Vanderzande, W. Maes, *Continuous flow polymer synthesis toward reproducible large-scale production for efficient bulk heterojunction organic solar cells*, ChemSusChem, **2015**, *8* (19), 3228

J. Kesters, S. Govaerts, **G. Pirotte**, M. Chevrier, N. Van den Brande, X. Liu, M. Fahlman, B. Van Mele, L. Lutsen, D. Vanderzande, J. Manca, S. Clément, E. von Hauff, W. Maes, *High-permittivity conjugated polyelectrolyte interlayers for high-performance bulk heterojunction organic solar cells*, ACS Appl. Mater. Interfaces, **2016**, *8* (10), 6309

L. D'Olieslaeger, **G. Pirotte**, I. Cardinaletti, J. D'Haen, J. Manca, D. Vanderzande, W. Maes, A. Ethirajan, *Eco-friendly fabrication of PBDTTPD: $PC_{71}BM$ solar cells reaching a PCE of 3.8% using water-based nanoparticle dispersions*, Org. Electron., **2017**, *42*, 42

G. Pirotte, S. Agarkar, B. Xu, J. Zhang, L. Lutsen, D. Vanderzande, H. Yan, P. Pollet, J. R. Reynolds, W. Maes, S. R. Marder, *Molecular weight tuning of low bandgap polymers by continuous flow chemistry: increasing the applicability of PffBT4T for organic photovoltaics*, J. Mater. Chem. A., **2017**, *5* (34), 18166

Acknowledgements

Met dit schrijven treed ik de laatste fase van mijn doctoraat in en komt er een einde aan een leerrijk, plezant en interessant hoofdstuk van mijn leven. In de volgende paragrafen zou ik dan ook graag de mensen willen bedanken die bij hebben gedragen aan dit avontuur en dit alles mogelijk hebben gemaakt. In eerste instantie zou ik graag mijn promotor willen bedanken, Prof. Dr. Wouter Maes. Het is ondertussen al vier jaar geleden dat je me gevraagd hebt om terug te keren naar de Universiteit Hasselt en je onderzoeksteam te versterken. Jouw voorstel om de flowchemie op gang te trekken binnen de wereld van organische zonnecellen was voor mij een schot in de roos. Na 4 jaar kan ik je met volle overtuiging zeggen dat dit inderdaad een prachtig project was met vele uitdagingen, zowel technische als chemische. Omwille van de beperkte technische flowkennis aan de UHasselt heb je me een soort 'carte blanche' gegeven om alles uit te zoeken, naar congressen te gaan en de nodige contacten te leggen. Ik dank je daar hartelijk voor want het heeft voor een extra ondernemende ervaring gezorgd waar ik later nog de vruchten van zal plukken. Wouter, je deur stond altijd open, je hebt me ondersteund in mijn droom om onderzoek in de States te doen, reageerde snel op vragen, ik heb genoten van onze discussies rond de flowverhalen, je hebt ieder schrijven van mij met volle overtuiging telkens geoptimaliseerd en je bent een op en top aangenaam persoon om door begeleid te worden. Ik zou dit avontuur vast en zeker opnieuw doen. Hartelijk bedankt!

De kiem van het flowverhaal aan de UHasselt is ontstaan bij mijn copromotor, Prof. Dr. Dirk Vanderzande. Ik zou ook graag jou willen bedanken voor je bijdrage aan mijn doctoraat. We hebben een aantal interessante discussies gehad over flowchemie en OPV, je hebt met enthousiasme mijn papers verbeterd en veel interesse getoond in mijn onderzoek. Die interesse en jou algemene passie voor organische chemie zijn op zijn allerminst aanstekelijk te noemen en hebben zeker gezorgd voor de nodige motivatie tijdens mijn doctoraat. Dirk, een dikke merci!

Then there is of course my second promoter, Dr. Laurence Lutsen. Generally everybody thanks you for guiding the daily operation of the labs and the orders. I would of course also like to thank you for that but I'd also like to say some extra words for you. Thank you for revising my papers, for interesting discussions on possible flow/OPV projects, your general interest in the flow topic and discussions on improving the practical work atmosphere. You trusted me to try to repair/clean equipment together with Pieter, which was an interesting experience that can come in handy in the future, and that you were always interested in my technical, chemical and structural suggestions. Laurence, thank you for your contribution to my PhD, well appreciated!

Next, I would like to thank the jury for taking the time to critically evaluate my work, to improve my scientific communication skills and to challenge me with interesting questions.

Special thanks also to Prof. Dr. Michael Singleton. Mike, my time in Bordeaux really put the foundations for my interest in organic chemistry. Your teachings in organic chemistry lab skills has proven its worth multiple times during my PhD. You and Aurore became friends for life and I'm happy that you have found your desired professor position in Belgium. Thank you for accepting my invitation to be part of the jury. It is an honour to chair this day with you and your critical review on my work will certainly be interesting again. Thank you very much, we'll drink to that!

I was given the opportunity to perform a part of my research in the United States and I would certainly like to thank Prof. Dr. Seth Marder for that. Dear Seth, thank you very much for receiving me with open arms in your research group, for your confidence in me for setting up the continuous flow project in your lab, sharing your great scientific insights with me and your guidance in writing down the flow story. Besides all the scientific help, I'm also greatfull that I met you as a person. You have a great personality and gave me a warm welcome. Although outsiders might not get it, I really enjoyed your 'Bash the Belgian' game and I can certainly say that I did not just made an additional work contact but that I met a great friend in the States with whom I really enjoy spending time with. Thank you for everything and hopefully we'll see each other again in the future!

From the Marder lab, I'd also like to thank several people. First my desk mate and processing mentor, Shruti. Thank you very much for the assistance, great time and may the world experience 'Shruti's magic' many times more! I wish you all the best with your new workspace in Natalie's group. Next, I'd like to thank Bing for all the GPC measurements and the batch experiments of the PCE11 story. I also enjoyed your admiration in the flow technology and working with you was a real pleasure. I hope your training on the flow equipment will come in handy in the future somewhere. Wish you also all the best! Then I'd like to thank Reddy and Tim for helping me out with getting started in the lab and taking care of my chemicals, Denise-Teresa-Christy-Tammy-Susan and Leslie for helping out with all the administrative paper work. Administration is always messy but your friendliness and enthusiasm during the process. I have never seen before and is well appreciated! Junxiang, thank you for synthesizing the monomers and sharing you great chemical insights with me. It is best that your wife doesn't find out that you are so good at cooking (chemical) stuff or she will also put you in the kitchen at home! Great to have met you! Elena, as one of the few Europeans at Gatech, it was also great to have met you and spend time with you. Eveline and I wish you all the best with your American adventure. Thanks

also to all the other people at GaTech for the warm welcome and wonderful experience.

Then there are two more people from GaTech that I would like to thank. First and for all, Dr. Pamela Pollet, thank you very much for your assistance for setting up the flow and your insights in the results. It was also great to have met you as a person and I really enjoyed talking with you. You are a worthy European ambassador in the States and I'm sure Americans will love Europeans because of you. Prof. Dr. John Reynolds, also special thanks to you for your warm welcome, pleasant discussions and revisions on the flow manuscript. You really put your effort in it and that is certainly appreciated.

Ik zou ook graag de Rotary Club Genk-Staelen willen bedanken en in het bijzonder Paul Beerden. Bedankt om mijn beursaanvraag voor de Rotary Foundation te ondersteunen en mijn avontuur in de States te verwezenlijken. We zullen ongetwijfeld nog van elkaar horen in de toekomst! Een dikke merci!

Verder wil ik graag iedereen bedanken van de DSOS en PRD groep. Soms was er wel wat competitiviteit tussen de twee groepen, maar altijd op een leuke manier. Het was voor mij een waar plezier om het labo te delen met iedereen, leuke gesprekken te hebben, plezante algemene OBPC-teamactiviteiten te doen en het is zonder twijfel dat deze twee groepen complementair samen heel wat moois hebben verwezenlijkt. Bedankt allemaal voor de fijne tijd samen, ik wens jullie elk stuk voor stuk een mooie toekomst toe.

Een aantal mensen zou ik toch graag nog persoonlijk willen bedanken:

Jurgen, ik denk dat de tijd tussen mijn aankomst en jou volledige incorporatie in de Genkse vriendengroep nog geen 4 maanden bedraagt. Van een gewone collega is geen sprake meer. Je bent een topkameraad waar ik op kan vertrouwen, leuke tijden mee kan beleven en maar al te graag een gerstenat mee nuttig! Ik wil je ook graag bedanken voor alle zonnecellen die je voor mij gemeten hebt en de talloze keren dat je me toch nog maar eens de fysica achter organische zonnecellen hebt uitgelegd. Jouw kennis van OPV is zonder twijfel een onmisbaar gegeven in de werking van de DSOS groep. Er zijn nog mensen die wat kunnen processen, maar als ik een staal aan jou geef dan weet ik dat dat op en top 100% is verwerkt en het was een eer om die mogelijkheid te hebben. Een welgemeende dikke merci en mogen we nog vele jaren vrienden zijn!

Pieter, je bent misschien niet de meest uitgesproken leidinggevende persoon, maar jouw positie als sleutelfiguur binnen de DSOS is werkelijk van onschatbare waarde. Je bent zeer toegankelijk voor iedereen en zal nooit afzien om iemand te helpen, beginneling of gevorderde. We hebben niet enkel talloze interessante discussies gehad waarbij we ons bogen over wettenschappelijke vraagstukken maar we gingen maar al te graag samen aan de slag om iets te repareren of uit

elkaar te draaien, om dan te zien hoe het allemaal werkt. Het was een waar genoegen aan je zijde te mogen werken in de voorbij 4 jaar en je advies en hulp is welgemeend geapprecieerd.

Joris, er is geen enkele vriend die ik langer ken dan jou en die mij beter kent dan wie dan ook. We hebben samen onze bachelor en master doorlopen en onze interesses zijn meermaals dezelfde gebleken. Na de master leek het even dat we niet meer op hetzelfde pad zouden belanden, maar ik ben blij dat je uiteindelijk toch hebt gekozen om een doctoraat te doen. Ook dit avontuur was weer fijn om met jou te beleven. We hebben veel over het werk gepraat en regelmatig onze frustraties, als die er waren, met elkaar gedeeld, en vonden elkaar hier ook in. Veel meer ga ik er hier niet over schrijven maar Joris, bedankt om al 27 jaar een top kameraad te zijn waar ik altijd op kan rekenen en leuke tijden mee kan beleven. Ik wens jou en Anke een super tijd tegemoet in Australië en mogen onze wegen zeker terug kruisen in de toekomst!

Ruben en Dries, als volgende generatie doctoraatsstudenten zijn jullie DSOS komen versterken. We hebben toch wel wat tijd samen in de G61 gestaan en de gesprekken aan de rotavap of de trekkast droegen bij tot een aangename werksfeer. Jullie zijn zonder twijfel twee enthousiaste en toffe personen en het was een waar genoegen om met jullie samen te werken. Ik wens jullie allebei een top toekomst toe en we zullen elkaar ongetwijfeld nog zien!

Dear Julija, a.k.a. babushka, it was great to have met you and shared an office with you. Each day I'm still missing your phonecalls with your mom, which everyone in a radius of 5 miles could hear, and you certainly contributed to an awesome work atmosphere. I wish you and Giedrius all the best with your little wonder and I know it is getting redundant, but we should meet up again soon!

Beste Veronique, ook jou wil ik graag bedanken. Het was een plezier om met jou de eerste twee jaar het kantoor te hebben gedeeld, we konden allebei de rust appreciëren. Bedankt om mij op weg te helpen met de Syrris, de van tijd tot tijd persoonlijke babbel en ik bewonder nog steeds jouw orde en structuur in je werkwijze. Dit was een grote hulp bij het overnemen van de flowzaken van jou. Het allerbeste ook aan jou en Jeroen toegewenst en nog veel succes bij Jansen, je doet dat goed!

Verder zou ik ook graag de mensen willen bedanken die heel wat metingen voor mij hebben verricht. Koen, Gunther en Huguette, jullie zijn zonder twijfel belangrijke spilfiguren binnen eenieders onderzoek van de OBPC groep. Niet enkel bedankt voor de talloze metingen die jullie verricht hebben, maar ook bedankt voor de aangename interactie en jullie moeite om iedereen zijn resultaten zo snel mogelijk te bezorgen. Voor deze moeite krijgen jullie mijn welgemeende appreciatie en het was een waar genoegen om met jullie samen te mogen werken.

Dan is er nog de grote maestro, Eugène Steegen, van het didactisch team. Gène, het was super aangenaam om regelmatig met je te babbelen en samen te lachen. Je was niet enkel altijd paraat voor een leuke babbel maar stond ook altijd klaar om te helpen als ik iets nodig had. Een welgemeende merci!

Johan en Koen van de metaalwerkplaats en Tinne van de glasblazerij, bedankt om de gekste constructies voor mij te fabriceren met een fantastische precisie. Het was een ware luxe om met zo een vakmensen samen te werken.

Als laatste maar zeker niet als minste, ben ik aanbeland bij de personen die misschien wetenschappelijk niet zoveel hebben bijgedragen aan mijn thesis, maar zonder wie ik dit avontuur ongetwijfeld niet tot een goed einde had kunnen brengen.

Mama, papa, broer en zus, allemaal bedankt om mij altijd te ondersteunen waar nodig, een luisterend oor te bieden bij frustratie en er gewoon altijd te zijn. Papa, ook bedankt om mij in contact te kunnen brengen met de Rotary, zonder dat budget was Amerika nooit gelukt. Eenieder die me goed kent, weet dat jullie me heel nauw aan het hart liggen en dat ik niet zonder jullie kan. Een hele opsomming voor wat jullie nog voor mij betekenen ga ik niet geven, maar ik ben trots op jullie als mijn familie en jullie steun voor dit avontuur is erg geapprecieerd!

Jan, Chrisha en oma Annie, ik heb de voorbije twee jaar regelmatig mogen genieten van een top keuken, lekker gebak, een warm onthaal en altijd een fijne babbel. De nodige zondagse ontspanning om dit avontuur tot een goed einde te brengen heb ik zeker kunnen genieten bij jullie. Jullie zijn absoluut drie personen met een warm hart en ik ben blij dat ik jullie heb leren kennen. Een dikke merci voor de ondersteuning!

Dan zijn er natuurlijk ook nog 'de diertjes'. Altijd paraat om elkaar uit de nood te helpen en steevast aanwezig in de Reyski's om bij Dirk te ontspannen na de werkweek, kortom een vriendengroep om U tegen te zeggen, onbetaalbaar. Laurent, Rob, Joris, Jurgen, Peter, Lennard, Michael, Vincent, Marco, Dries, Brando, Jeroen en de rest van de bende, een dikke merci en mogen we nog jaren vrienden blijven!

Allerbeste Eveline, ik kan misschien wel zeggen dat jij de grootste ontdekking tijdens mijn doctoraat was. Ben ik blij dat je me aangesproken hebt op de heidefeesten! We zijn ondertussen al enige tijd samen en we vormen een sterk team. Bedankt om er altijd voor mij te zijn en het deed me genoegen om te zien hoe je meeleefde in iedere up en down van mijn doctoraat. Je bent me gevolgd naar de andere kant van de wereld en we hebben daar een avontuur beleefd om nooit te vergeten. Je hebt me gesteund, iedere dag voor lekker eten gezorgd na het werk, super leuke ontspannende momenten bezorgd, de nodige peptalk gegeven en me bewonderd voor wat ik doe, echt waar een welgemeende merci

en bedankt om dit avontuur tot een goed einde te brengen. We gaan ongetwijfeld nog super leuke tijden tegemoet en ik kan geen betere partner wensen!

Bedankt allemaal/thank you everyone!

Geert